People's Democratic Republic of Algeria
Ministry of Higher Education and Scientific Research
University of 20 aout 1955-Skikda
Faculty of Sciences
N° : ……. Department of Physics

Thesis

Presented to obtain the degree of doctorate

Specialty: Materials physics

Thesis entitled:

Study of the structural, optical, and electrical properties of copper oxide thin films undoped and doped

Presented by:

ZEROUALI Madiha

Defended on: 09/05/2024 before the jury composed of:

M^{r}.Otmani Amara	Professor	University of 20 aout 1955- Skikda	President
M^{r}. Daira Radouane	MCA	University of 20 aout 1955- Skikda	Supervisor
M^{r}. Boudjema Bouzid	Professor	University of 20 aout 1955- Skikda	Co-supervisor
M^{r}. Sferdjla Hocine	MCA	University of 20 aout 1955- Skikda	Examiner
M^{r}. Lekmine Farid	MCA	University of Abbes Lghrour-Khenchela	Examiner
M^{rs}.Bouras Dikra	MAB	University of Mohamed-Cherif Messaadia- Souk Ahras	Invited

Academic Year

2023/2024

Dedication

I dedicate this thesis:

To my dear parents

To my sisters and my brother

To all "Zerouali" family

To all my colleagues and everyone helped me.

Madiha

Acknowledgments

First of all, I thank GOD Almighty for giving me the will and the courage to complete this thesis. I also thank my parents, sisters, and brother for their encouragement, support and sacrifice.

A big thanks to my supervisor of thesis “Dr. **Daira Radouane**” For his acceptance of taking charge of my work and his keen interest in my research. I really thank him for his constant support and the trust he has placed in me and his encouragement.

Also, thanks to my co- supervisor of thesis “Pr.**Boudjema Bouzid**” for welcoming me, then for guiding me, and benefiting from his scientific skills.

I would like to extend my gratitude to **Mr. Othmani Amara** , Professor at Skikda University, for graciously accepting the presidency for my thesis. I am also thankful to **Mr. Sefardjella Hocine** , MCA at Skikda University, for the honor of serving as an examiner for this work. Additionally, I express my deepest appreciation to **Mr. Lekmine Farid**, MCA at Khenchela University for generously agreeing to participate in the jury and review my thesis.

Many thanks to my friend “**Dr. Bouras Dikra**”, MAB at Souk Ahras University for accepting to take over my work and for her keen interest in my research. I thank her for her continued support, trust in me, and encouragement.

I also thank the laboratories for receiving me to do the thin layers and characterization:

- The Laboratory of Active Components and Materials (LCAM) of the Larbi Ben M'Hidi University of Oum El Bouaghi (Algeria). I especially thanks very much **Dr. Bouras Dikra**, who received me in her laboratory and helped me to prepare the samples, without forgetting the director and the engineers of the laboratory for having received me.
- The Moltech Anjou Laboratory of the University of Angers (France). I especially thanks very much **Pr. Barillé régise**, Who received me in his laboratory and helped me.
- Laboratory of Structures, Properties and Inter-Atomic Interaction (LASPI²A) laboratory of the Abbes Laghrour Khenchela University (Algeria).

.

List of Figures

List of tables

Contents

Chapter II :Experimental deposition and characterization techniques

Chapter III : Effect of spraying times for copper oxide thin films on the water contact angle

Chapter IV: Elaboration and characterization of Al-doped copper oxide thin films for photocatalysis application

Chapter V: Elaboration and characterization of Ag-doped copper oxide thin films for photocatalysis application

General introduction

General introduction

Scientists' interest in science and technology at the nanoscale has been actively and intensely growing for many years to the present day. Therefore, scientific research and industrial development paved the way for nanoscience and nanotechnology. It is known that this domain of research is emerging and has a significant impact on the industrial, medical, and environmental fields. Metal oxide particles and nanostructured semiconductor materials in particular have become very important and indispensable tools [1], thanks to their wide use in modern science and technology due to their extraordinary physical and chemical properties [2].

Contemporary research indicates that the lotus leaf employs nanotechnology to achieve a self-cleansing surface characterized by non-wetting properties, super water-repellency and super hydrophobicity. The self-cleaning characteristic shown by the lotus leaf can be attributed to its unique surface structure. The lotus leaf possesses a nanostructure characterized by cone-like protrusions that are randomly arranged [3]. Self-cleaning coatings may be broadly classified into two categories: hydrophobic and hydrophilic. These distinct types of coatings exhibit varying behaviors in relation to water, enabling them to effectively clean surfaces. The first method facilitates the movement of water droplets over surfaces, causing them to take away dirt particles by sliding and rolling. On the other hand, the second method employs certain metal oxides to create a thin layer on the water's surface, enabling it to remove dirt from the surface [4].

Azo dyes are complex chemical compounds that often provide difficulties in terms of degradation. During the processing stage, they can also produce more hazardous intermediates. Due to the latter two factors, the remediation of the azo dye Orange II (Acid Orange 7) is particularly concerning when it comes to contaminated dyes in water [5]. The expansion of this field has thus been substantial. It encompasses semiconductor physics, surface science, chemistry, materials science and chemical engineering [6]. The field of heterogeneous photocatalysis has developed rapidly over the past four decades. It has seen many advancements, particularly in the fields of energy and the environment where it has been of significant interest and focus [6,7]. Photocatalysis is a process in which the rate of a chemical reaction is enhanced by the presence of a catalyst when exposed to light.

At present, water pollution is considered as a serious problem in the environment posing a threat to humans and living organisms due to chemical pollution resulting from agricultural or industrial wastes. This prompts us to find solutions to it by using thin films of copper oxide,

undoped and doped with different elements for self-cleaning and photocatalysis applications as well as degradation of Orange II. It represents the most colored material used in industry, so it is the most polluting one. In addition, Orange II is a carcinogenic dye.

Thin films of copper oxide (CuO) have been attractive as one of effective catalysts due to the advantages of non-toxicity, good adaptation to the environment, and low cost [8]. Also, it has a large light absorption coefficient and a high activity in the photocatalysis splitting of water into H_2 [9]. CuO is a p-type transition metal oxide semiconductor with a direct band gap, Eg= 1.2 eV to 2.2 eV[10], enabling its use in several applications such as gas sensors [11,12], antibacterial activity [13], solar cells [14], and photocatalysis [9].

Doping a suitable metal cation like Al^+ and Ag^+ into the CuO lattice seems to be the most constructive approach because it not only reduces the band gap but also improves the electrical properties of CuO [15]. Aluminum oxide is widely used as a carrier for various catalysts. Its effect as a carrier on catalyst performances has been widely studied [16, 17]. Also, silver oxide is one of the most important p-type semiconductors due to its remarkable chemical reactivity in solution. Silver oxide is mostly attractive for photocatalysis applications [6].

The objective of this study is the elaboration of thin layers of copper oxide by spray pyrolysis method on a glass substrate for different spray times and thicknesses. It was then used in the application of self-cleaning. Also, the elaboration of films of CuO copper oxide undoped and doped by Ag and Al with atomic contents like 5%, 15%, 25% and 50% with respect to copper were obtained by the method of sol-gel spin coating to improve structural, morphological, optical and electrical properties for the increase in the yield of degradation in the photocatalysis application such as the degradation of the Orange II dye under UV irradiation.

The thesis is divided into five chapters :

The first chapter is devoted to the largest part to a bibliography on copper oxide as well as its structural, optical, electrical and catalytic properties as well as its applications. Also, the general idea of dyes especially the Orange II dye and its principle of degradation are exposed.

The second chapter describes in detail the experimental procedure used during this thesis work. This is essentially a description of the method of synthesis of CuO, $Cu_{1-x}Ag_xO$, and $Cu_{1-x}Al_xO$ films where x is the doping content by spray pyrolysis and sol-gel spin coating. It describes also the characterization techniques used. Thin layers have been studied by X-ray

diffraction (XRD), UV-Visible spectrophotometry, spectroscopy (FTIR), scanning electron microscope, four points method and water contact angle. The basic principle of their operation is provided.

The third chapter of this study focuses on the analysis and interpretation of the findings derived from the examination of the films produced by the pneumatic spray pyrolysis technique. Specifically, the investigation explores the impact of varying spraying durations on the properties of the films as well as the influence of the film thickness on the surface characteristics with the intention of assessing their potential for self-cleaning applications.

The fourth chapter studies the effect of Al doped copper oxide thin films obtained by the sol-gel spin coating method on structural, morphological, electrical and photocatalysis properties for the degradation mechanism of the Orange II dye.

The fifth chapter studies the effect of Ag doping of the copper oxide thin film obtained by the sol-gel spin coating method on the photocatalysis properties for the degradation mechanism of the Orange II dye.

The dissertation manuscript ends with a general conclusion in which we have summarized the main results obtained as well as the importance and perspectives that can be expected from this dissertation work.

Chapter I :

Copper oxide properties and photocatalysis application

I.1. Introduction

The human race rapid technological advancement over the last centuries has resulted in the unpleasant phenomenon of water contamination which threatens the ability of life on earth. Physical and chemical approaches have thus been devised to combat this significant issue.

Photocatalysis is a straightforward and cost-competitive process that works through the activation of a semiconductor with light. Copper oxide has been chosen as it is a semiconductor with interesting properties for this application.

This chapter focuses on copper oxide thin films, their structural, optical, and electrical properties and their applications. A reminder on the principle of photocatalysis is also provided.

I.2. Thin films

I.2.1. Definition

A thin film is a thin layer of one material deposited on top of another one, the latter being called the substrate [18]. It has been greatly reduced in thickness with the technology advances so that it varies nowadays from a single atomic layer to a few nanometers "nm" and up to a few micrometers "µm" (typically, in most cases, these thin films are layers 10 - 100 nanometers thick) [19]. The fundamental difference between matter in the solid state and in the thin layer state is the role and property of boundaries that are generally neglected for bulk materials while in the thin layer case, surfaces and interfaces play a major role. The smaller the thickness, the more critical the two-dimensional topological effect becomes. However, if the thickness exceeds some threshold, the dimensionality problem becomes minimal, and the material regains the known properties of the solid material [20]. Also, the thin layer films may see its properties affected by those of the substrate on which it is standing. For example, a thin film of the same material and thickness can have significantly different physical properties when deposited on an amorphous insulating substrate such as glass or on a semi-conducting monocrystalline silicon substrate [21].

I.2.2. Steps to formation of thin films

In the synthesis process of thin films, the coating material must pass through a conductive medium and come into direct contact with the substrate to form a thin film on a solid surface (substrate). A portion of the coating particles adheres or chemically reacts with the substrate when they land on it. The particles can be either atoms, molecules, ions, or molecular fragments coming from molecules that have been ionized or fragmented.

Nevertheless, all thin film deposition techniques consist of four consecutive phases :

- **Source :** The fundamental constituent of the thin film to be generated may initially consist of a solid, a liquid, or a gas [22].
- **Transport :** The homogeneity of the flow of species throughout the transport stage onto the substrate surface is a crucial property to preserve but it is influenced by several parameters that are contingented by the medium in which the transport occurs.
- **Deposition :** The third stage in the fabrication of thin films involves the application of a layer onto the surface of the substrate. This phase encompasses the processes of nucleation and fusion. The deposition process is influenced by various factors, including the source and transport mechanisms as well as the primary surface conditions of the substrate. These surface conditions encompass characteristics such as surface roughness, contamination levels and other relevant factors. Additionally, the bonding coefficient of the material arriving on the substrate surface and the temperature of the substrate also play a significant role in determining the deposition behavior [23].
- **Analysis :** The final stage of the production process involves the examination and analysis of the thus-deposited film [24].

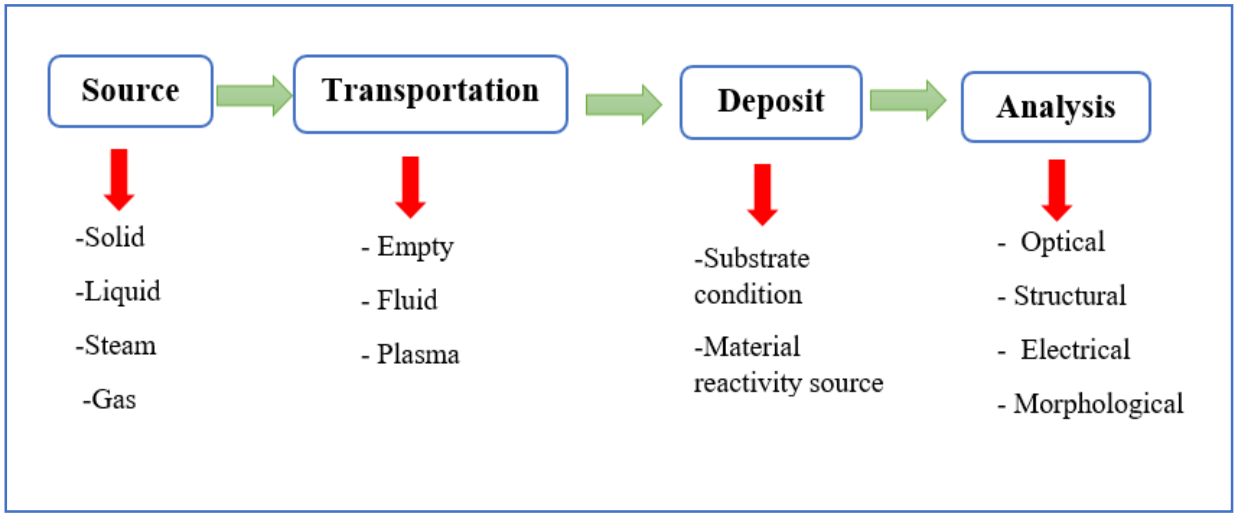

Figure I.1. Schematic diagram of the steps of the thin film fabrication process.

I.2.3. Mechanisms of growth of thin films

A thin film formed on the surface of a substrate will undergo two phases : a nucleation phase (germination) followed by a growth phase.

I.2.3.1. Nucleation

The process of nucleation of a thin layer can be summarized as follows :

- The phenomenon of atoms (or molecules) being adsorbed onto the substrate surface with a statistical sequence of nucleation.
- The growth by surface diffusion of the atoms or molecules on the substrate surface.
- The bonding between the precipitated atoms and the substrate resulting in the formation of stable bonds. The islands thus formed grow into islands of larger dimensions until finally they form a continuous layer through the process of the filling of spaces between the already-grown islands [25].

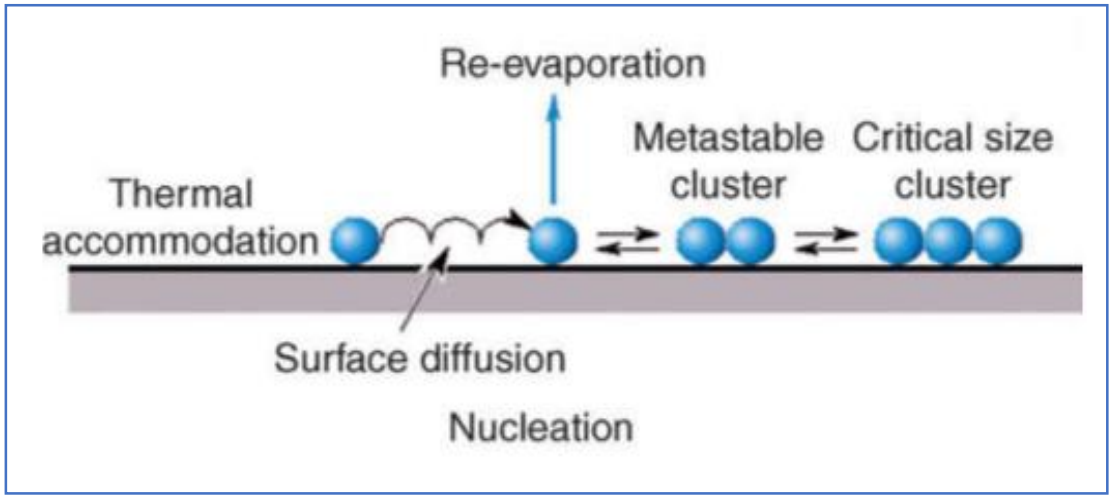

Figure I.2. Schematic representation of processes leading to nucleation [26].

I.2.3.2. Growth of thin films

Depending on the interaction between the substrate and the deposited atoms, three different nucleation modes can be observed during the formation of thin films [27].

- **Frank-Van der Merwe mechanism (FVM)**

This mechanism consists of creating a monoatomic layer on the entire substrate. Therefore, it is a two-dimensional building of the thin film of matter layer by layer. It is confirmed by the observation that the layers of atoms are more closely bound to the substrate rather than to the other layers themselves.

- **Volmer-Weber mechanism (VW)**

The growth mechanism is not two-dimensional but rather three-dimensional. Indeed, this growth mode corresponds to the growth of islands, both in x and y in the plane direction, as well as along the vertical z direction. These islands can merge to form, in the end, a compact layer of atoms within a film, tightly linked to each other rather than to the substrate [28, 29].

- **Stranski-Krastanov mechanism (SK)**

The growth begins similarly to the Frank Van-der-Merve (2D) growth, but after a few atomic layers, the growth develops three-dimensionally. This growth mechanism is often considered as an intermediate between the FVM and the VW models [28.30].

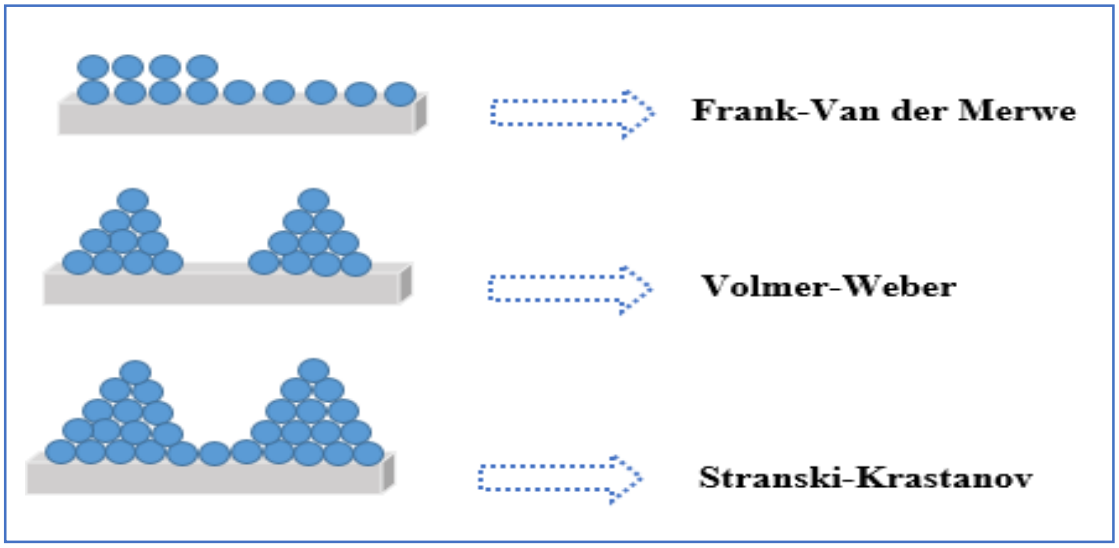

FigureI.3. Diagram of the different thin film growth mechanisms.

I.2.4. Applications of thin films

The implementation of thin film fabrication technologies has led to numerous applications in a wide variety of fields. The applications of thin layers are vast and we cannot mention them all because development. Research in this field still continues to develop day by day [31].

- **Microelectronics :** diode, transistor, LED lamps, solar cells.
- **Optics :** Thin layer technology is used mainly for two types of applications, on the one hand, reflective layers and on the other hand to the contrary anti-reflection layers.
- **Decoration :** Another aspect of thin film technology is its use in the luxury industry for decorative applications such as eyewear and jewelry.
- **Chemistry :** corrosion resistance, gas sensors, catalytic coatings, protective layers.
- **Magnetic :** information storage (computer memory), hard drive read heads.

I.3. Cupric or Tenorite copper oxide

I.3.1. Reason for choosing copper oxide

This phase of copper oxide is used in various applications such as solar cells, gas sensors, and photocatalysis applications. Other reason supporting this choice is chemical stability, excellent electrical conductivity, non-toxicity, low cost yielding economical advantages, .industrializablility [32, 33, 34].

I.3.2. Crystallographic properties

Cupric oxide, CuO, known as tenorite [35] has a monoclinic crystalline structure with lattice parameters a = 4.6859 Å, b = 3.4283 Å, c = 5.1232 Å and β = 99.541° [36]. It crystallizes within space group C2/c [37]. Each copper (or oxygen) atom has four oxygen (or copper) close neighbors : the copper atoms are at the center of a rectangle of oxygen, while the oxygen atoms are at the center of a deformed copper tetrahedron [35]. CuO crystals present a multitude of morphologies that depend on the method and the conditions of synthesis [38]. Atomic positions within the unit cell [39] for CuO are :

- Copper : (1/4, 1/4, 0), (3/4, 3/4, 0), (1/4, 3/4, 1/2) and (3/4, 1/4, 1/2)
- Oxygen : (0, y, 1/4), (0, 1/2 + y, 1/4), (0, y, 3/4) and (1/2, 1/2 - y, 3/ 4) with y = 0,416.

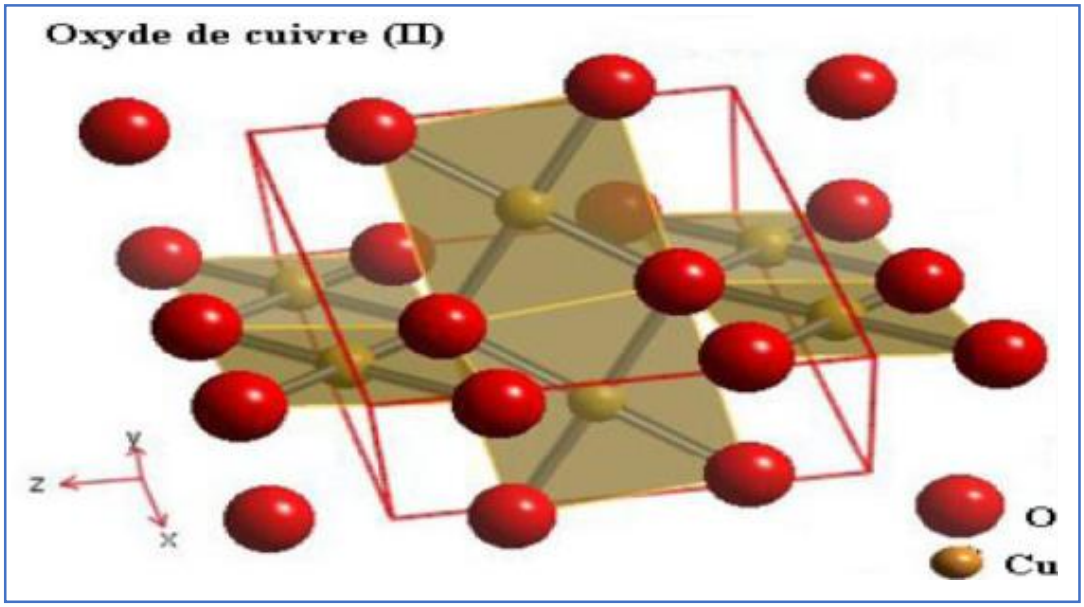

FigureI.4. Crystal structure of CuO. Oxygen atoms (large red spheres) and Cu atoms (small yellow spheres) [40].

TableI.1. The main crystallographic characteristics of CuO [41]

Characteristics	Value
Density (g/cm^3)	6 .51
The volume of a cell (10^6 pm^3)	81.12
Cu-O bond length (Å)	1.96
O-O bond length (Å)	2.62
Cu-Cu bond length (Å)	2.90

I.3.3.Electrical properties

Copper oxide is a p-type semiconductor at room temperature. Its direct band gap Eg ranges from 1.2 to 2.1 eV. Because of the existence of acceptor levels attributable to copper vacancies, oxides with metal defects by cationic vacancies or oxides with excess oxygen by interstitial anions releasing holes generally endow to the CuO semiconductor material a low conductivity. There have been notable disparities seen in resistivity levels though with a pronounced correlation between resistivity and the elaboration process employed. The conductivity of CuO can be controlled in a low partial pressure environment during its formation. Additionally, CuO is sensitive to the presence of adsorbed molecules, indicating its significant potential for chemical and environmental detection. This sensitivity is even observed with a small quantity of impurities in the compound, highlighting its temperature stability [37-39, 41, 42].

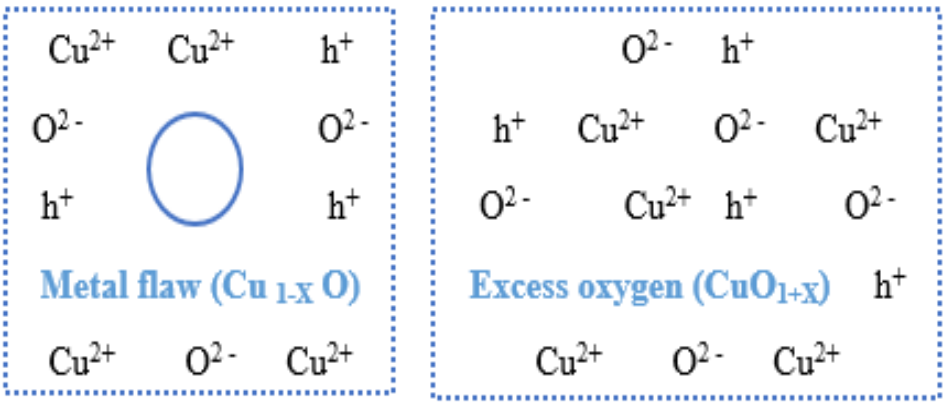

Figure I.5. Structural defects of metal oxides.

I.3.4.Optical properties

The optical characteristics of CuO play an essential role in its beneficial use as an absorber layer in optoelectronic devices in general and solar cells in particular. High solar spectrum absorption in the visible range is essential for this application. Preparation conditions and deposition methods also affect structural characteristics, film surface morphology, and optical properties [43]. The band gap of the materials determines the absorption threshold with reported values between 1.2 to 2.1 eV. On the other hand, the researchers also found a higher band gap, up to 4.13 eV. Therefore, CuO absorbs in the UV region and substantially absorbs the visible spectrum due to a broader band gap [35, 39].

I.3.5.Physical properties

Copper oxide CuO is a solid substance characterized by its black coloration. It possesses a density of 6.31 g/cm^3 and exhibits notable thermal properties, with melting and evaporation points recorded at 1064°C and 1100°C, respectively. Due to its potential for cost-effective synthesis and its exceptional electrochemical characteristics, CuO stands out as a highly desirable material for applications in electrical and optical sensing. Due to its low symmetry, CuO exhibits ferroelectric and antiferromagnetic properties. Many methods to prepare copper oxide CuO are available, such as thermal oxidation, precipitation, sputtering, chemical vapor deposition (CVD), electrochemical deposition, sol-gel, spray pyrolysis, and pulsed laser deposition [38, 44, 45].

Table I.2. Some physical properties of CuO [38, 45].

Properties	Value
Dielectric constant	18.1
Refractive index	1.4
Effective hole mass	0.24 m_0
Hole mobility	0.1-10 cm^2/VS
Specific heat capacity (Cp)	460 ± 10 J kg^{-1} K^{-1}
Molecular mass	79.55 g mol^{-1}
Volumic mass	6.32 g cm^{-3}

I.4. Cuprous oxide Cu_2O

I.4.1. Crystallographic properties

Cuprous oxide Cu_2O crystallizes in a simple cubic structure with lattice parameter a = 4.271 Å, broken down into two sub-lattices : a face-centered cubic lattice formed by the Cu^+ cations and a centered cubic lattice formed by O^{2-} anions. The copper atoms are thus coordinated to two oxygen atoms while each oxygen atom is bonded to four copper atoms [46]. Cuprous oxide crystallizes in the space group Pn3m in which a quarter of the tetrahedral interstitial spaces are found to be occupied by oxygen atoms [44, 47].

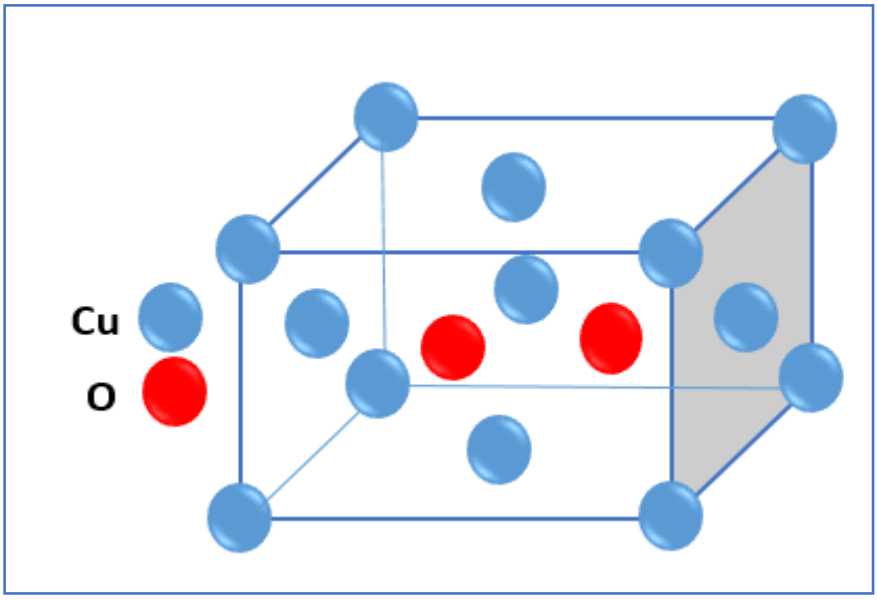

Figure I.6. Crystal structure of Cu_2O.

Table I.3. Summary of the main structural characteristics of Cu_2O [44,46].

Material	Cu_2O
Volume ($Å^3$)	77.83
Molar volume ($cm^3.mol^{-1}$)	23.44
Volumic mass ($g.cm^{-3}$)	6.106
Z	2

I.4.2.Physical properties of Cu_2O

Cu_2O is a p-type semiconductor. The electrical conductivity is often explained by the presence of excess oxygen linked to the formation of V_{Cu} copper vacancies or interstitial oxygen. These defects give to Cu_2O a p-type electrical conduction with significant mobility of positive carriers at ambient temperature, up~100 $cm^2 .V^{-1}.s^{-1}$ in the form of a thin layer [35].

Table I.4. Physical properties of Cu_2O [42].

Physical property	Value
Fusion point	1235˚C
Relative dielectric constant	7.5
the electron mass in the conduction band	0.98me
the hole mass in the valence band	0.58me
Cu–O bond length	1.85 Å
O-O bond length	3.68 Å
Cu - Cu bond length	3.02 Å
largeur de la bande interdite (Eg)	2.09 eV

I.5. Oxidation of copper to Cu_2O

Within the temperature range of 150 to 200°C and in the presence of air, copper undergoes oxidation leading to the formation of Cu_2O [48]. Therefore, the presence of the cuprous phase is significantly influenced by variations in temperature and oxygen partial pressure. The structure is modified, oxygen is introduced, and the arrangement of the copper atoms results in a +65% increase in molar volume when the copper oxidizes to Cu_2O. The alteration in volume has the potential to induce porosities or imperfections within the microstructure of the material [49]. The principle is rather simple : oxygen diffuses through the copper sheets and reacts to produce Cu_2O. To obtain copper oxide as a single phase, the oxygen content, as well as the temperature and duration of the calcination, must be controlled [46].

$$4Cu + O_2 \rightarrow 2Cu_2O \qquad \text{(I.1)}$$

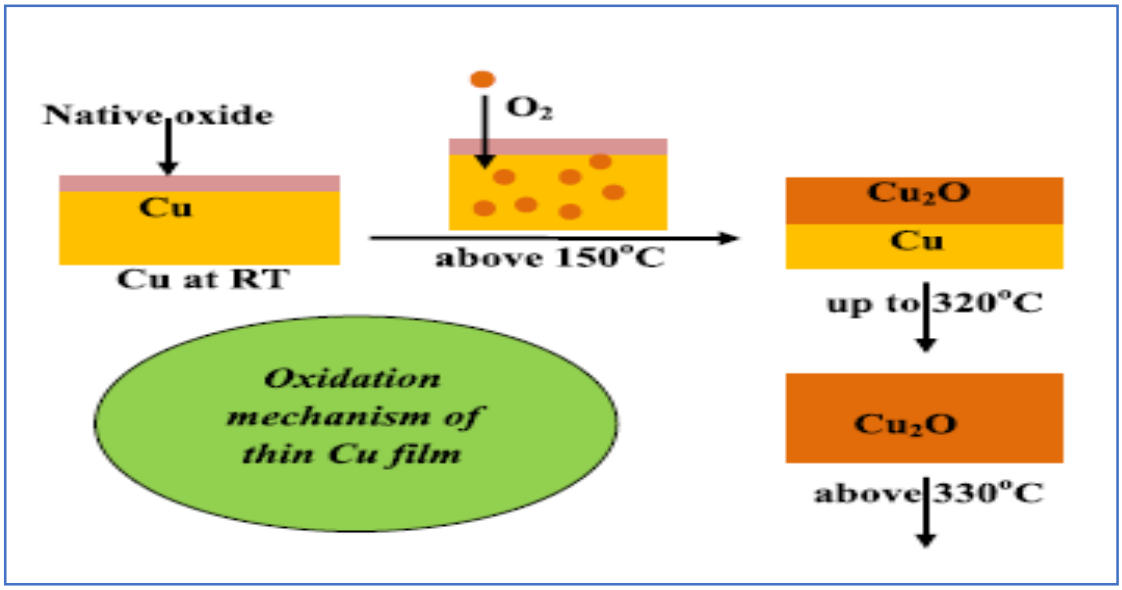

Figure I.7. Mechanism of growth of Cu_2O from copper metal [48].

I.6. Cu_2O oxidation to CuO

CuO is obtained by the oxidation of Cu_2O at temperatures beyond from 330°C [48]. CuO is continuously formed by the oxidation of Cu_2O and never by direct oxidation of metallic copper. As the enthalpy of formation of Cu_2O is always lower than the enthalpy of formation of CuO, it is thermodynamically impossible to form CuO directly from copper. Therefore, the only systems that can be observed are copper with Cu_2O and Cu_2O with CuO [49]. Copper in air should therefore oxidize entirely at room temperature of 300 K under oxygen pressure of $P(O_2)$ = 0.2 atm if the kinetics is not considered. It is therefore interesting to give a particular interest to the kinetic aspects of this oxidation, and notably the size of the copper particles. Indeed, the kinetics of the oxidation reaction is all the more rapid as the size of the copper particles is small [46].

$$2Cu_2O+O_2 \rightarrow 4CuO \qquad \text{(I.2)}$$

I.7. Applications of CuO

Copper oxides have been extensively investigated due to their semiconducting properties which make them suitable for several applications, such as solar cells [50], gas sensors [48] and photocatalysis.

I.7.1. Solar cells

Solar cell technology for future energy has improved in several technical areas. Cost reduction is one of the most crucial concerns in producing traditional solar cells which use silicon as a material semiconductor. [39]. Due to the high cost of silicon solar cells, new photovoltaic devices need to be developed using inexpensive, non-toxic materials and energy-efficient methods [51]. CuO semiconductors have the qualities of suitable materials with high optical absorption coefficients, low thermal emissivity and low manufacturing costs. CuO is an exciting material for solar cells because the material under consideration exhibits p-type semiconductor characteristics with its band gap closely approximating the ideal energy band gap for efficient utilization in solar cell applications [39]. Producing solar panels using cupric oxide as a potential active layer has therefore attracted much attention. Various deposition processes have been used, including electro-deposition, RF sputtering, sol-gel, and plasma evaporation.

The characteristics of solar cells based on CuO are intricately linked to the method of deposition. For example, the ZnO/CuO interface of solar cells produced by the electro-deposition process has a higher density of defects which significantly impacts the solar cells efficiency. The layers utilized in this context are ZnO, Cu_2O, ZnO:Sn and C_{60}, and they all impacts the solar cells efficiency. By manipulating the optical and chemical characteristics of the buffer layer, several current studies seek to increase the efficiency of solar cells. Furthermore, diligent endeavors have been undertaken to develop a thin film with soft and smooth consistency as a window layer for solar cells based on copper oxide (CuO) [43].

I.7.2.Gas sensor

For years, metal oxide semiconductors (MOS) have been utilized for the detection of reducing gases, including hydrogen, ethanol, carbon monoxide (CO) and hydrogen sulfide (H_2S). Such materials like pure phase CuO or CuO bonded to other MOS in a composite material have been explored. The growing interest in various CuO nanostructures such as nanowires and thin films can be attributed to their very high surface-to-volume ratio. The enhancement of device performances in semiconductor nanostructures is thus anticipated [52]. The p-type copper oxide semiconductor under investigation for gas sensing applications has garnered significant attention in academic research due to its advantageous characteristics, including its affordability, exceptional stability, and non-toxic nature. For the detection of various gases, several researchers have focused on creating unique CuO nanostructures [53]. Gas sensors have gathered much interest as integrated devices into daily life for precise

monitoring and control of ambient humidity for human comfort and prospective applications in industries such as robotics, aerospace, agriculture,and health [54].

I.7.3. Photocatalytic application

Multiple studies have shown that the use of CuO for the photocatalytic degradation of organic contaminants in aquatic environments is possible. The utilization of CuO has been employed in the process of photocatalysis degradation of methylene blue, facilitated by exposure to sun irradiation [55]. To control the efficiency of photocatalysis, one can use an active medium for the preparation of the pollutants such as the use of lactic acid (LA), methanol (MeOH), triethanolamine (TEOA) and so on. The photocatalyst efficiency for of H_2 generation in solution has been reported to improve with the increasing redox potential of the hole scavenger. Currently, the process of producing H_2 from CuO based on photocatalysts is usually carried out in an aqueous solution of MeOH [56]. Research studies have revealed the superior stimulating activity of metallic nanoparticles using copper oxide as the perfect support [57]. Hence, CuO is a good catalyst in the rose bengal (RB) dye degradation. In particular, A. Al Gamdi and al. [58] studied a thin layers of CuO deposited by RF sputtering in 600 s. A degradation of 100% of methylene blue under visible light in 3 hours was observed. In addition, another study on the Au-CuO_2-CuO composite deposited by RF magnetron sputtering method showed dye degradation with percentages 73.1% for methyl orange and 86.2% for methylene blue in 28 mins of sun exposure, see Kavita Sahu and al. [59].

I.8.Copper oxide doping

I.8.1.Aluminum doped Copper oxide

Aluminum is an elemental substance characterized by its atomic number, which is Z=13. Its symbol is Al and it is a member of the poor metal family. Found in the periodic table in period 3 and column 13, its electronic configuration is [Ne] $3S^2 3P^1$ and ionic radius 0.54 Å. CuO doping with Al atomic element is used to improve the CuO thin film catalytic properties. Aluminum oxide is extensively employed as a support material for several catalysts. Extensive research has been conducted on the impact of transportation on catalyst performance. It has been observed that acidic carriers have a greater propensity to enhance the electron deficiency of noble metals compared to essential supports. These carriers are distinguished by their substantial surface area playing a crucial role in determining the distribution and the states of the active components, thereby influencing the activity in various reactions. Additionally, acidic carriers exhibit excellent thermal stability and possess high mechanical strength [60, 61].

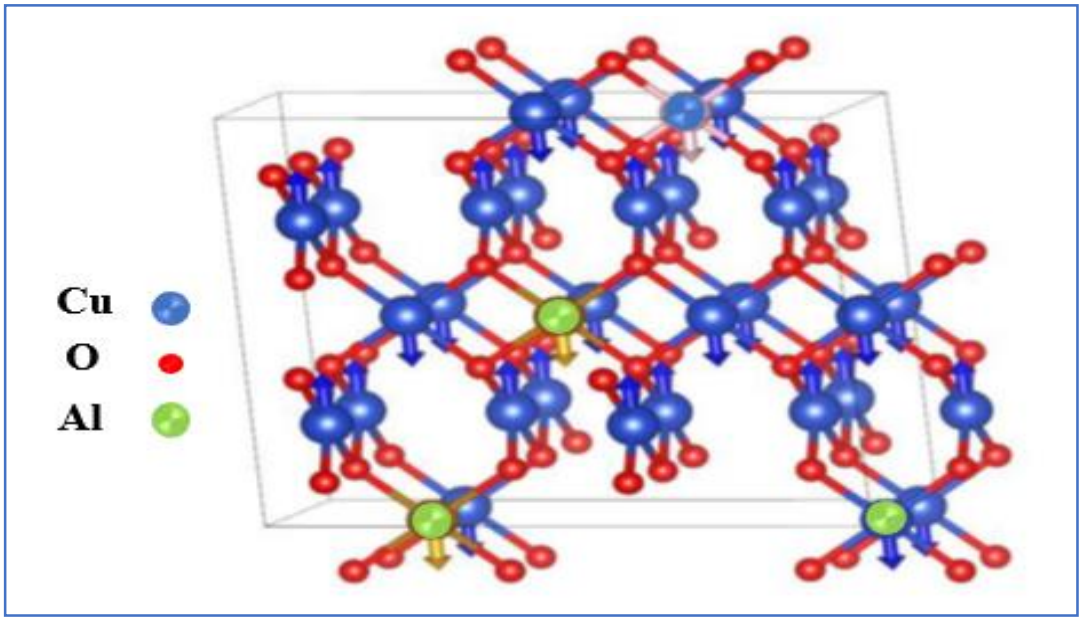

Figure I.8. Crystalline structure for Al-doped CuO [62].

I.8.2.Silver doped Copper oxide

Silver is classified as a metal element with the atomic number 47, is denoted by the symbol Ag, and belongs to the family of transition metals. It is found in the element table in period 5 and column 11, with ionic radius 1.15 Å. CuO doping with Ag atom is used to improve the catalytic properties too. Ag atom doping has been used to enhance the degradation of Orange II in photocatalysis because researchers have been widely attracted by the silver-oxygen (Ag-O) bond and its utilization in several fields including high-density optical storage devices, gas sensors, photovoltaic cells, photodiodes and antibacterial coatings owing to its innovative applications

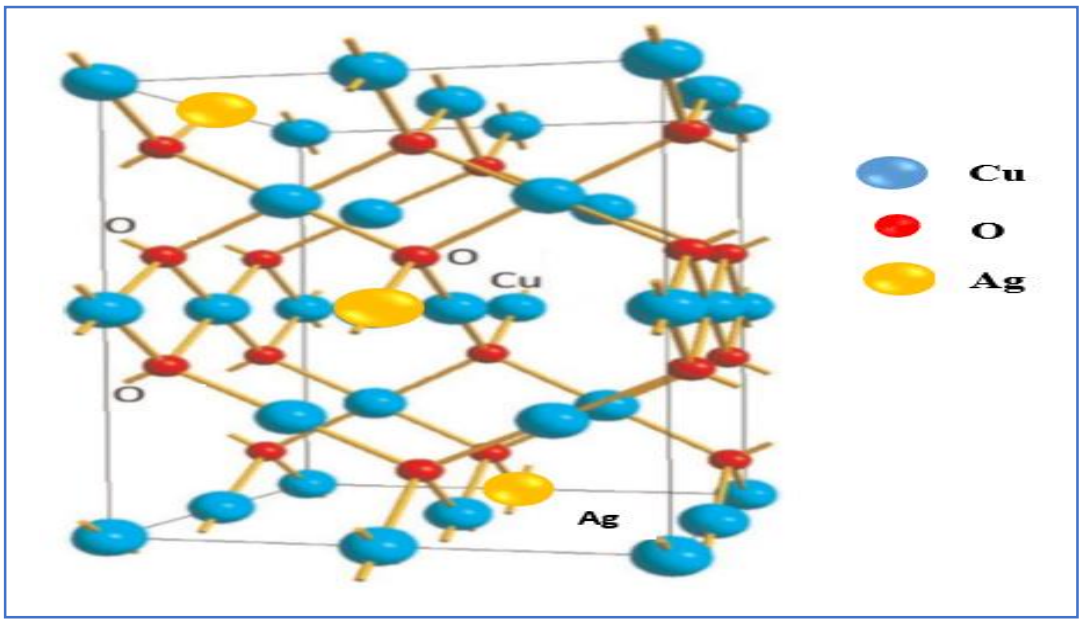

Figure I.9. Crystalline structure for Ag-doped CuO [63].

I.9. Dyes

I.9.1. Origin of dyes

Throughout the course of human history, dyes have been employed in a wide range of applications that permeate all facets of our everyday existence. These applications encompass the realms of paper, skin and clothes where dyes have been utilized for the purpose of painting and dyeing. The utilization of natural dyes persisted until the mid-19th century. Inorganic pigments such as manganese oxide, hematite and anchor were employed in these cases. Conversely, natural organic dyes were extensively employed, particularly within the textile industry. The most common colors were coming from aromatic compounds predominantly obtained from botanical sources. This includes alizarin and indigo. The synthetic dye business began in 1856 when English scientist W. H. Perkin discovered the first synthetic color, "mauve" when he was trying to create artificial quinine to cure malaria (aniline, basic dye)..Perkin secured a patent for his innovative discovery and then established a production line, a development that was swiftly followed by other individuals. Emerging synthetic dyes have recently entered the commercial market. The acceleration of this tendency was facilitated by Kekule's 1865 discovery of the molecular structure of benzene. Therefore, by the beginning of the 20th century, synthetic dyes had almost wholly replaced natural colors [64]. It was in 1876 that Witt first recognized that colored substances comprised an entire distinctive group. He named this group "chromophore" from the Greek words "chromo" for color and "phore" for

"which transmits". He observed that a hydrocarbon - an uncolored compound - became colored by adding a chromophore. Thus, it is transformed into a chromogen, that is to say, into a more or less intensely colored molecule [65]. All aromatic compounds are electromagnetic energy absorbers, but only those that can absorb visible light (380 to 750 nm) are pigmented [66]. Thus, the absorption spectrum of the molecule is due to the presence of a chromophore group, most often with double bonds. Also, the chromogen turns into a dye if it has the second auxochrome group. The fixation of the dyes on the substrates is made possible by the auxochromic groups. Auxochromes can intensify their hue. Examples of auxochromes include the hydroxyl (-OH) and amine ($-NH_2$) groups. (Table I.5). This list has been supplemented as a molecule can acquire color from additional components [67].

Table I.5. Main chromophore and auxochrome groups, classified by increasing intensity [68].

Chromophore groups	Auxochromic groups
Azo (-N=N-)	Amino ($-NH_2$)
Nitroso (-NO ou –N-OH)	Methylamino (-NHCH3)
Carbonyl (=C=O)	Dimethylamino ($-N(CH_3)_2$)
Vinyl (-C=C-)	Hydroxyl (-HO)
Nitro ($-NO_2$ ou =NO-OH)	Alkoxyl (-OR)
Sulphide (>C=S)	Electron donating groups

I.9.2. Definition of dyes

A dye is a chemical substance that interacts with the medium in which it is placed, causing the dye to dissolve and distribute the characteristic of the dye. This characteristics, which results from a specific affinity between the dye and the medium, often a fiber, is the source of most problems encountered during dyeing procedures. Synthetic dyes must meet several criteria depending on the application and use to extend the life of the colored products to which they are applied: abrasion resistance, photolytic color stability, resistance to chemical oxidation (particularly to detergents), resistance to microbial attacks [69]. We have only been interested in azo dyes and acid dyes in this work.

I.9.2.1. Azo dyes

Azo dyes are estimated at a production of around 350,000 tons per year. Azo dyes are recognized as the predominant group of synthetic dyes due to their distinctive molecular structure which involves the linkage of two benzene rings through an azo group (-N=N-). The

group of dyes in question is now the most extensively utilized in terms of applications, as it accounts for over 50% of the global output of coloring agents. These organic compounds are very resistant to biodegradation. Azo dyes fall into several categories: water-soluble basic, acid, direct and reactive dyes, water-insoluble non-ionic disperse and mordant azo dyes [70-72].

I.9.2.2. Acid or anionic dyes

They are soluble in water and are called acidic or anionic dyes because of their sulfonate or carboxylic groups because certain animal fibers, such as wool and silk, as well as certain modified acrylic fibers like nylon and polyamide, are permitted to undergo dyeing processes inside a mildly acidic solution. The affinity between dye and fiber arises from the formation of ionic connections between the sulphonic acid moiety of the dye and the amino groups present in the textile fibers. The majority of these dyes exhibit azo (yellow to red), anthraquinone, or triphenylmethane (blue and green) characteristics [73, 74].

I.10. Reasons to choose the Orange II dye

We chose the Orange II dye because of its wide use in our daily lives, representing more than 50% of colored materials used in industries. It is therefore also the most polluting consequently. Also, Orange II is a human carcinogenic dye. It is resistant to bacterial attack in the aquatic environment and maintains its concentration percentage during light analysis. It is also soluble in water[75].

I.11. Orange II

Orange II (OII) or acid orange 7 (AO7) is an azo (anionic) acid dye, soluble in water that does not degrade [76]. The structure of this dye consists of a sulfonate (SO_3) and an azo group with aromatic cycles within the molecule. Used in the plastics industry, textile industry (leather, decoration), printing (ink, paper), and pharmaceutical industry, Orange II is a toxic dye under its two forms: azo and hydrazine [77].

Table I .6. Orange II identity sheet [76, 77].

Denomination	Acid Orange 7, Orange II
Chemical name	Orange Acide 7 ; 4-(2-hydroxy-1-naphthylazo) benzenesulfonic acid sodium salt ; Sodium4-[(2-hydroxy-1- naphtyl)azo benzenesulfonate].
Brute formula	$C_{16}H_{11}N_2NaO_4S$
Chemical structure	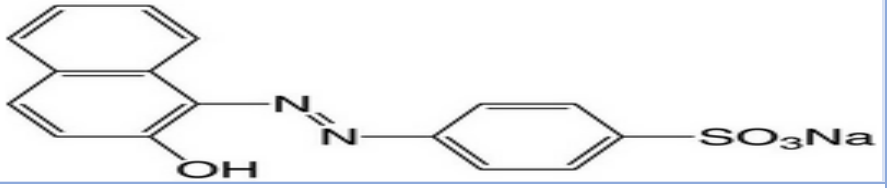
Molecular weight (g/mole)	350,32

λ (nm)	485
Family	Azo Anionic Acid Dye
Color	Brilliant orange
State	powdery
Water solubility (g/L)	116
Fusion point °C	164

I.12. Heterogeneous photocatalysis

I.12.1. Definition

Photocatalysis refers to the phenomenon wherein the acceleration of a chemical process is facilitated by the presence of a catalyst that is exposed to light. The utilization of active semiconductor oxide catalysts in heterogeneous photocatalysis has garnered significant interest over the last twenty years, mostly due to its high application efficiency. Given the current energy and environmental constraints, developing efficient photocatalytic materials is essential [78]. Pollutant degradation usually occurs by photocatalysis reactions and increases under UV irradiation when semiconductor photocatalysis are excited and e^- and h^+ pairs are generated. The catalysts activity for photocatalysis is contingent upon both the adsorption behavior of pollutants and the efficacy of separating electron-hole pairs [79].

I.12.2. The photocatalytic process

The photocatalysis process may be categorized into five distinct stages [80-83] :

- **Transfer of the pollutant from the liquid phase to the surface of the catalyst**

The phenomenon described is the process by which molecules of pollutants disperse towards the surface of a solid material when exposed to light. This mass transfer expresses the transport of a compound from a region where it is in high concentration to an area where it is in low concentration. This leads to a concentration gradient at the solid/fluid interface.

- **Adsorption of reactive molecules on the surface of the catalyst**

Adsorption results in intermolecular bond breaking and the formation of bonds with the surface. It can be classified into two families :

- Chemisorption is the result of a chemical phenomenon wherein the adsorbent and the adsorbed species create robust covalent bonds. In general, it is irreversible.

- Physisorption is the binding of molecules to a solid by Van der Walls forces. These electrostatic and low-energy bonds are easily reversible.

- **Reaction on the surface of the adsorbed phase**

The surface interaction of adsorbed reagents is the most essential step in the photocatalytic reaction. The production of oxidants is due to the photo-induced excitation of the catalyst under

irradiation (radicals, for example). These reactive species will reduce the adsorption of nearby pollutants.

- **Desorption of reaction products**

This desorption step is generated either by breaking bonds, releasing intermediate products or through competition and preferential affinity with other molecules.

- **Transfer of products from the surface of the photocatalyst to the solution**

The products diffuse towards the fluid. Note that this cycle can be perpetuated until complete mineralization or the cessation of the photochemical reaction when the by-products are no longer oxidizable.

I.12.3. Mechanism of heterogeneous photocatalysis

Heterogeneous photocatalysis relies on the absorption of photons with energy equal to or greater than the energy band gap, i.e. hv ≥ Eg, of the semiconductor under investigation. The excitation of the electrons from the valence band to the conduction band results in the formation of a hole in the valence band, facilitating the development of an electron-hole pair (e^-/h^+). An oxidation site, often referred to as a hole, and a reduction site, symbolized as é, are two distinct locations within a chemical system where oxidation and reduction reactions occur, respectively. The chemical entities accountable for the process of photocatalysis encompass electron-hole pairs and active oxygen species. Oxygenated radicals formed, in particular $OH^{\cdot}$, $O_2^{\cdot}$ from electrons and holes generated by irradiation will be at the origin of oxidation-reduction reactions, which are of particular interest for the degradation of organic pollutants [84, 85].

In order to produce hydroxyl radicals $OH^{\cdot}$, the holes of the valence band interact with H_2O, and superoxide radicals $O_2^{\cdot -}$ are formed. The white hue of the solution is intensified as a result of the interaction between electrons in the conduction band and oxygen molecules. This enhancement is particularly pronounced when the active layers are formed using low gap materials, such as CuO with an energy gap of only 1.2 eV.

$$CuO + h\upsilon \longrightarrow e_{CB}^- + h_{VB}^+ \quad \text{(I.3)}$$

$$O_2 + e_{CB}^- \longrightarrow O_2^{\cdot -} \quad \text{(I.4)}$$

$$H_2O + h_{VB}^+ \longrightarrow OH^- + H^+ \quad \text{(I.5)}$$

$$OH^- + h_{VB}^+ \longrightarrow OH^{\cdot} \quad \text{(I.6)}$$

$$\text{pollutant} + h_{VB}^+ \longrightarrow P^+ \quad \text{(I.7)}$$

$$\text{pollutant}^{+} + OH^{\cdot} \longrightarrow CO_2 + H_2O \qquad \text{(I.8)}$$

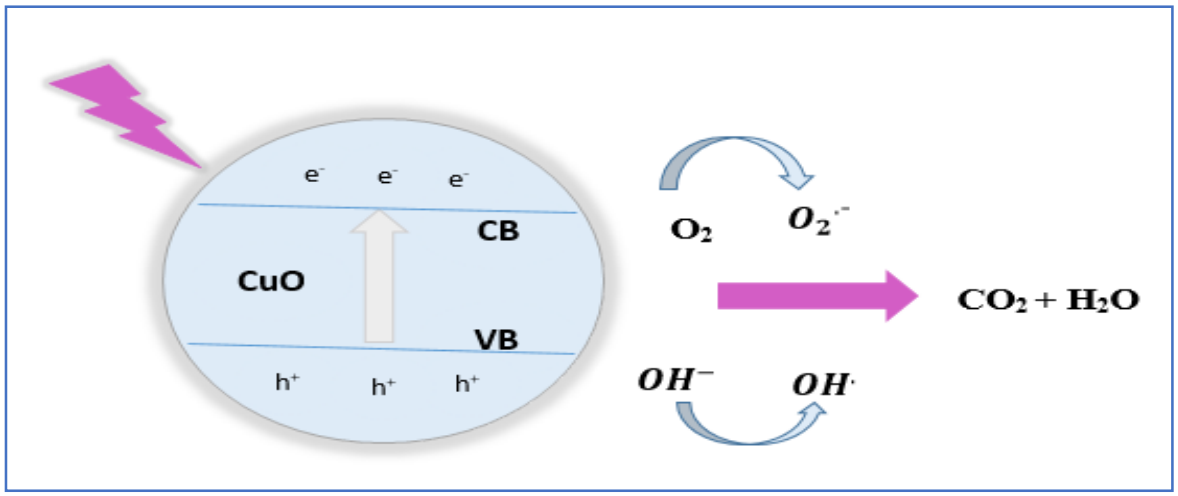

Figure I.10. Principle of CuO photocatalysis.

I.12.4. Factors influencing heterogeneous photocatalysis

Like any reaction, photocatalytic reactions will be subject to a set of physical parameters such as the mass of the photocatalyst, the absorption spectrum of the incident light, the number of incident photons, the concentration of reactants or even the temperature and the pH [86]. The main factors influencing heterogeneous photocatalysis are [87-89] :

- ✓ **The catalyst concentration**

Numerous researches have been conducted to examine the impact of varying concentrations of photocatalysts on the process of photocatalytic reactions. They have demonstrated that the concentration of electron-hole pairs has a proportional relationship with the catalyst, which corresponds to the rate of onset of the photocatalysis reaction. At high catalyst concentrations, the solution becomes opaque, opacifying effects indeed appear preventing light from penetrating through to the center of the reactor and thus affecting the yield of the photocatalysis reaction.

- ✓ **The initial concentration of the pollutant**

Generally, degradation efficiency in a photocatalysis process decreases with increasing pollutant concentration. At high concentration of pollutants, the catalyst surface is impeded in its ability to be penetrated by photons. The Langmuir-Hinshelwood model is the most commonly used to study the phenomenon of adsorption at low concentrations.

✓ **The luminous flux**

Several authors have demonstrated that the concentration of electron-hole pairs in the semiconductor is proportional to the flux of photons. This verifies the photo-induced origin of the activation of the catalytic process. When the luminous flux value is too high, the recombination rate of electron-hole pairs increases.

✓ **Specific surface and particle size**

Many photocatalysis processes show a linear relationship between the rate of degradation and the amount of substrate adsorbed on the surface of the photocatalyst. Mass unit of photocatalysis solids increases without affecting the surface characteristics due to the higher number of adsorbed molecules surrounding the e^-/h^+ regions. Therefore, a larger specific surface area allows us to consider an increased photocatalysis activity. The particle size variation also influences the band gap energy (Eg) and therefore the number of adsorbed photons. It has been shown that the smaller the particle size, the smaller the probability of recombination of electron-hole pairs and the easier the pollutants to react with the hydroxyl radicals formed on the surface [79,89].

✓ **pH**

The pH is one of a reaction medium physical and chemical parameters. The influence of pH on the rate of decomposition in the photocatalysis reaction is challenging to elucidate owing to its multifaceted involvement throughout the course of the reaction. Conversely, the surface charge can be influenced by the pH of the aqueous solution. The latter may exhibit either a positive or a negative charge, depending on the pH of the solutio .Indeed, the surface of the photocatalyst is positively charged at $pH < pH_{PZC}$, negatively charged at $pH > pH_{PZC}$ and neutral when the pH takes the value of the pH corresponding to the potential of zero charge (pH_{PZC}). As the pH increases, there is a decrease in the quantity of positively charged sites and an increase in the quantity of negatively charged sites. This fact favors the adsorption of orange II dye to the electrostatic attraction between hydroxide ions (OH^-) and cationic coloring ions [90-93].

✓ **Temperature**

In general, the degradation rate is not affected by temperature since the semiconductor creates pairs (e-/h+) via the absorption of light radiation. Nevertheless, at low temperatures (-40°C down to 0°C), the desorption of the product becomes a limiting phase. After a temperature of about 80°C, the adsorption of the pollutant becomes the limiting phase, slowing down the degradation rate [94]. The effect of temperature on the rate of a photocatalysis reaction can be explained within the framework of the Langmuir−Hinshelwood model. The temperature

increase promotes the pollutant's desorption and the intermediates produced, thereby increasing the reactivity of the surface [95].

I.12.5. Advantages and disadvantages of photocatalysis [83, 96].

I.12.5.1. Advantages of photocatalysis

The advantages of photocatalysis can be listed and are :

- ✓ Produce at the conditions of room temperature and atmospheric pressure.
- ✓ Simple and economical installation.
- ✓ It is a non-destructive and non-selective technique.
- ✓ It has been found to be efficacious in mitigating the impact of contaminants present in low quantities.
- ✓ Energy consumption is low.
- ✓ No chemical additives.
- ✓ The catalyst is non-toxic, active in different physical forms, and inexpensive.

I.12.5.2. Disadvantages of photocatalysis

Likewise, the disadvantages of photocatalysis can be listed and are :

- ✓ Limitation by diffusion on the surface of the semiconductor.
- ✓ The recombination of photo charges generated between the times of their formation can also decrease the efficiency of the process.
- ✓ The photocatalysis is only activated by UV irradiation, which limits the effectiveness of this technology in the visible and interior applications.
- ✓ Efficiency and limited lamp life.

I.12.6. Degradation rate

The degradation absorption rate can be calculated utilizing the subsequent equation [44] :

$$\eta(\%) = \frac{C_0 - C_t}{C_0} * 100 \qquad \text{(I.9)}$$

with C_0 the initial absorbed concentration of dye and C_t its absorbed concentration at time t. Photocatalysis degradation based on copper oxide under UV irradiation is a heterogeneous photocatalysis and generally follows the first-order kinetic expression of Langmuir Hinshelwood [80, 97, 98]. In this model, the surface coverage and the initial concentration of the pollutant are related to the absorption constant, as given by the following equation :

$$\theta = \frac{k_{ads}.C_0}{1 + k_{ads}.C_0} \qquad \text{(I.10)}$$

with θ the surface coverage, K_{ads} the pollutant adsorption constant in units of L/mol and C_0 the equilibrium pollutant concentration in units of mol/L.

In the case of the Langmuir-Hinshelwood model, the limiting step is the degradation reaction of the pollutant on the active site located at the surface of the photocatalyst. The speed of this reaction is given by the following equation :

$$r = -\frac{dC}{dt} = k_c.\theta = k_c.\left(\frac{k_{ads}.C_0}{1+ k_{ads}.C_0}\right) \quad \text{(I.11)}$$

with *r* the reaction rate in units of mol/L/min, and k_c the kinetic constant of the reaction in units of mol/L/min. Therefore, when the concentration of pollutants is $C_0 > 10^{-3}$, mol/L, the term $k_{ads}.C_0$ is very large compared to unity and the reaction is of order 0. However, in a dilute medium, if the concentration of pollutants is $C_0 < 10^{-3}$,mol/L, the term $k_{ads}.C_0$ becomes negligible compared to unity and the reaction is first ordered We can thus solve the equation as follows:

$$-\frac{dC}{dt} = k_c k_{ads} C_0 = kC_0 \quad \text{(I.12)}$$

$$-\frac{dC}{C_0} = kdt \quad \text{(I.13)}$$

$$[-\ln C]_{C_0}^{C} = kt \quad \text{(I.14)}$$

$$\ln\left(\frac{C_0}{C}\right) = kt \quad \text{(I.15)}$$

The variation of function $\ln\left(\frac{C_0}{C}\right)$ as a function of time is thus linear and the slope provides the rate constant k.

Chapter II :

Experimental deposition and characterization techniques

II.1 Introduction

After detailing the properties of CuO and their applications, we will look at the deposition techniques and the characterizations of these materials.

As it is known, the techniques for depositing thin layers are very numerous, which is why we will limit ourselves to only describing the principle of the spray pyrolysis and sol-gel spin-coating methods as well as the type of devices used for the characterization of the thin layers used in this study in the reason of clarifying the way from where we could have the results presented, a task discussed in the next chapter.

II.2.Thin film deposition methods

In order to generate a thin layer film on a solid substrate, the coating material particles must pass through a conducting medium in intimate contact with the substrate. Particles can be atoms, molecules, ions, or molecular fragments. The transport medium may be solid, liquid or gaseous, and even vacuum [99]. There are two main categories of methods for producing thin layers, either physical methods or chemical methods. The main methods used to deposit thin layers utilize a combination of chemical and physical deposition techniques. The different production methods are presented in the diagram of Figure II.1.

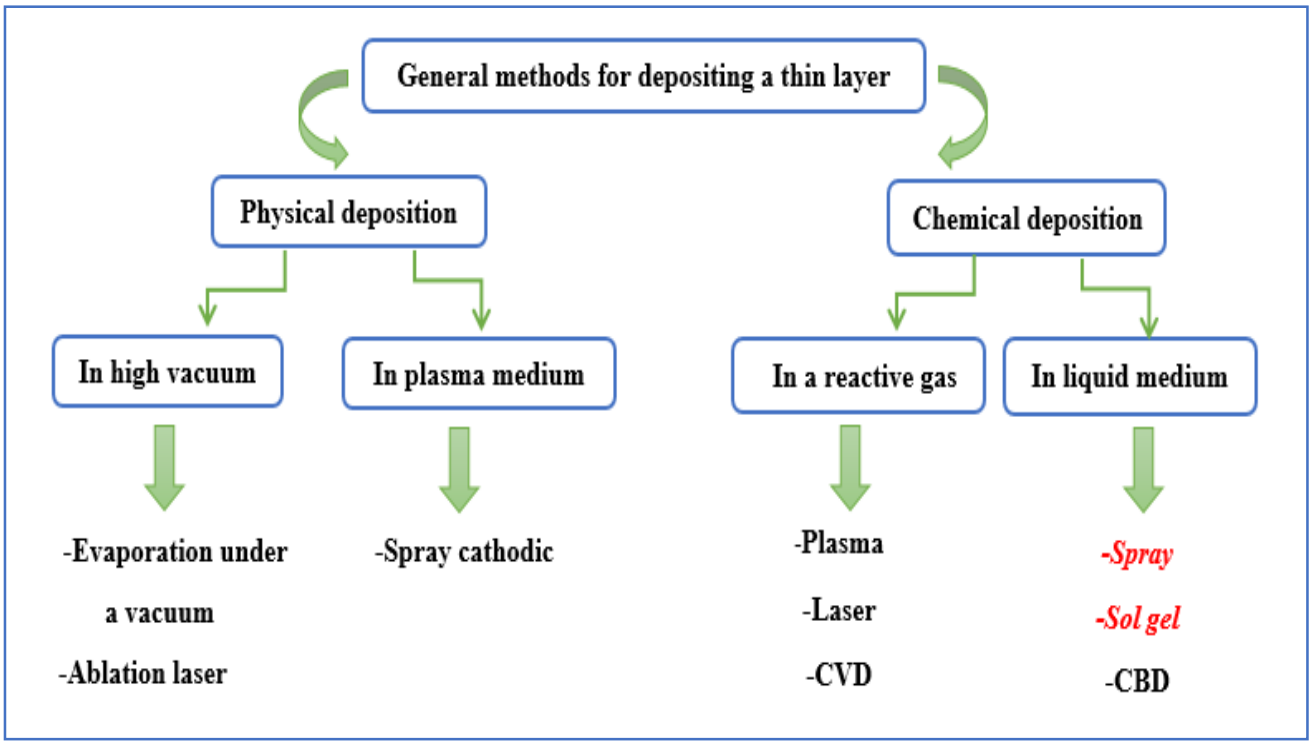

Figure II.1. Thin film deposition techniques.

In our research, we have used the method of spray pyrolysis and sol-gel for the synthesis of thin layers of CuO. The latter method has also several advantages over the other.

II.2.1. Spray pyrolysis

II.2.1.1. Definition

The process commonly referred to as spray pyrolysis is widely utilized. The process in question consists of two main actions : spray and pyrolysis.

- ✓ **Spray :** With this phenomenon, a liquid jet consisting of small droplets is discharged from a spray apparatus.
- ✓ **Pyrolysis :** With the phenomenon, a liquid undergoes a transformation of decomposition of its chemical components under heat without interaction with oxygen or other oxidants into smaller volatile molecules [100].

II.2.1.2. Spray

Two methods are commonly used to spray the solution.

- ✓ **Pneumatic spraying :** Fog production is done by compressed gases which absorb the liquid and causes it to explode.
- ✓ **Ultrasonic spraying:** Aerosols are generated by high-frequency vibrations within the solution localized towards the free surface of the liquid. The formation of a geyser occurs when the ultrasound beam is directed towards the interface between the gas and the liquid, with the height of the geyser being controlled with the strength of the sound producing the vibrations. The geyser in question generates aerosols by the process of inducing vibrations at the liquid surface and causing cavitation at the gas-liquid contact. This process is known as the pyro sol procedure [100].

II.2.1.3. Pyrolysis

When the droplet touches the substrate surface, several processes occur with the evaporation of the residual solvent, the droplet diffusion and the salt decomposition. There are several models available. Viguie and Spitz put out a series of mechanisms that manifests themselves as the substrate temperature increases [101].

Process I : The aerosol droplets are deposited onto the heated substrate in a direct manner. The solvent undergoes evaporation, resulting in the decomposition of the initial substance and the subsequent formation of the product layer. In order to generate thicker films, the procedure necessitates the use of successive deposition techniques to achieve high film density, with

thicknesses often less than 1 µm. Nevertheless, this procedure requires a significant amount of time. Furthermore, when the thickness of the layer rises, it is seen that the layer tends to exhibit porosity and the formation of fractures. The aforementioned procedure aligns with the fundamental concept of spray pyrolysis.

Process II : Prior to coming into contact with the heated surface of the substrate, the solvent undergoes evaporation. In order to generate the required material layer, the precursor undergoes surface reactions, either degrading or engaging into chemical transformations. It does not transit through the gas phase.

Process III : The solvent undergoes a process of evaporation when it approaches the surface of the substrate. The primary material experiences a phase change into a gaseous phase when it is in close proximity to the heated surface. The precursor molecules experience diffusion across the surface, subsequently undergoing a reaction that results in the production of products through breakdown and subsequent chemical reactions. The process employed by the director frequently results in films that exhibit a notable level of intricacy and remarkable cohesiveness.

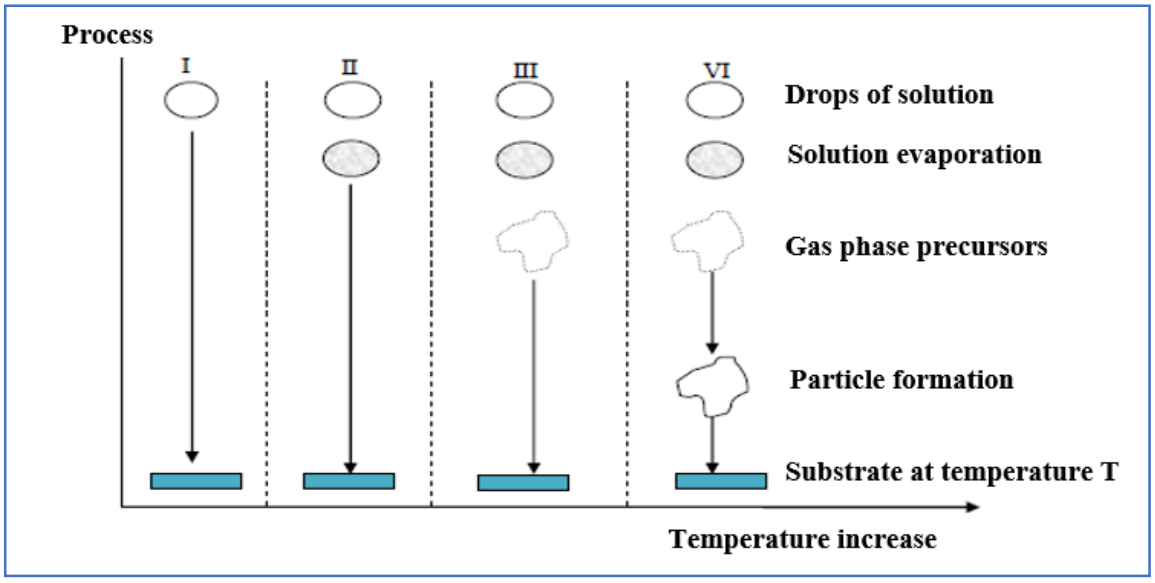

Figure II.2. Presentation of the different processes that can occur in Spray depending on the deposition temperature [103].

II.2.1.4. Principle of spray pyrolysis

In order to disperse the constituent components of the substance into small droplets, a conventional pneumatic system or an atomizer equipped with an ultrasonic generator is employed. With the aid of these systems, it is possible to create a jet of small droplets, each measuring only a few tens of micrometers in diameter. The jet hits the heated substrates surface at a high enough temperature to allow the breakdown of the products dissolved in the solution and to start the processes likely to yield the desired material. At elevated temperatures, volatile components resulting from the reactions will be promptly removed, leaving just the chemicals to be deposited onto the substrate. The substrate holder can be static or animated by a movement to improve the uniformity of the deposited layers [103].

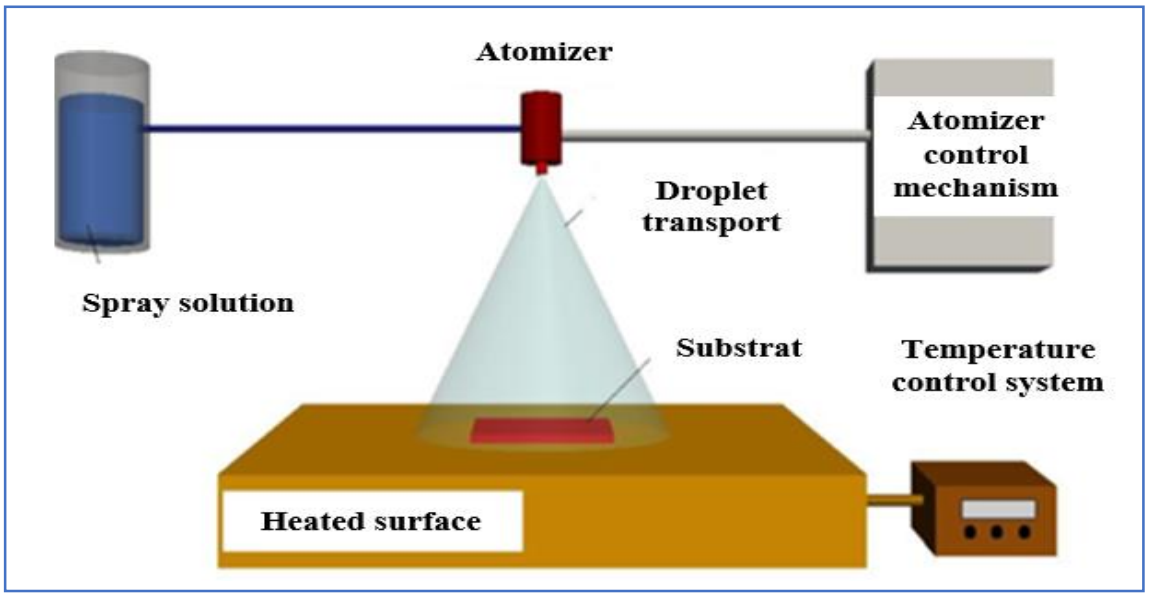

Figure II.3. Schematic representation of the spray pyrolysis deposition process [104].

II.2.1.5. Advantages

Apart from its simplicity, the spray pyrolysis technique has many advantages.

- ✓ Spray pyrolysis is an easy and inexpensive method for preparing semiconductor thin films.
- ✓ The method provides a convenient approach for doping films with various elements in desired proportions by introducing them into the spray solution in a suitable manner.

- ✓ It is able to create uniformly thick, highly-quality adherent films. Spray pyrolysis has the advantage of not requiring high-quality targets or a vacuum at any point, which is crucial if the technique is to be applied in industrial settings.
- ✓ The manipulation of spray parameters allows for the effective control of deposition rate and film thickness throughout a broad spectrum [105].

II.2.2. Sol gel method

II.2.2.1.Definition

The sol-gel process, although known for more than 150 years, has only experienced significant growth in the last two decades. Before discussing the chemistry of the sol-gel process, it is necessary to recall a few definitions.

- ➢ **Sol :** Stable dispersion of colloidal particles in fixed-size liquids particles. The latters must be denser than the liquid.and thus small enough so that the forces responsible for dispersal are not overcome by gravity.
- ➢ **Gel** : Stable expansion of a connected three-dimensional solid network dispersed throughout a liquid medium. The gel is referred to as colloidal if the solid network contains colloidal particles. The sub-colloidal chemical constituents of the solid network units are macromolecules [106].

During a sol-gel synthesis, the molecular precursors contained in the starting solution, the “sol”, polymerize according to various mechanisms and form a network of oxides, the “gel”. A drying step followed by heat treatments eliminates the organic compounds to form the inorganic oxide material. The sol-gel technique is particularly well suited to the fabrication of uniform substances, in the shape of thin layers, with high optical performance [22].

The picture provides a schematic representation of the several stages involved in the synthesis of materials using the sol-gel technique.

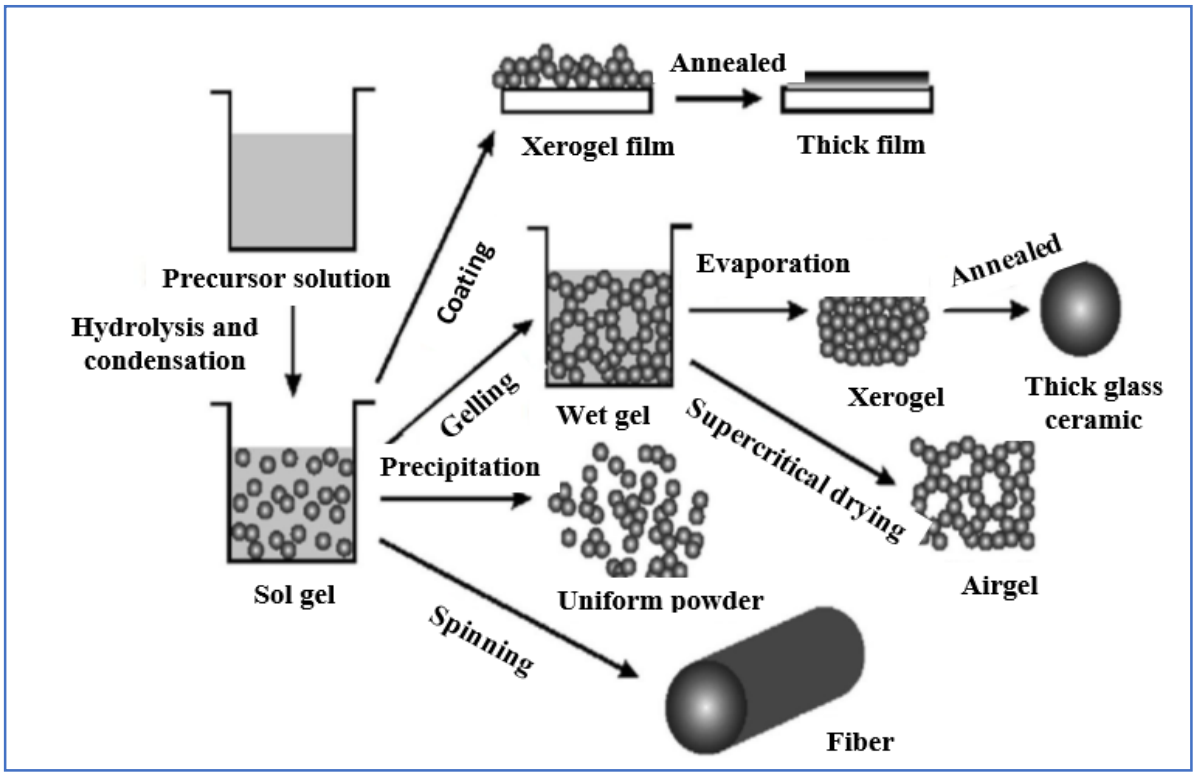

Figure II.4. Stages and potential of sol-gel chemistry [107].

II.2.2.2. Pathways of the sol-gel process

II.2.2.2.1. Inorganic (colloidal or aqueous)

This process is inexpensive, but difficult to control, which is why it is still of very little use. The precursors used are metal salts such as acetates, chlorides and nitrates in aqueous solutions and the hydrolysis is then carried out by simple pH variation which can be ensured by the addition of a complexing agent. Condensation, for its part, leading to precipitation consists of the production of polymeric structures by O-X-O bonds with the elimination of water molecules. Note that the inorganic route (sometimes called the precipitation method) is the basis of many industrial powder manufacturing processes. This is the preferred method for the synthesis of ceramic materials. It involves two steps :

a) Variation in the pH of the solution : the decrease in pH leads to the formation of protonated species (powders) and the increase in pH leads to denser species (films).

b) Polycondensation with the elimination of water molecules [108].

II.2.2.2.2. Organometallic (polymeric)

The second process uses metal precursors of the alkoxide type of formula $M(OR)_n$, where M is a metal, for example Cu, Al, Ag or a metalloid (for example Si) and R an organic alkyl group C_nH_{2n+1}. This particular pathway enables the acquisition of materials with a significant level of purity and will be consistently referenced throughout the remainder of this study. In both instances, the reaction is triggered by the process of hydrolysis of the precursors, facilitating the creation of M-OH groups. Then comes the condensation of the precursors, initially hydrolyzed, to finally lead to the formation of a branched network of oxide nature (M-O-M) [109]. We recall here that for the synthesis of our samples, we have used in our work the (organometallic) method.

II.2.2.3. Reaction mechanism

Metal alkoxides are initially dispersed in an organic solvent, often alcohol. The sol-gel transition, also known as solidification, is initiated by an inorganic polymerization mechanism that involves two distinct reactions. The processes of hydrolysis and condensation of alkoxides are of significant academic interest [110].

II.2.2.3.1.Hydrolysis

Hydrolysis is a chemical reaction in which the action breaks a covalent bond of a water molecule. In the case of the hydrolysis of an organometallic precursor, alcohol groups R-OH appear [111]. The aforementioned reaction is iteratively performed on every organic group that is connected to the metal atom and can be expressed in the following manner:

$$M(OR)_4 + H_2O \longrightarrow HO\text{-}M(OR)_3 + ROH \qquad (II.1)$$

II.2.2.3.2. Condensation reaction

The hydrolysis process results in the formation of groups (HO-M(OR)-1), which can undergo two reactions. Firstly, they can react with each other resulting in the production of a water molecule (oxolation). Alternatively, they can react with a molecule M of the alkoxy (OR), leading to the formation of an alcohol molecule (alkoxylation). This process also facilitates the creation of one or more metal-oxygen-metal (MOM) bridges, where the oxygen atom acts as a bridge connecting two metal atoms M. The result is the creation of a gel whose viscosity is worse however. Solvents and unreacted precursors are present in this gel. This procedure is governed by the following reactions at room temperature.

This mechanism of a metal alkoxide (OR) [40,112] is a condensation which if it produces a water molecule is called “oxolation” :

$$(OR)_3M\text{-}OH + HO\text{-}M(OR)_3 \longrightarrow (OR)_3M\text{-}O\text{-}M(OR)_3 + H_2O \quad (II.2)$$

If it produces an alcohol molecule, it is called “alcoxolation” :

$$(OR)_3M\text{-}OR + HO\text{-}M(OR)_3 \longrightarrow (OR)_3M\text{-}O\text{-}M(OR)_3 + HOR \quad (II.3)$$

II.2.2.4. Spin coating

The "spin-coating" technique consists in producing, by centrifugation, a thin layer from an excess solution deposited on a substrate. Preparation of a layer, therefore, goes through four essential phases:

- ✓ The deposit of the excess solution (a few drops) on the surface of the substrate.
- ✓ Acceleration : it is the beginning of the rotation, its forces cause the solution to flow uniformly over the sample and move the liquid away from the center towards the outside of the substrate because the centrifugal force makes it possible to separate in a liquid solution the solid particles of different densities.
- ✓ The much accelerated constant rotation : allows the ejection, in the form of droplets, of the excess of the sol, as well as the reduction of the thickness of the layer in a uniform way.
- ✓ Evaporation : during this phase, the substrate always rotates at a constant speed and the most volatile solvents are evaporating first, which emphasizes how thin the deposited film is [113,114].

These four stages of deposition of a thin layer are schematized in this figure :

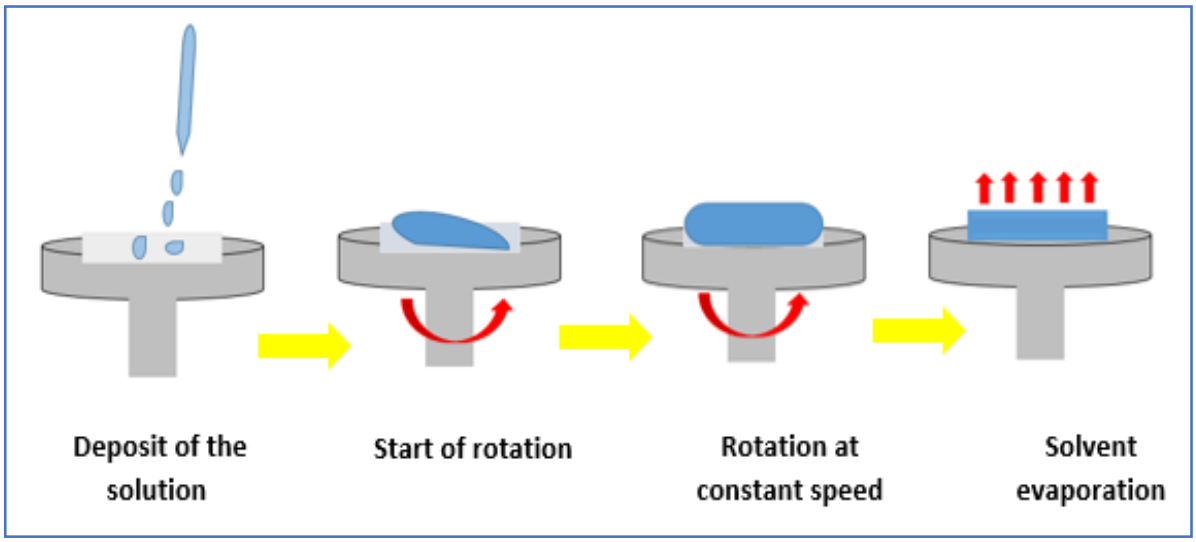

Figure II.5. Deposition of thin layers by the process of spin coating.

This technique has the advantage of obtaining very homogeneous layers with a constant thickness at any point of the layer. Its implementation is easy [113].

II.2.2.5. Dip-coating

The support is immersed in the colloidal solution containing the "sol" then removed respecting very controlled and stable conditions in order to obtain a film of regular thickness after evaporation of the solvent, excess liquid drainage and polymerization of the deposit. The film is known as a xerogel film as gel still contains solvent [115,116].

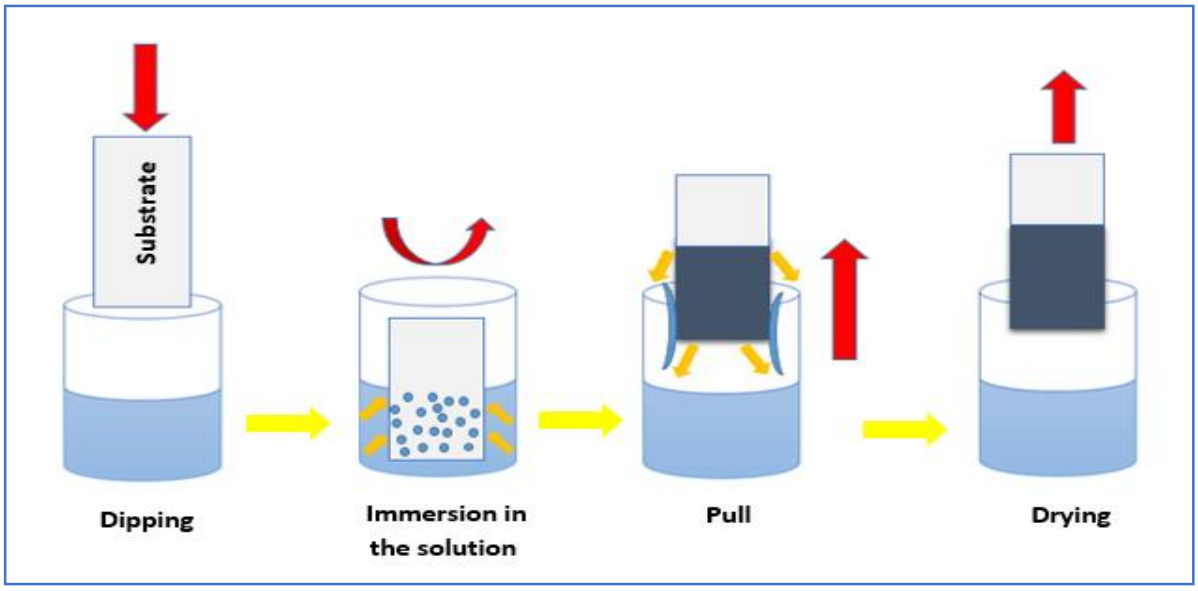

Figure II.6. Schematic representation of the principle of deposition by dip coating.

II.2.2.6. Advantages

Apart from its simplicity, the sol-gel technique has several advantages [117].

- Ease with which homogenous stoichiometric coatings may be manufactured.
- Control of the chemical composition and microstructure of the coating.
- High level of purity.
- Fairly good adhesion.
- Coating of complex substrates.
- Ability to manipulate various synthesis settings.

II.2.2.7. Disadvantages

- Long process times.
- High cost of raw materials.
- Lifetime of certain solutions produced by sol-gel process is sometimes very short.
- Procedure is difficult to reproduce.

II.3. Experimental part

II.3.1. Preparation devices

II.3.1.1. Cleaning substrates

Before depositing thin layers, there is a very important step, which is the substrate cleaning. This process is used to remove all traces of grease and impurity. We used glass substrates to achieve a deposit of thin layers based on copper oxide. The substrate surface cleaning process was carried out at the Structures, Properties and Inter-Atomic Interaction Laboratory (LASPI²A) of the Abbes Laghrour University of Khenchela using an ultrasonic bath of the "Fisherbrand" type, see Figure II.7. The protocol was the following :

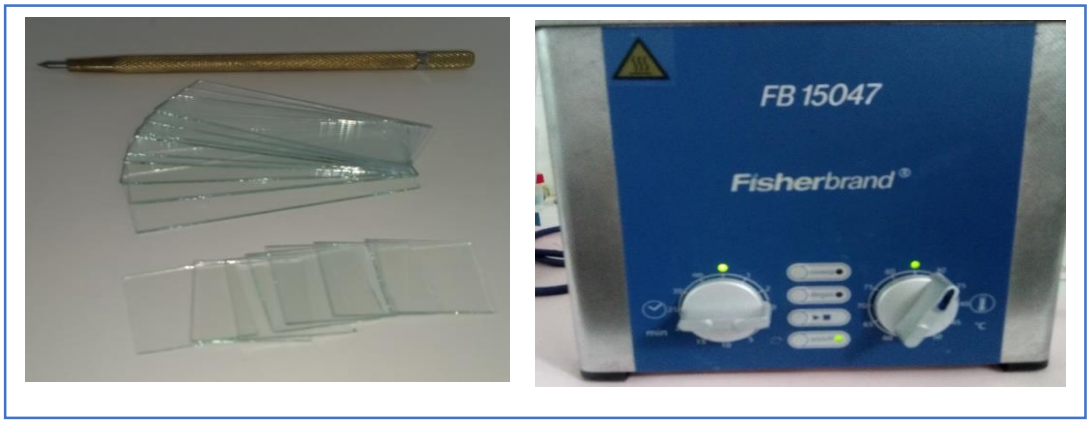

Figure II.7. Cleaning of substrate by ultrasonic bath.

- ✓ Cutting of the substrates.
- ✓ Ultrasonic bathing with acetone for 3 mins.
- ✓ Rinsing with distilled water.
- ✓ Ultrasonic bathing with methanol for 3 mins.
- ✓ Rinsing with distilled water.
- ✓ Drying.

II.3.1.2. Electronic Balance

The measurement of the masses of the precursor was carried out with a sensitive balance of the Ohaus type with an accuracy is 0.0001 g as shown in Figure II.8 used in the Active Components and Materials laboratory (LCAM) of Oum El Bouaghi University.

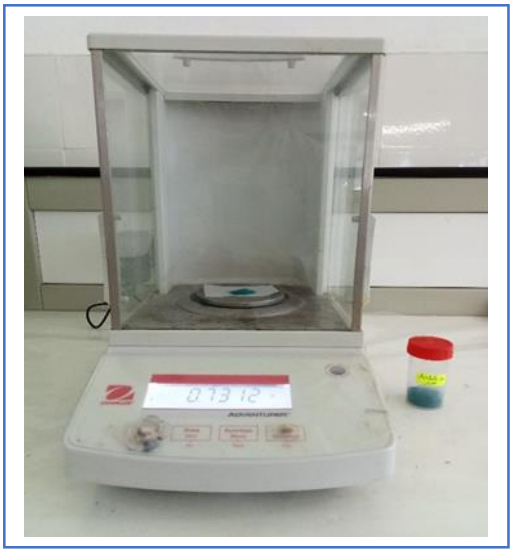

Figure II.8. Balance electronic.

I.3.1.3. Magnetic stirrer

The magnetic stirrer is a device used to agitate solid elements in a suitable solvent. We used the magnetic stirrer STUART US152 type as shown in Figure II.9 in use in the Active Components and Materials Laboratory (LCAM) of Oum El Bouaghi University.

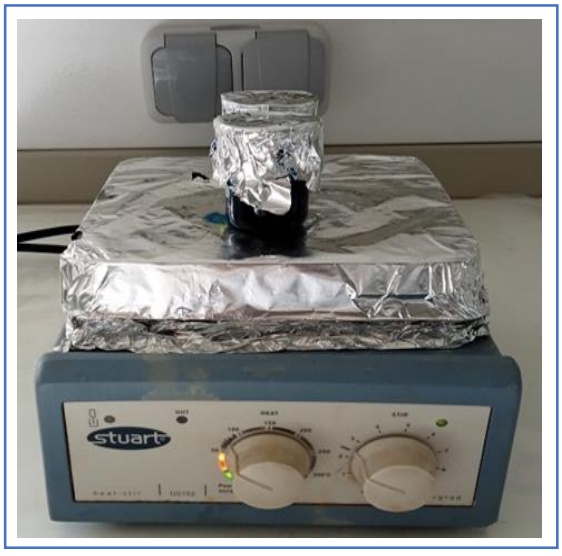

Figure II.9. Magnetic stirrer.

II.3.1.4. Drying oven

For drying, a Memmert type dryer was used, as shown in Figure II.10 present in the Active Components and Materials Laboratory (LCAM) of Oum El Bouaghi University.

Figure II.10. Drying oven.

II.3.1.4. Oven

For the sample annealing, we used a high-temperature furnace type WISD-FHX-03 shown in Figure II.11 and.used in the Active Components and Materials Laboratory (LCAM) of Oum El Bouaghi University.

Figure II. 11. Oven.

II.3.2. Preparation of thin layers

II.3.2.1. Elaboration by pyrolysis spray method

The copper oxide thin films were synthesized using the pneumatic spray pyrolysis technique. The flow rate of the precursor solution was maintained at 20 ml/h while the spray times varied between 5 mins, 10 mins, 15 mins, 20 mins, 25 mins and 30 mins. The precursor used was copper nitrate $Cu(NO_3)_2$ with a molarity of 0.1 M. The films were deposited onto a glass substrate that was heated up to a temperature of 400°C. The distance between the spray nozzle and the substrate surface was set at 25 cm. The angle between the beaker and the substrate was 90 degrees.

Table II.1. Properties of precursor used in the spray pyrolysis method.

Name	Copper nitrate
Chemical formula	$Cu(NO_3)_2$
Volumic mass	3.05 g/cm^3
Molar mass	187.56 g/mol

Thin films deposition by pneumatic spray pyrolysis (SP) was carried out at the Structures, Properties, and Inter-Atomic Interaction (LASPI²A) laboratory of the Abbes Laghrour Khenchela University.The experimental device used is shown in the following figure .

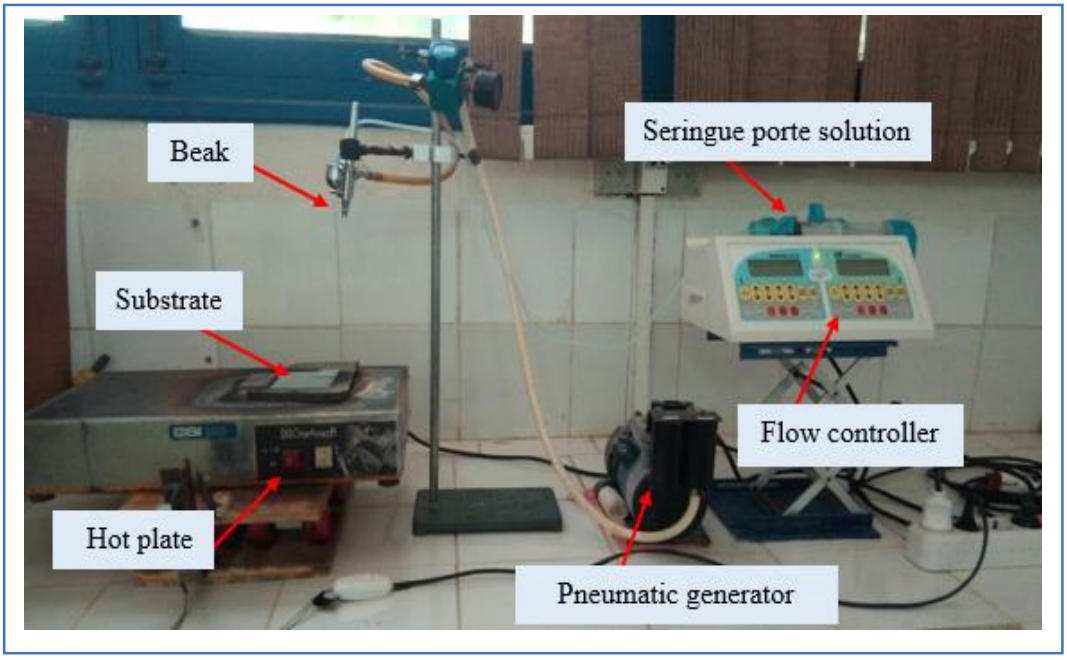

Figure II.12. Device for depositing thin layers by pneumatic spray pyrolysis.

II.3.2.2. Elaboration by sol gel spin coating method

In this study, a sol-gel spin coating technique was employed to deposit thin films of CuO onto a glass substrate. To create a 0.2 M solution, the copper acetate precursor was dissolved in pure ethanol (C_2H_6O) with a purity of 96%. In order to investigate the impact of doping rates using Ag and Al on the thin layers of CuO, we conducted an experiment including the preparation of four distinct percentage solutions : 5%, 15%, 25% and 50%. These solutions were created using aluminum acetylacetonate and silver nitrate. Additionally, a certain volume of monoethanolamine (MEA) was added to achieve a molar ratio of 3 (n (MEA) / n (sol)). Subsequently, the solution is subjected to thermal treatment with magnetic stirring at a temperature of 70°C for a duration of 2 hours.

Next, the substrate should be placed in the oven and subjected to a temperature of 50°C for a duration of 10 minutes. The precursor solutions were applied onto substrates using a syringe through the spin-coating technique. The substrates were securely placed on a rotating speed support and spun at 3000 rpm for a duration of 30 seconds. Following each deposition, the samples were subjected to drying at a temperature of 250°C for a period of 10 minutes in an oven. This process was repeated four times. Subsequently, the specimen underwent a heat treatment process within an oven set at a temperature of 500°C for a duration of 2 hours.

Table II.2. Properties of the precursor used in the sol gel spin coating method.

Name	Copper acetate	Aluminum acetylacetonate	Silver nitrate	(MEA)	Absolute Ethanol
Chemical formula	$Cu(CH_3COO)_2.2H_2O$	$Al(C_5H_7O_2)_3$	$AgNO_3$	C_2H_7NO	C_2H_6O
Volumic mass	1.88 g/cm^3	1.42 g/cm^3	4.35 g/cm^3	1.02 g/cm^3	0.7 g/cm^3
Molar mass	181.63g/mol	324.31 g/mol	169.87 g/mol	61.08 g/mol	46.06 g/mol

The process of depositing thin layers by sol-gel spin coating was conducted at the Laboratory of Active Components and Materials, located at the University of Oum El Bouaghi. The experimental procedure is illustrated in the accompanying diagram.

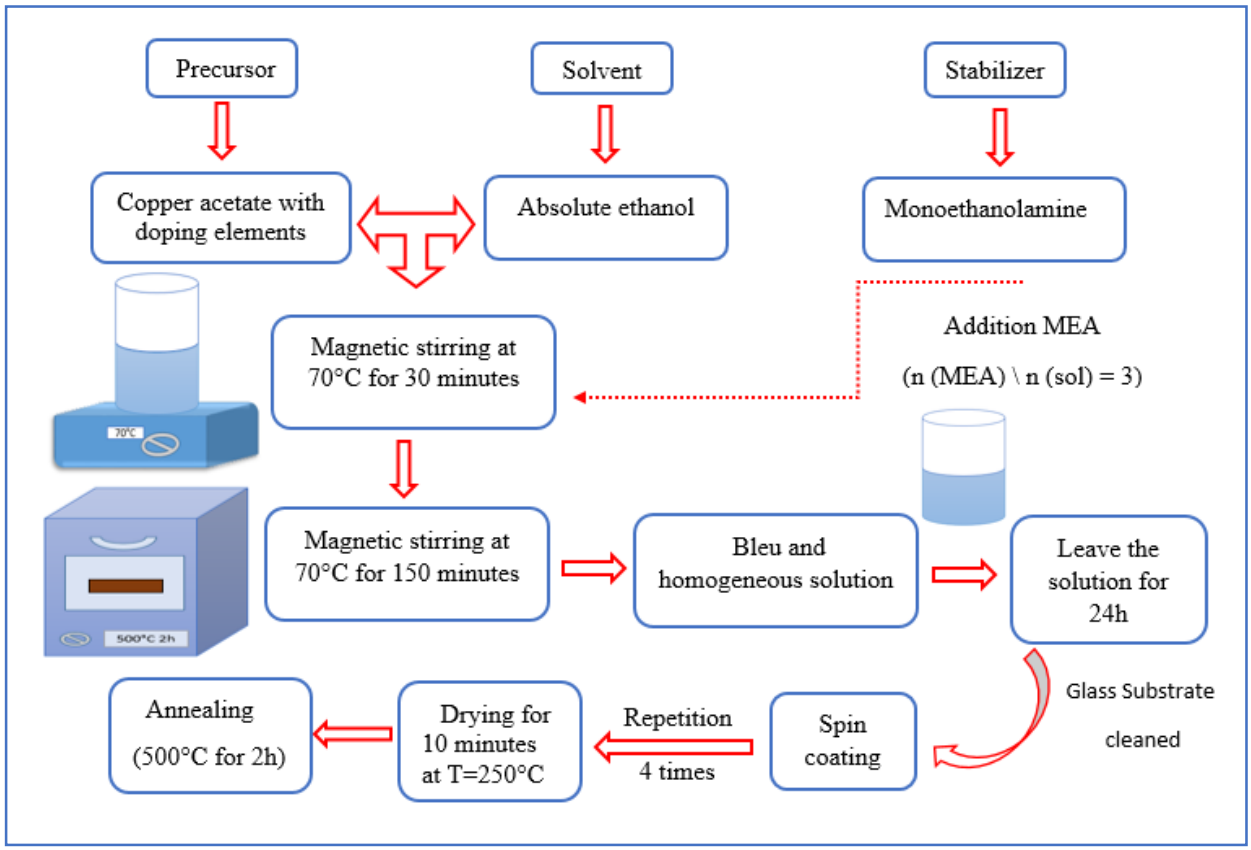

Figure II.13. The steps of preparing the solution by the sol gel method.

II.4.Characterization methods

II.4.1. X-Ray diffraction

It is the most important technique for the determination of structural properties. Used to identify the type of network and the inter-particular distance of the planes, as well as the measurements of stress, texture and crystallite size.

II.4.1.1.X-Ray production

X-Rays are produced by the interaction of electrons with a metallic target. These electrons are emitted by a tungsten filament heated by the Joule effect. They are accelerated by an electric field created by a potential difference V between a cathode constituted by the filament and an anode constituted by the target. An order of magnitude of the low energy efficiency η=((photon energy)/ (electron energy) in % is given by the following formula :

$$\eta = 1{,}1\text{x}10^{-9}\ \text{Z.V} \qquad \text{(II.4)}$$

with Z the atomic number of the target and V the potential difference between the anode and the cathode (in Volts).

Most of the energy is therefore lost in the form of heat, which must be eliminated by cooling the anode, generally by circulating water [118].

II.4.1.2. Principle of X-Ray diffraction

X-ray diffraction is employed for characterizing crystalline materials and relies on the interaction between the crystal lattice and X-rays [119]. X-rays refer to a kind of electromagnetic radiation characterized by wavelengths ranging from 0.01 to 10 nm. But the domain used for material characterization is 0.1-10 nm. The principle of this method consists in placing the sample in a monochromatic X-ray beam of wavelength λ which becomes a source of diffracting radiation. These diffracted rays are then recovered by a detector in the form of intensities. This method is used to identify known structures or sometimes to detect and characterize new structures for catalytic purposes [120]. The diffraction pattern recorded is determined by the Bragg condition :

$$2.d.sin\theta = n.\lambda \qquad \text{(II.5)}$$

With d representing the inter-reticular distance of the crystal lattice, λ is the wavelength of the incident beam,n is an integer that represents the order of the reflection and θ represents the angle of incidence of the X-rays with respect to the surface of the sample.

In the same compound, several plane families can be present. It is for this reason that a fairly wide angular sweep is performed. The variation of the angle makes it possible to determine the

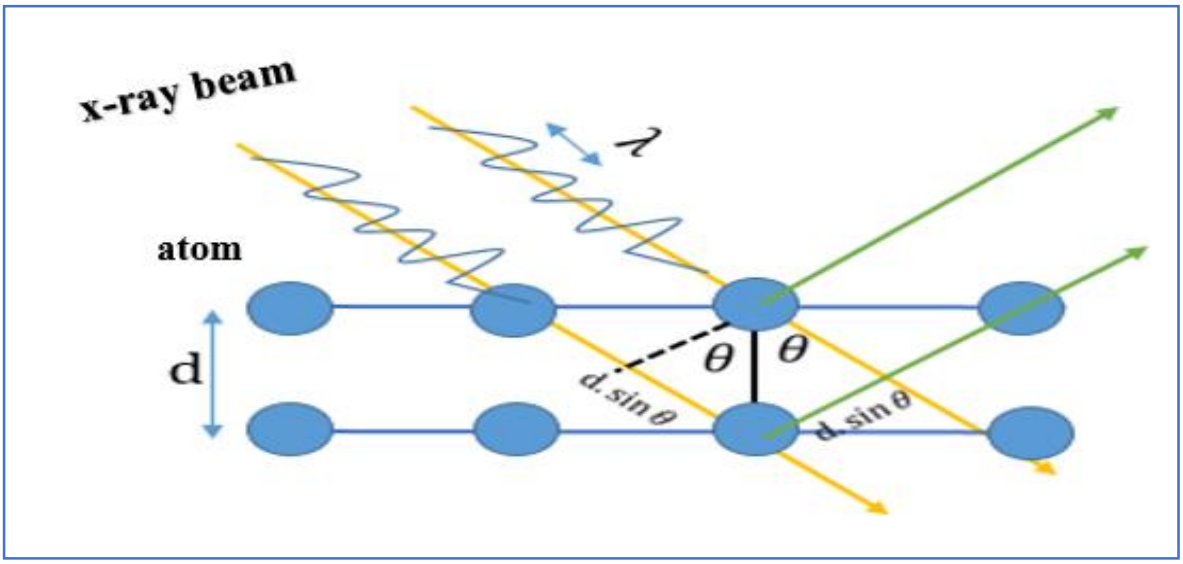

Figure II.14. Schematic representation of the principle of X-ray diffraction.

the angles for which n is an integer in the Bragg equation. The angle being thus known and the wavelength being predetermined and constant, it is then possible to determine the reticular distance *d*. The determination of the relative intensity of the diffraction peaks involves the division of the absolute intensity of a given peak by the absolute intensity of the most prominent peak, followed by the conversion of this ratio into a percentage value. Absolute intensity values are generally not used because they vary with instrumental and experimental settings. The number of detected atoms that correspond to this peak plane and the density of the atoms electron cloud are directly related to the area beneath the peaks. The diffraction pattern is specific and unique to a single phase, even if phases have the same chemical composition. The position of the peaks, as well as their relative intensities, is used for comparisons in databases thus leading to the identification of the phase(s) present [121].

II.4.1.3.Determination of lattice parameters

The comparison between the J.C.P.D.S files of code N:041-0254 and the spectrum of the sample will allow us to determine the lattice parameters. Indeed, each diffraction angle corresponds to a reticular plane (h, k, l) and a distance d in the Bragg formula. However, we know that for a unit cell, there is a relationship linking the planes (h, k, l) and the inter-particular distance d_{hkl} of the sample [122,123]. In our case, it is the monoclinic lattice of CuO whose expression of the distance between planes (hkl) is given in the following form :

$$\frac{1}{d_{hkl}} = \frac{1}{\sin\beta}\left(\frac{h^2}{a^2} + \frac{k^2 \sin\beta^2}{b^2} + \frac{l^2}{c^2} - \frac{2hl\sin\beta}{ac}\right)^{\frac{1}{2}} \quad \text{(II.6)}$$

II.4.1.4. Determination of crystallite size

Initially, it is possible, from the diffraction spectra to calculate the size of the crystallites of the phases of the deposits using the Scherrer formula given by the relation [124]:

$$D = \frac{0.9\,\lambda}{\beta.\cos\theta} \quad \text{(II.7)}$$

with D the crystallite size in nm, β is the width at half height expressed in radians, θ is the diffraction angle in degrees, λ is the wavelength of the X-ray beam in Å. Also the microstrain ε can be expressed as follows [125] :

$$\varepsilon = \frac{\beta\cdot\cos\theta}{4} \quad \text{(II.8)}$$

The density of dislocations δ can be evaluated by the formula :

$$\delta = \frac{1}{D^2} \quad \text{(II.9)}$$

To calculate the crystallite size and the internal strains, we used the Williamson-Hall plot method, namely [126-128].

$$\beta \cos(\theta) = \varepsilon(4 \sin(\theta)) + \frac{k\lambda}{D} \quad \text{(II.10)}$$

II.4.1.5. Texturing coefficient

We can find in diffraction patterns crystal orientation and preferred growth directions. The quantification of these peaks is achieved by utilizing the Barret-Massalski formula to get the texture coefficient [129].

$$T_{C_{hkl}} = \frac{\frac{I_{hkl}}{I_{0\,hkl}}}{\frac{1}{N}\sum \frac{I_{hkl}}{I_{0\,hkl}}} \quad \text{(II.11)}$$

with $T_{C_{hkl}}$ the texture coefficient of the line (hkl), I_{hkl} the intensity of the line (hkl), $I_{0_{hkl}}$ the reference intensity of the line (hkl) and .Nis the number of peaks considered.

II.4.1.6. Equipment used

In our work, we used a Brucker AXS D8 ADVANCE type diffractmeter. The X-rays were generated using a CuK_α radiation source which emitted X-rays with a wavelength of 1.5418 Å. The samples were analyzed under grazing incidence. The source of the beam remains fixed and strikes the sample kept horizontal at an angle of incidence of a few degrees. Only the detector moves and scans the desired angular range, applying to the cathode of the X-ray tube a voltage of 40 KV and a current of 40 mA. The scanning range of the detector is 10 to 45° (Bragg angle) [130].

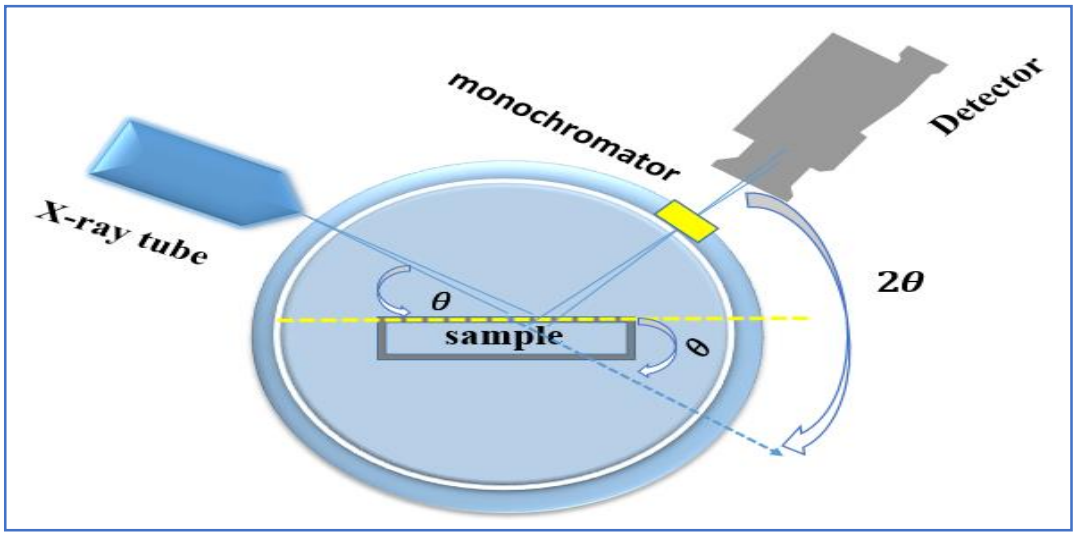

Figure II.15. Diagram of the operation of an X-ray diffractometer.

Figure II.16. BRUKER-AXS type D8 ADVANCE diffractometer.

II.4.2. Fourier Transform Infrared Spectrometry (FTIR)

II.4.2.1. Definition

Infrared spectroscopy, a sensitive and commonly used technique, is based on the phenomenon of absorption. It makes it possible to obtain molecular information when the absorption bands are directly related to the binding force constant between atomic nuclei. This mode of characterization results from the modification of the induced electric dipole moment of the atoms triggering modes of vibration characteristic of the molecular groups of the compound [131].

II.4.2.2.Principle of IR spectroscopy

The Fourier transform infrared spectroscopy (FTIR) method is based on the material ability to absorb infrared light. It allows for the analysis of the material chemical functions by spotting the distinctive vibrations of chemical bonds. The molecular vibration energy range corresponds to the infrared region between 4000 cm^{-1} and 400 cm^{-1} [132]. The energy of photons emitted in this range is not sufficient to produce electronic transitions within materials but can induce the excitation of chemical bonds between atoms. Thus, incident infrared photons will be absorbed when the energy they carry corresponds to the excitation energy of an atomic bond in the material which depends on the chemical environment of the bonds, the mass of the atom as well as the nature of the bonds. Consequently, a material of a given chemical composition and structure will correspond to a set of excitation modes making it possible to identify the chemical bonds characteristic of the material. These excitation modes can be calculated using "group theory" and are listed in tables, thus facilitating the identification of chemical bonds [133]. The IR transmission spectra were obtained by utilizing a VERTEX 70 spectrophotometer.

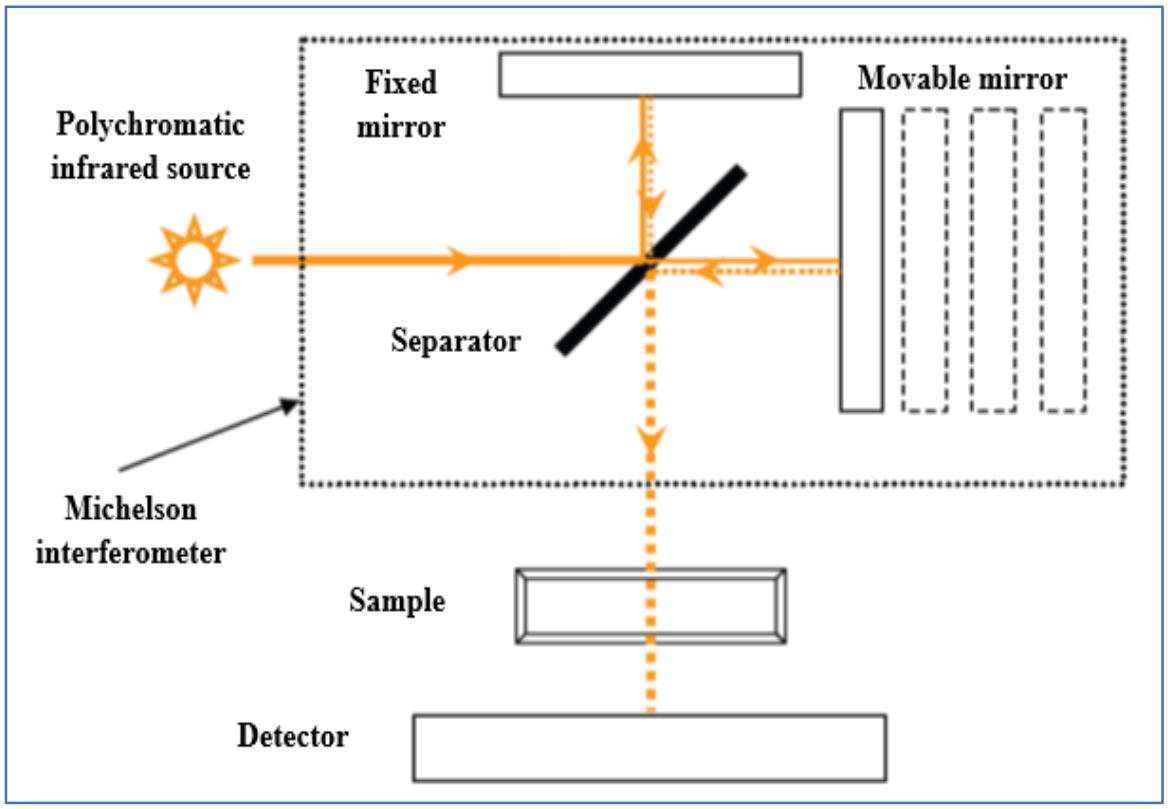

Figure II.17. Principle of IR spectroscopy [133].

II.4.2.3. Equipment used

In this work, the infrared spectroscopy (FTIR) VERTEX70-BRUKER type shown in Figure II.18 was used in the Active Components and Materials Laboratory (LCAM) of Oum El Bouaghi University.

.

Figure II.18. Infrared spectrometer.

II.4.3.Profilometer

The profilometer is used to measure the vertical exterior thickness of a sample. A microneedle is lowered on the sample and placed on a high-precision platform [134]. The device consists of a stylus needle with a diamond tip that moves horizontally on the surface of the sample which allows profile registration. The measurement of the thickness by this method requires the realization of a step on the sample, between an area covered during the deposition and another not covered. This step is obtained thanks to a cover placed on one end of the substrate. Tracking on the surface is ensured by a camera attached to the pointing device. A computer connected to the device is equipped with software allowing the measurement of variations in height and displaying them in the form of a profile.This device also makes it possible to analyze the surface roughness (variation in the thickness of layers) [135].

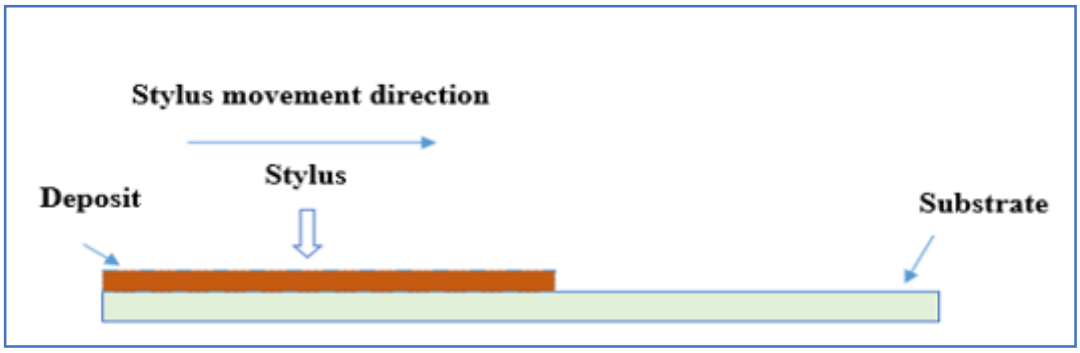

Figure II.19. Principle of measuring thickness by profilometer.

II.4.4. Scanning Electron Microscopy

II.4.4.1. Definition

Scanning Electron Microscopy produces high-resolution images of a sample surface that reveal details about its morphology like shape, size and arrangement of particles, topography (determination of surface defects, texture) [136].

II.4.4.2. Principle

The radiation involved is a beam of electrons striking the sample and causing several phenomena [120] including :

- Emission of secondary electrons.
- Backscattering of some of the primary electrons.
- Emission of X-rays.
- Emission of photons.

More precisely :

- ✓ **Secondary electrons :** low energy electrons come from the external surface of the sample. Consequently, the provided data offers insights into the sample topography. The more the surface sample contains a relief, the more secondary electrons there are (edge effect).
- ✓ **Backscattered electrons** : electrons coming from a depth under the surface a little more important. They are much more energetic than the secondary electrons. They provide a map of the chemical contrast according to the atomic number Z and therefore of the chemical composition of the sample [136].

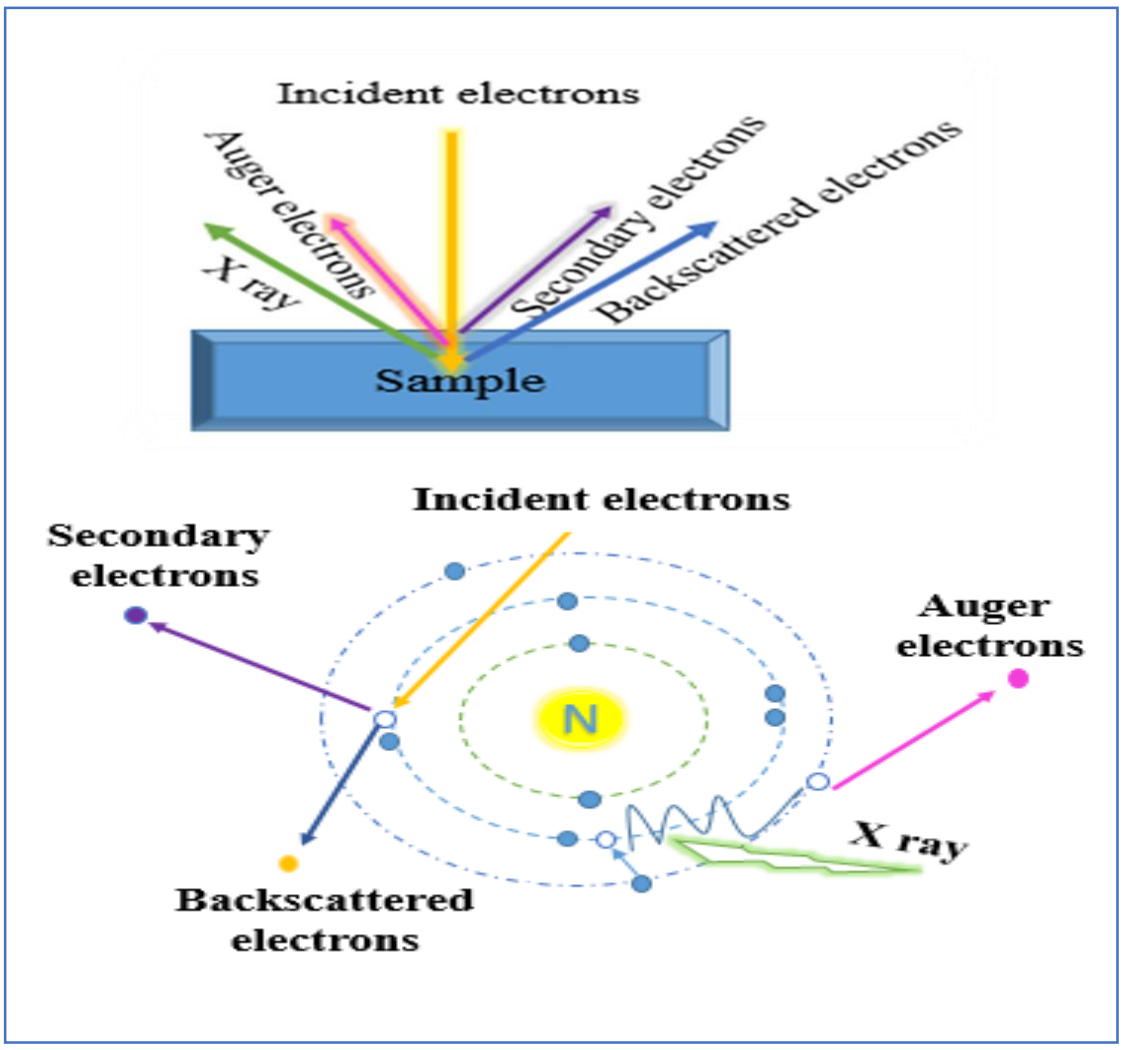

Figure II.20. Principle of matter interaction with electron.

An electron gun sends an electron beam toward the sample. This electron beam is effectively concentrated by the utilization of a magnetic lens to obtain a very fine and focused beam. The secondary electrons produced following the bombardment of the sample by the electron beam are detected by the detector. These secondary electrons are amplified and interpreted to reconstruct an image according to the intensity of the electric current produced. The sequential acquisition of the picture is achieved by systematically displacing the electron beam across the surface of the material, point by point. The quality of the images thus obtained depends greatly on the sample analyzed [137].

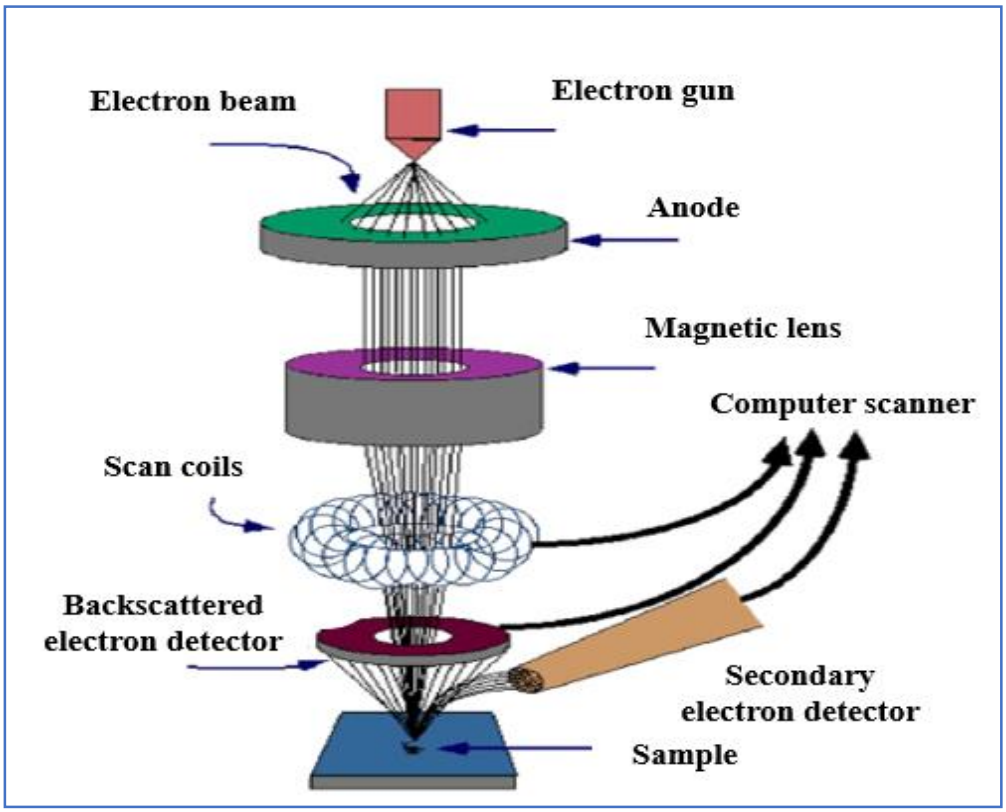

Figure II.21. Block diagram of the scanning electron microscope [138].

II.4.4.3. Energy dispersive spectroscopy

Energy dispersive spectroscopy (EDS) was utilized to examine the sample microscopic chemical composition. The energy carried by the incoming electron beam induces excitation in the electrons situated in the inner layers of the atoms, leading to their ejection, namely atom ionization. The emission of an X photon occurs as a result of the displacement of an electron from such a higher energy shell and the subsequent relaxation of the expelled charge. The energies in question are determined by the electron shell within each respective element and may be effectively employed for the purpose of identifying distinct elements present within a given sample [139].

II.4.4.4. Equipment used

Films morphology were examined using an environmental scanning electron microscope SEM type (Thermoscientific PrismaE).

Figure II.22. Picture for scanning electron microscopy.

II.4.5. Raman spectroscopy

II.4.5.1. Definition

Raman spectroscopy is an analysis the proposed an approach founded on the investigation of molecular vibrations. It complements infrared spectroscopy. It is based on the phenomenon of inelastic light scattering. The sample is excited by a monochromatic radiation, usually a laser beam [140]. The energy variation observed for the photon then provides information on the rotational and vibrational energy levels of the molecule or material concerned. Raman spectroscopy provides a wide range of information. It can be used to characterize short-, medium- and long-range structural order, as well as a compound bond type and crystal structure. Its performance is particularly remarkable. It is the spectroscopic method with the best resolution (one micron) for identifying and characterizing compounds or phases. Its ability to identify amorphous systems is also unrivaled [141,142].

II.4.5.2.Principle

The principle of Raman spectroscopy is relatively simple. It involves shining monochromatic light onto the sample to be studied, and analyzing the scattered light. The scattering of monochromatic radiation by molecules gives rise to low-intensity radiation with frequencies different from those of incident radiation. These frequency changes, linked to the vibrational and rotational energies of the molecules, are specific to each molecule and the intensity of the scattered radiation is therefore characteristic of the material [143].

Scattering can be:

- ✓ Rayleigh or elastic : the incident radiation is elastically scattered without any change in energy.
- ✓ Inelastic scattering or Raman scattering (Stokes or Anti-Stokes).
- ✓ The diagram depicted below provides a visual representation of the Rayleigh and Raman scattering processes.
- ✓ If the frequency $\nu_{diff}(\nu_0 - \nu_{vib})$ of the scattered photon is lower than that of the incident photon ν_0, the molecule gains vibrational energy (and the photon loses energy), forming a Stokes line.
- ✓ If, on the other hand, the incident photon is scattered at a frequency ν_{diff} $(\nu_0 + \nu_{vib})$ there is a loss of vibrational energy for the molecule (and a gain of energy for the photon), which corresponds to the anti-Stokes line of much lower intensity [114,142].

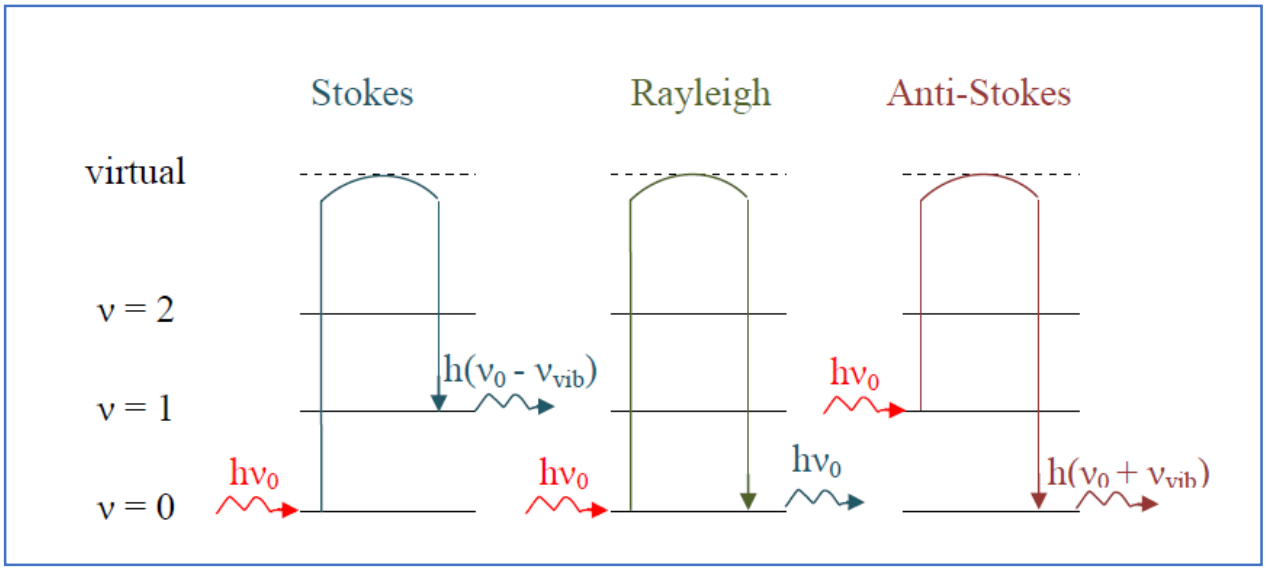

Figure II.23. Raman and Rayleigh diffusion mechanisms in case of $\nu_0 >> \nu_{vib}$.[142].

II.4.6.Resistivity measurement using the four-point technique

Four metal spikes are applied to the sample. The probe is comprised of four contacts that are arranged in a linear fashion and are evenly distributed. The source supplies an electric current, denoted as I, which flows via the external terminals. The voltage V is measured across the terminals of the two inner tips.

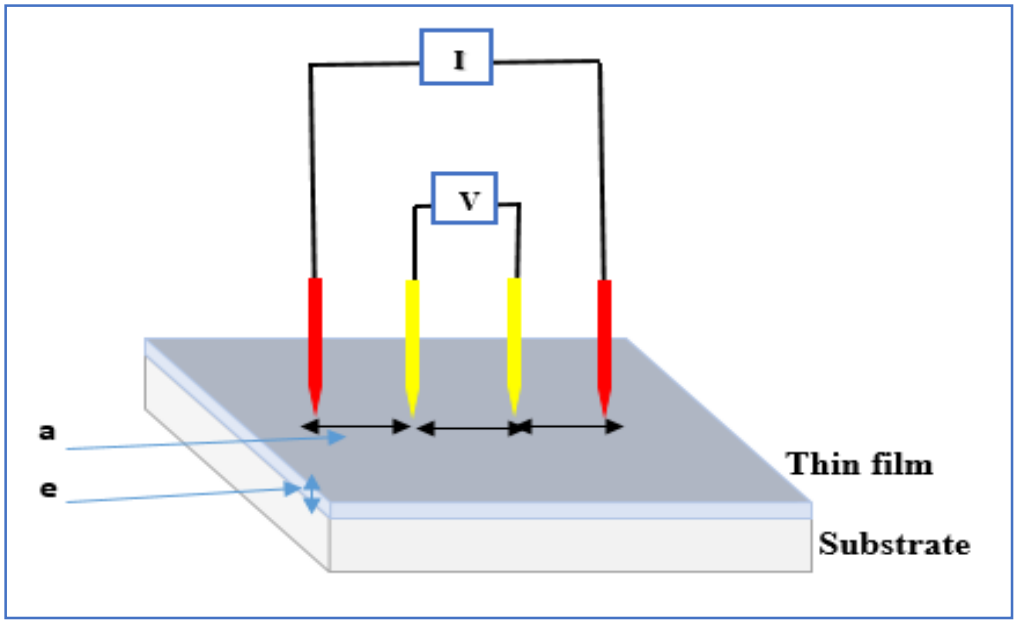

Figure II.24. Diagram showing how to measure resistance using four-point method.

To find the resistivity and electrical conductivity of our films, we used a four-point measuring device, model KEITHLEY 2400 shown in Figure II.25. Used in the Laboratory of Semiconductor and Metallic Materials (LMSM) of Biskra University.

Figure II.25. Real picture of Keithley 2400 type 4 point device .

The resistivity is linked to the measurement of the $\frac{\Delta V}{I}$ ratio according to the relationship :

$$\rho = \frac{\Delta v}{I}.e.\frac{\pi}{Ln2} \qquad \text{(II.12)}$$

The square resistance of a layer is defined by the resistance of a sample whose length is equal to the width. In the case of a uniformly doped layer [144,145], the sheet resistance R_D of a layer of thickness *e* is linked to the resistivity ρ by the relationship :

$$R_D = \frac{\rho}{e} \qquad \text{(II.13)}$$

with ρ the film resistivity and *e* the film thickness.

II.4.7. UV-visible spectroscopy

UV-Visible spectrophotometry is a method for studying the optical properties of thin layers. This study focuses on the interaction between matter and electromagnetic radiation inside the near ultraviolet (UV) to extremely near UV region. The recorded spectra give the transmittance or absorbance as a function of the wavelength of the radiation [146].

II.4.7.1. Principle of UV-visible spectrophotometer

The UV-visible spectrophotometer has three primary components, namely the radiation source, the sample and the reference holder and a detector. The light emitted from the source has a polychromatic nature at its output [147]. To determine the percentage of light transmitted by the layer, the spectrophotometer sends a beam of monochromatic light divided into two components: one component passes through the sample and the other serves as a reference. The transmittance T is defined as the ratio between the intensity of the transmitted light I_t and the incident light I_0. The specular reflection R is the ratio between the intensity of the reflected light I_r and the incident light I_0 [148].

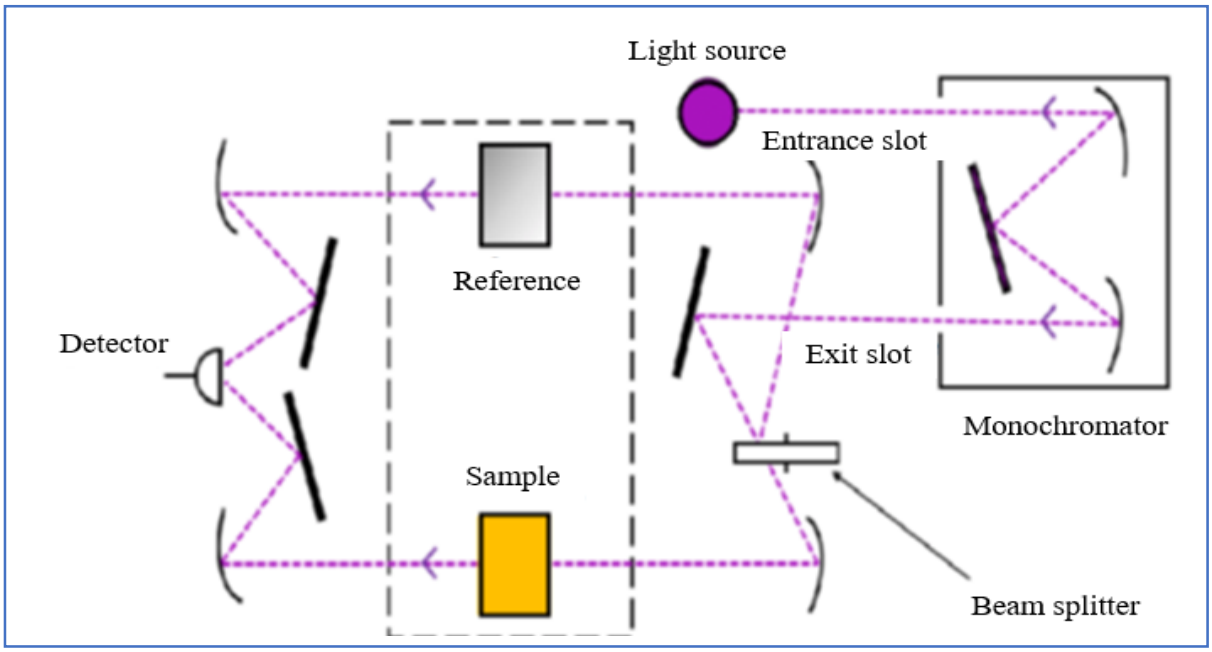

Figure II.26. Principle of operation of UV-visible spectroscopy [150].

II.4.7.2. Determination of the absorption coefficient

If we know the thickness of the layer in the spectral region where light is absorbed, we can determine the absorption coefficient for each transmission value. The beer-lambert law makes it possible to link the transmitted flux and the thickness of the *e* layer with the absorption coefficient [149]. Hence :

$$\frac{I}{I_0} = \frac{T}{100} = e^{-\alpha \cdot e} \qquad \text{(II.14)}$$

with T the transmittance, I_0 the Intensity of incident light, I the transmitted light intensity, α the absorption coefficient and *e* the thickness of the deposited layer. If the transmittance T is expressed in %, the absorption coefficient is given by

$$\alpha = \frac{1}{e} \ln \frac{100}{T\%} \quad \text{(II.15)}$$

This approximate relation is established, neglecting the reflections at all the interfaces : air-layer, air-substrate and layer-substrate [149].

II.4.7.3. Determination of the extinction coefficient

The relationship between the absorption coefficient of the film and the extinction coefficient K is shown in equation (II.16) [149].

$$K = \frac{\alpha \cdot \lambda}{4\pi} \quad \text{(II.16)}$$

II.4.7.4. Determination of the optical gap

The determination of the electronic band gap of the films is deduced from the slope of the curve $(\alpha h\nu)^2$ as a function of hν. Several formulas have been proposed, including:

$$\alpha h\nu = D \cdot \left(h\nu - E_g\right)^{1/2} \quad \text{(II.17)}$$

where D is a constant,,Eg is the electronic band gap in eV,hν the energy of a photon eV knowing that :

$$h\nu(\text{eV}) = \frac{hc}{\lambda} = \frac{1.24}{\lambda(\mu m)} \quad \text{(II.18)}$$

The plot of $(\alpha h\nu)^2$ as a function of the energy of a photon (E= hν) and by the extrapolation method,determination of the intersection of the tangent with the x-axis provides the electronic gap Eg of the material [151].

II.4.7.5. Calculation of the Urbach energy disorder

The Urbach energy is described as the width of the energy band resulting from localized circumstances inside certain band gaps that are characteristic of disordered or weakly crystalline materials. Spectral dependence of the absorption coefficient (α), and the photon energy (hν) is called the "Urbach's empirical rule" which can be expressed by the following relationship:

$$\alpha = \alpha_0 \cdot \exp\left(\frac{h\nu}{E_U}\right) \quad \text{(II.19)}$$

By finding the ln α as a function of hν, we can then graphically determine the value of E_U [152]. Indeed :

$$\mathrm{Ln}\alpha = \mathrm{Ln}\alpha_0 + \frac{h\nu}{E_U} \quad \text{(II.20)}$$

With α the absorption coefficient, α_0 a constant, E_U the Urbach energy and hν the energy of a photon in eV.

II.4.7.6. Equipment used

In this study, the optical properties measured were the transmittance T to deduce the electronic band gap energy of CuO-based nanocatalysts. The transmission spectra of the deposits were carried out within the research Laboratory on the Physical Chemistry of Surfaces and Interfaces (LRPCSI) of the University of Skikda on a UV-visible type spectrophotometer Shimatzu 1700 in the range of wavelength between 200-900 nm.

Figure II.27. Picture showing of the Shimatzu 1700 UV-visible spectrophotometer.

II.4.7.6. Beer Lambert law

From UV-Visible spectroscopy, the absorption of solutions can be determined by the Beer-Lambert law. The analytical applications of UV-visible molecular absorption spectro-photometry relate to molecules in solution. They can be qualitative and quantitative [153]. The analytical technique is often used in a quantitative mode to determine the absorption of a chemical entity in a solution [154]. The absorption phenomenon can be evaluated by the ratio

between incident intensity I_0 and transmitted intensity I of the beam transmitted in the same direction [153,155]. Hence, the absorbance (A) or optical density is defined by :

$$A = -\log_{10}\left(\frac{I}{I_0}\right) = \varepsilon LC \qquad \text{(II.21)}$$

where I and I_0 are the light intensity transmitted and incident on the solution, A is the absorbance or optical density at a wavelength λ, C is the molar concentration of the solution and L is the thickness of the solution through which the luminous flux passes and ε is the molar absorptivity in units of L. mol^{-1}. cm^{-1}.

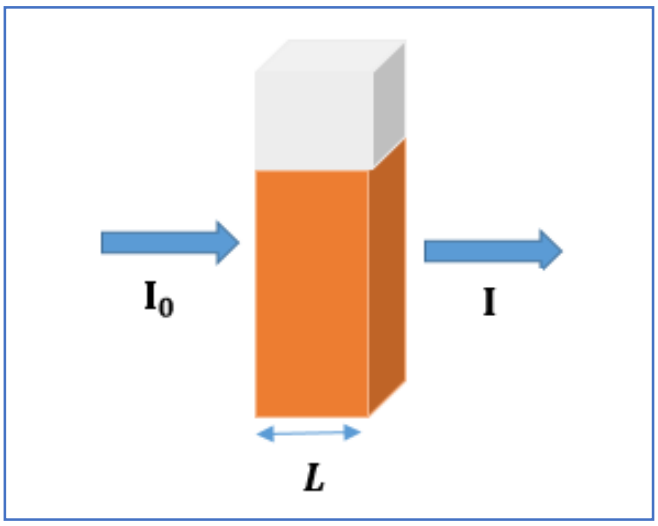

Figure II.28. Diagram illustrating the concept of absorbance.

II.5. Water contact angle goniometer

II.5. 1.Definition

Figure II.29 is a representation of the angle formed by a liquid on a solid surface and is measured only with pure liquids and pristine solid surfaces [156]. It measures the wettability of a surface and describes the extent to which a liquid spreads over a solid when it comes into contact with it.

II.5.2. Principle

The goniometer consists of a light source and an adjustable level, a control, a camera recorder and a computer for data analysis. The slow inflow and outflow of water through a tunnel is then measured through a small needle. The needle is close to the sample and a drop of water falls on the tip of the needle. The video is recorded as water is slowly drawn from the

syringe into droplets with the needle as the waterfront moves into the sample. Each image in the video is analyzed to determine the focal angle at the time the image was captured [157], as shown in Figure II. 29.

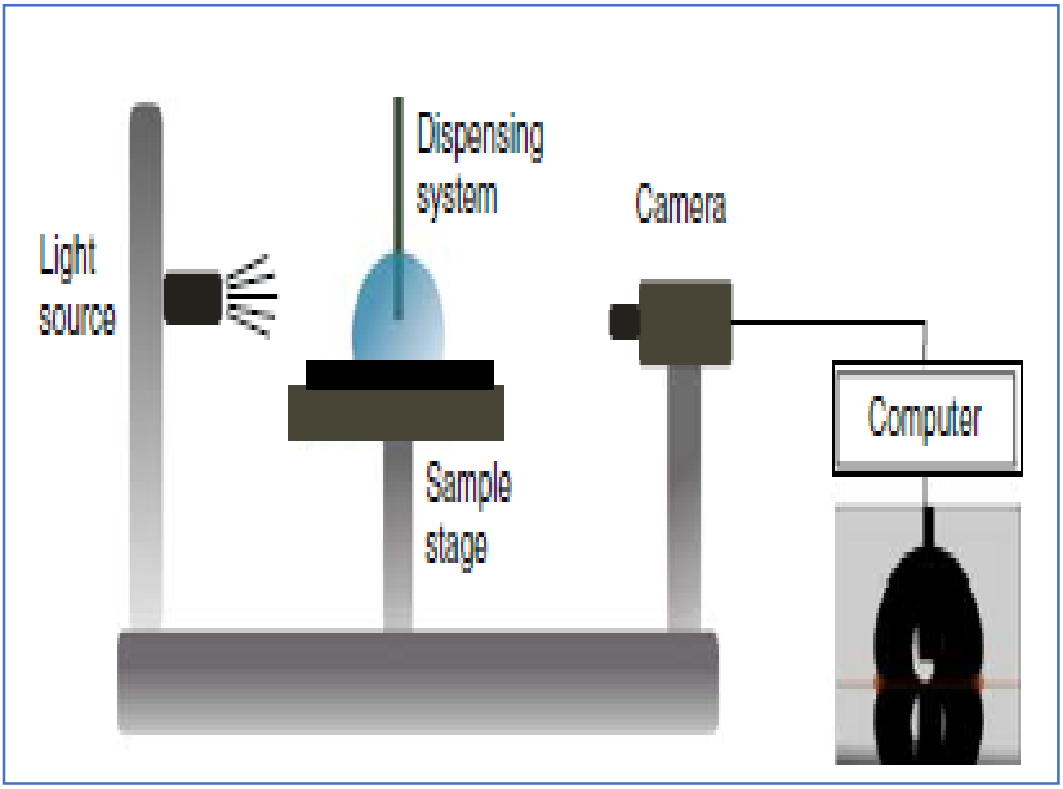

Figure II.29. Principle contact angle goniometer [157].

II.6. Photocatalysis application

In studying the dye activity of Orange II with copper-based catalysts, a volume of 25 ml of Orange II solution is placed in a beaker containing samples prepared under UV irradiation and each time after one hour a volume of 2 ml of the solution is taken to measurement of its absorbance by UV-visible spectrophotometry. We have noticed that every hour there is a change in the color of the solution towards clearing with decrease in the intensity of absorption. The effectiveness of the photocatalysis application depends on the nature of the oxides which verify the effect of copper oxide doping on the catalytic characteristics. Photocatalysis was applied in the laboratory of Active Components and Materials, University of Oum El Bouaghi.

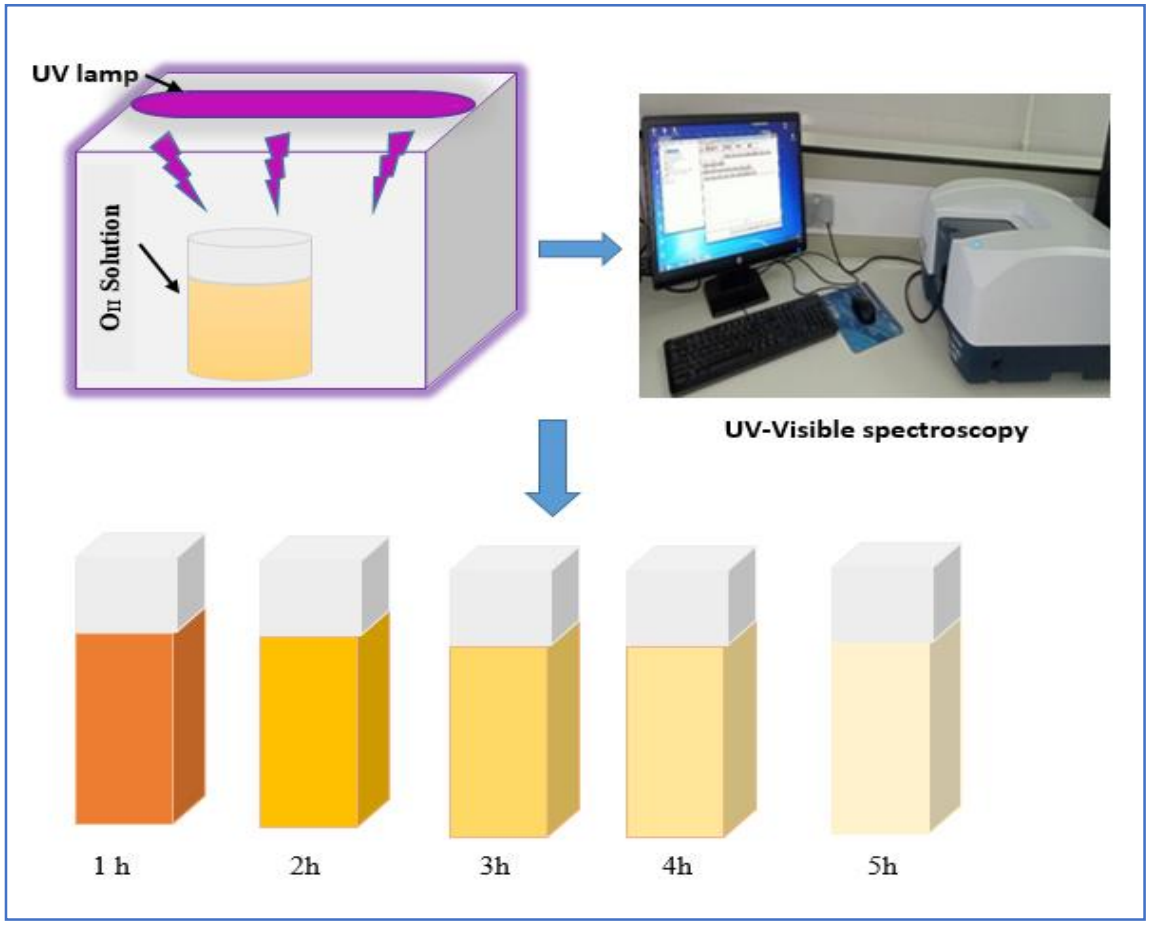

Figure II.30. Principle of the photocatalysis application.

Chapter III:

Effect of spraying time for copper oxide thin films on the water contact angle

III.1.Introduction

In this study, copper oxide thin films were fabricated using the pneumatic spray pyrolysis technique on a glass substrate. The deposition process involved heating the substrate to 400°C, and different spraying times (5min, 10min, 15min, 20min, 25min, and 30min) were employed. A precursor concentration of 0.1M was utilized for the deposition process. The structural, optical, and electrical properties of these films were investigated through various characterization techniques, including X-ray diffraction (XRD), Fourier-transform infrared spectroscopy (FT-IR), UV-visible spectroscopy, and the four-point method. Furthermore, the synthesized films were applied in the field of nanotechnology as self-cleaning films, and the surfaces were evaluated using the water contact angle measurement.

III.2.Thickness measurement

Figure III.1 presents the variation in the thickness of copper oxide (CuO) as a function of different spraying durations (t= 5, 10, 15, 20, 25, 30 min) using the pneumatic spray pyrolysis technique. The films exhibited variations in thickness ranging from 102 to 650 nm. The thickness of the samples exhibits a positive correlation with the duration of the spraying process.

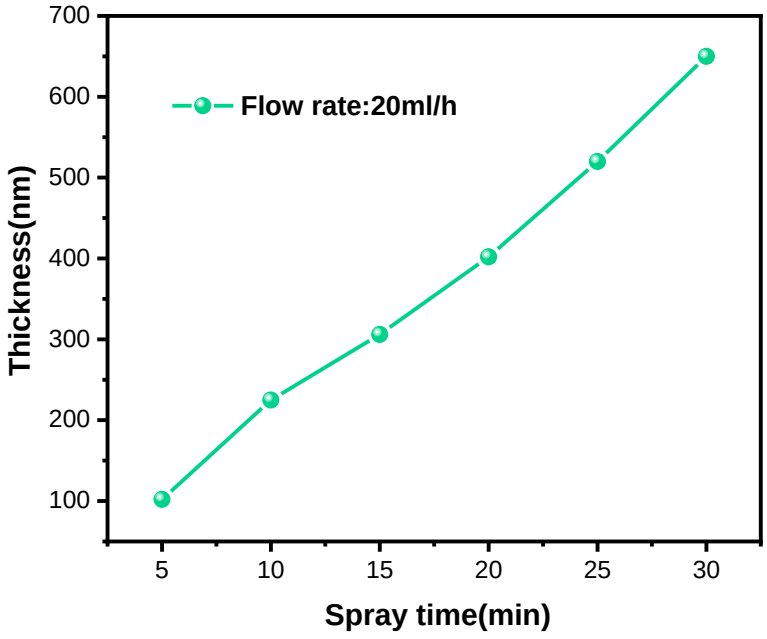

Figure III.1. Thickness of copper oxide as a function of spraying time.

III.3.Structural properties

III.3.1.X Ray Diffraction

The structural characteristics of copper oxide thin films for various spray durations ranging from 5 minutes to 30 minutes have been identified by XRD. The presence of multiple diffraction peaks at specific angles, namely 2θ = 32.35°, 35.44°, 38.62°, 53.43°, 66.16°, and 68.30°, can be observed in Figure III.2. These peaks correspond to distinct crystal planes, specifically (002), (110), (111), (020), (-311), and (220). This observation is consistent with the JCPDS code 00-041-0254, which provides supporting evidence for the presence of the monoclinic structure of the tenorite phase. This observation indicates that the thin films possess a polycrystalline structure. The observed samples exhibit a distinct and heightened peak that corresponds to the (111) crystallographic plane. The literature commonly indicates that CuO thin films exhibit a predominant orientation along the (111) plane, which is consistent with previous research findings [158,159]. Upon increasing the duration of spraying, it was observed that the intensity of the two primary peaks exhibited an increase. The enhancement of both growth and crystallinity was observed in these layers. This observation is substantiated by the heightened intensity of the peaks.

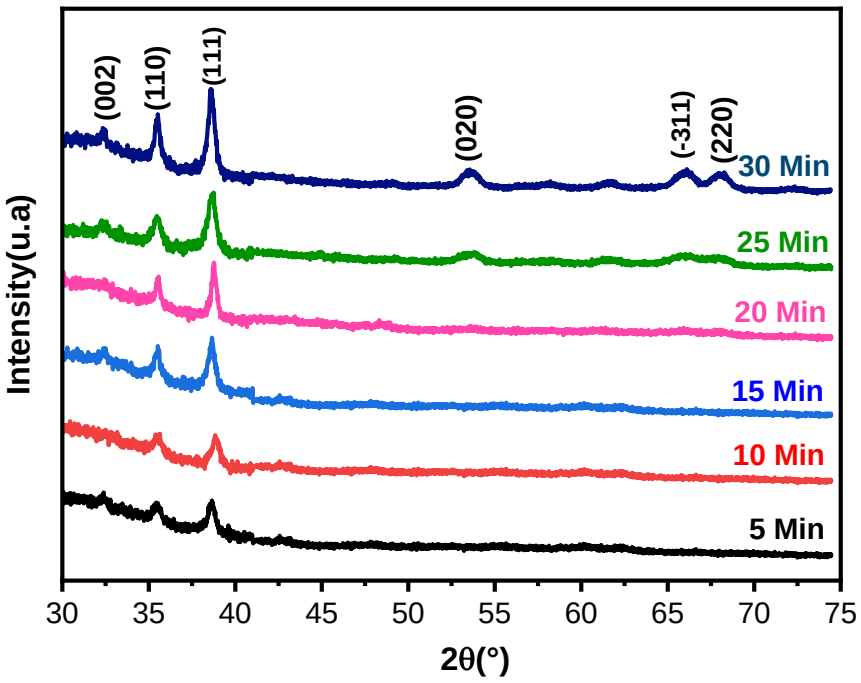

Figure III.2. XRD spectra of undoped CuO thin films deposited at 400 °C.

III.3.2.Texture coefficient

When determining the texture coefficient (Tc) and finding the preferred orientation of these films, equation (II.11) is used. Figure III.3 represents the variation of texture coefficient for the two planes (110) and (111) for the films of copper oxide at different spraying times. We notice that the texture coefficient in all the films (>1) in two planes (110) and (111) confirms the existence of a preferential orientation along the plane (110) and (111).

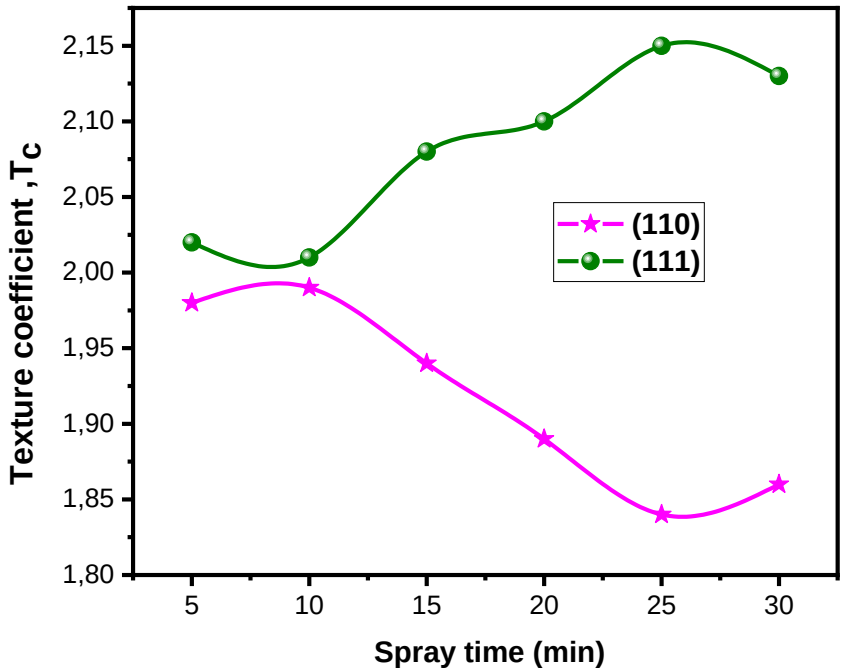

Figure III.3. Texture coefficient as a function of spraying time at (110) and (111).

III.3.3.Crystallite size and microstrain

The crystallite size ranges from 14 nm to 23 nm, as indicated in Table III.1. These measurements were obtained by the (111) plane. It is worth noting that the optimal crystallite size is observed at the 20-minute. Figure III.4 depicts the relationship between microstrain and crystallite size in relation to spray time. It is observed that these two variables exhibit an inverse correlation. An increase in crystallite size reduces micro-strain within the lattice, consequently leading to a decrease in microstrain within the crystal lattice of copper oxide.

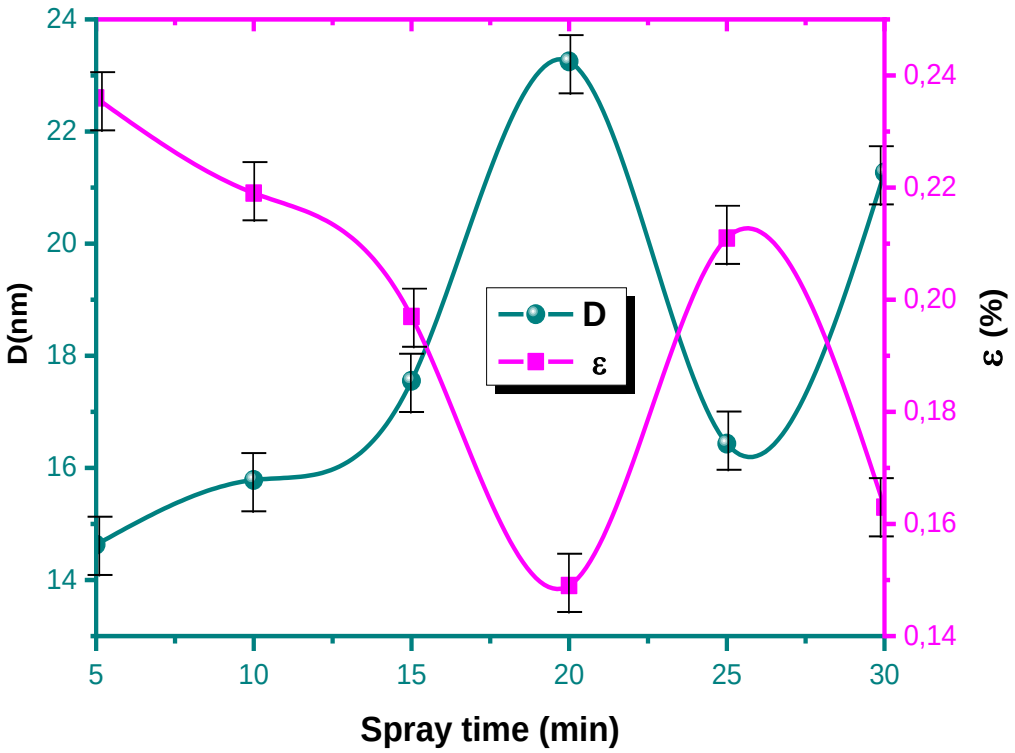

Figure III.4. Crystallite size and microstrain of the films as a function of spray time.

III.3.4.Lattice parameters

The lattice parameters and volume of the films with a monoclinic structure are provided in Table (III.1). It is important to highlight that the experimental lattice parameters align with the theoretical parameter obtained from the JCPDS code (00-041 -0254).

Table III.1. Lattice parameters of the samples.

Phases	Plane (hkl)	2θ (°)	FHWM β(°)	D (nm)	**ε** (10^{-4})	**δ**10^15 (Lines/ m^2)	a (Å)	b (Å)	C (Å)	**β**(°)	v ($Å^3$)
5min	(111)	38.62	0.543	14±0.04	22.36	5,10	4.68	3.41	5.14	99.20	80.79
10min	(111)	38.85	0.503	15±0.05	20.7	4,44	4.68	3.42	5.13	99.25	81.29
15min	(111)	38.62	0.452	17±0.03	18.61	3,46	4.68	3.41	5.14	99.12	81.30
20min	(111)	38.76	0.342	23±0.01	14.08	1,89	4.66	3.43	5.14	99.71	81.14
25min	(111)	38.63	0.483	16±0.02	19.89	3,90	4.63	3.42	5.14	99.19	80.38
30min	(111)	38.61	0.373	21±0.01	15.36	2,26	4.64	3.43	5.14	98.99	80.85

III.4.Vibration spectroscopy investigations using FT-IR

The FTIR spectroscopy technique was employed to analyze the thin films that were produced, with the aim of gaining a deeper understanding of their chemical compositions and the interactions that govern their properties. In the range of 400-2500 cm^{-1}, infrared (IR) spectra of CuO thin films were recorded, as depicted in Figure III.5. Multiple absorption bands were identified, including peaks at 413 cm^{-1}, 424 cm^{-1}, 462 cm^{-1}, 478 cm^{-1}, 529 cm^{-1}, 575 cm^{-1}, 478 cm^{-1}, 529 cm^{-1}, 718 cm^{-1}, and 908 cm^{-1}, which are attributed to the Cu-O band. Additionally, another author's band at 1540 cm^{-1} and 1650 cm^{-1} corresponds to the vibration of the O-H band, indicative of the vibrational mode of the hydroxyl group bond to the adsorbed water. These findings align well with existing references [160-162].

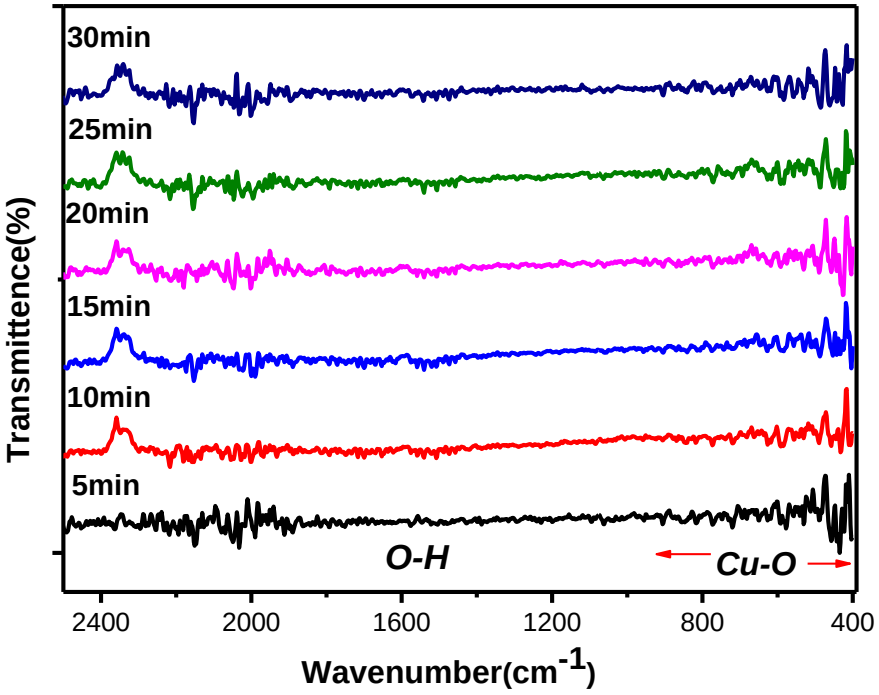

Figure III.5. FTIR spectra of copper oxide thin films for different spray times

III.5.Optical properties

III.5.1.Transmittance spectra

Figure III.6 displays the transmittance spectra of CuO that were acquired at various spray durations within the wavelength range of 200 nm to 900 nm. From this figure, it becomes evident that the transmittance exhibits an upward trend as the wavelength of light increases across all samples. There are two distinct regions that can be identified based on their optical

properties. The first region exhibits an average transmittance exceeding 50%, with the highest transmittance occurring at approximately 65% in the wavelength range above 500 nm. In contrast, the second region, which falls within the visible spectrum, demonstrates significant absorption due to the energy of incoming photons being close to the absorption edge (specifically, the energy value of the forbidden band).This absorption phenomenon is also associated with fundamental absorption (wavelengths less than 500 nm), resulting in a complete cancellation of transmittance below 400 nm. The observed transition wavelength is in agreement with the optical gap energy of the investigated copper oxide layers. All photons with energy levels exceeding the gap threshold, and consequently all photons with wavelengths below 500 nm, are absorbed rather than being transmitted. The observed absorption phenomenon can be attributed to the electronic transition band. The exploitation of transmission variation in this particular region is utilized for the purpose of determining the gap. Conversely, there is an observed displacement of the absorption threshold towards lower energies, corresponding to longer wavelengths. The observed shift can be ascribed to the heightened concentration of unbound carriers within the material [163].In the spray time of 5min, it represented a good transmittance in the visible range accuse of the lower thickness.

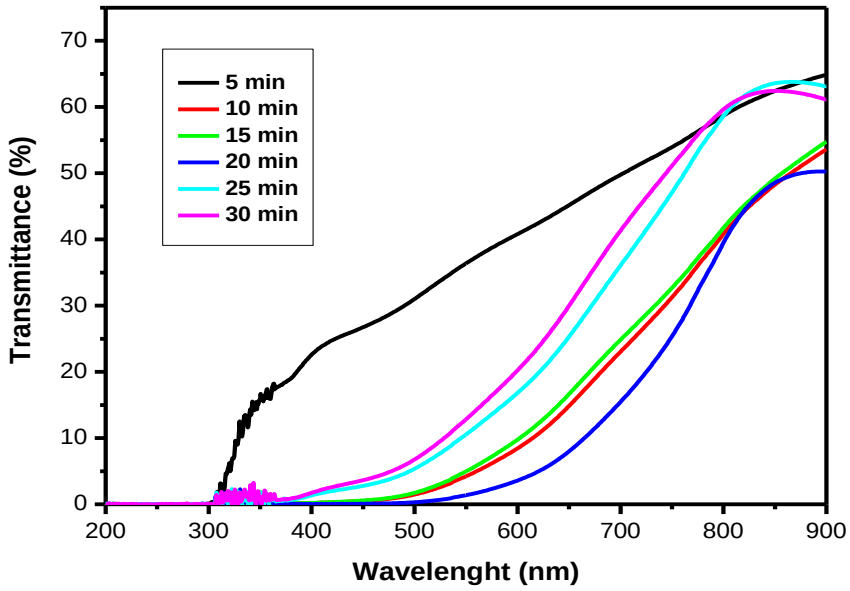

Figure III.6. Variation of the transmittance of CuO films deposited at different Spray times.

III.5.2.Energy gap

Figure III.7 shows the plot of $(\alpha h\nu)^2$ as a function of the energy of a photon $h\nu$ and by the extrapolation method, we have represented the optical gapE_g. The values of the gap energy are influenced by various factors, such as the duration of the spray and the thickness of the material. A variation in the optical gap is observed, with the gap energy values ranging from 2.65 eV to 1.91 eV. The minimum value of the gap energy is represented by a spray time of 20 minutes. The observed phenomenon can be attributed to the successful crystallization of our layer, which serves as evidence for the significant size of the crystallites achieved during the specified spray time. Additionally, the low transmittance observed suggests a substantial deposition of material.

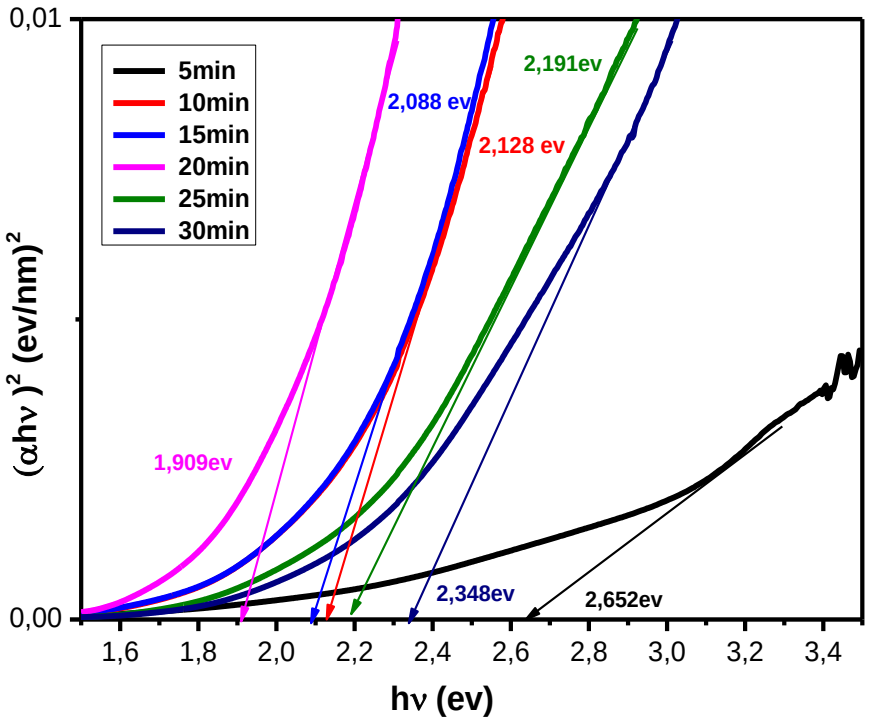

Figure III.7. Variation of $(\alpha h\nu)^2$ as a function of the photon energy of copper oxide for different spray times.

III.5.3.Dielectric Constant (ε)

The dielectric constant is a fundamental optical parameter and is written as

$$\varepsilon = \varepsilon_1 - i\varepsilon_2 \qquad \text{(III.1)}$$

Where ε_1 is the real part of the dielectric constant, which is related to the energy stored in the material, and ε_2 is the imaginary component of the dielectric constant, which is related to the energy dissipation in the material [164].

III.5.3.1.Real part of dielectric constant (ε_1)

A real part of the dielectric constant is calculated from the following relation

$$\varepsilon_1 = n^2 - k^2 \qquad \text{(III.2)}$$

The following spectra show the variation of the real part of the dielectric constant as a function of the energy of a photon. The progressive increase of the real dielectric constant values can be observed in Figure III.8 as the photon energy increases. Subsequently, a sharp decrease is observed in the high energy range for all the films that were prepared. The curves exhibit similarities to the refractive index curves as a result of the relationship between the real part of the dielectric constant and the refractive index values, as described by equation (III.2), in conjunction with the values of the extinction coefficient. It is evident that the impact of the extinction coefficient is significantly smaller in comparison to the influence of the refractive index. Consequently, it can be disregarded, particularly when dealing with low photon energies.

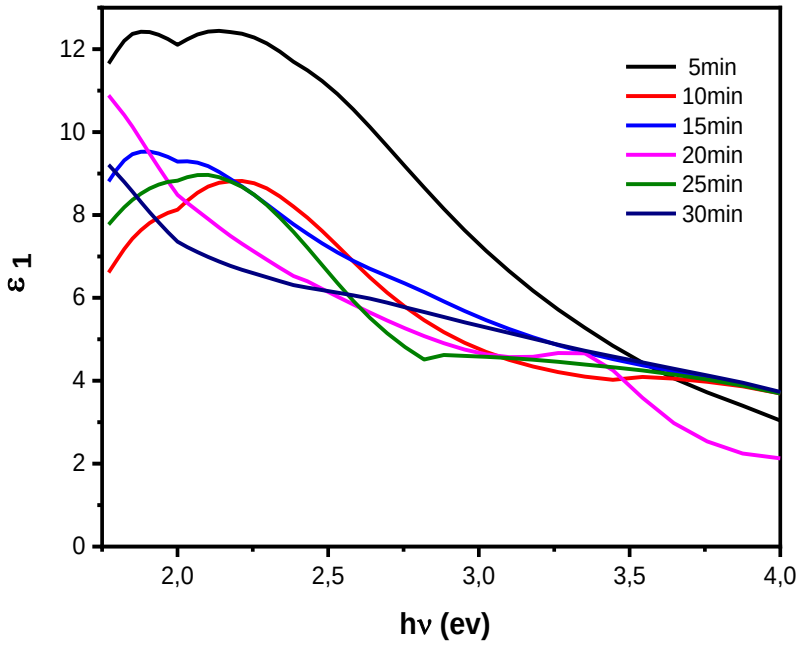

Figure III.8. Variation of the real part of the dielectric constant as a function of the energy of a photon.

III.5.3.2.Imaginary part of dielectric constant (ε_2)

The imaginary part of the dielectric constant is calculated from the following relation

$$\varepsilon_2 = 2nk \qquad \text{(III.3)}$$

The variation of the imaginary part of the dielectric constant as a function of the incident photon energy with the evolution of the spray time is represented in Figure III.9 as it is noted that the imaginary part of the dielectric constant almost increases with the increase of the spray time. This increase is shown by the increase of the absorption energy. This result is in good agreement with the extinction coefficient results. In all films, the peaks of the curves creep towards low photon energies (long wavelengths), and note also the 5min spray time film is shown the value 1 as the highest value of the imaginary dielectric constant.

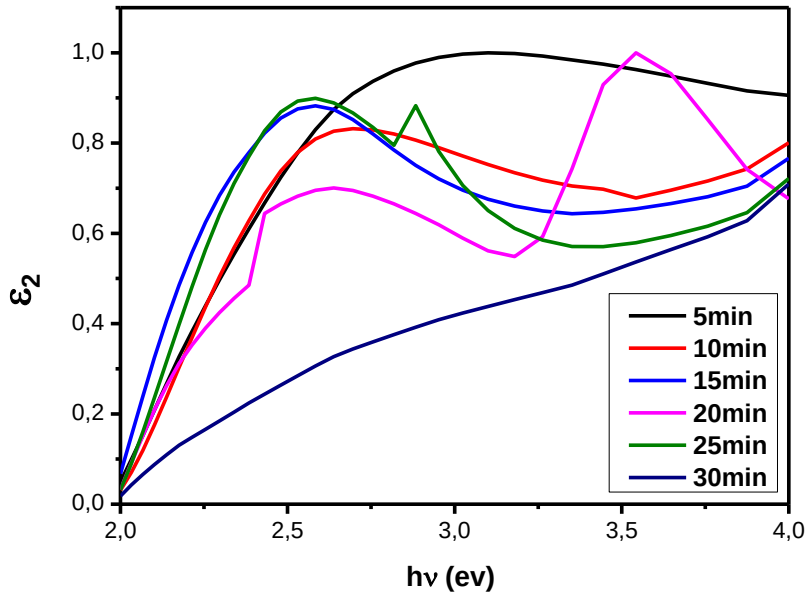

Figure III.9. Variation of the imaginary part of the dielectric constant as a function of the energy of a photon.

III.6.Electrical properties

The electrical conductivity (σ) and resistivity (ρ) of CuO thin films, which are acquired through the process of spraying time, can be determined using the four-point method.

The figure III.10 displays the relationship between electrical conductivity and resistivity with respect to spray time. A notable trend of diminishing and augmenting electrical conductivity is observed as the duration of spraying is increased, ultimately culminating in a peak value of 0.34 Ω^{-1} .cm^{-1} at a spray time of 20 minutes. This outcome aligns with the findings reported in the reference literature [165]. And the other values of electrical conductivity are in agreement with the references [166,167].The augmentation of electrical conductivity is strongly correlated with the augmentation of free charge carriers and the reduction of crystalline defects resulting from the increase in crystallite size in comparison to other factors. The observed relationship between electrical conductivity and gap energy indicates a strong correlation, whereby a decrease in gap energy corresponds to an increase in electrical conductivity. The decline in electrical conductivity can be attributed to the reduction in crystallite size, which consequently leads to the presence of grain boundaries and defects that can augment the optical gap energy.

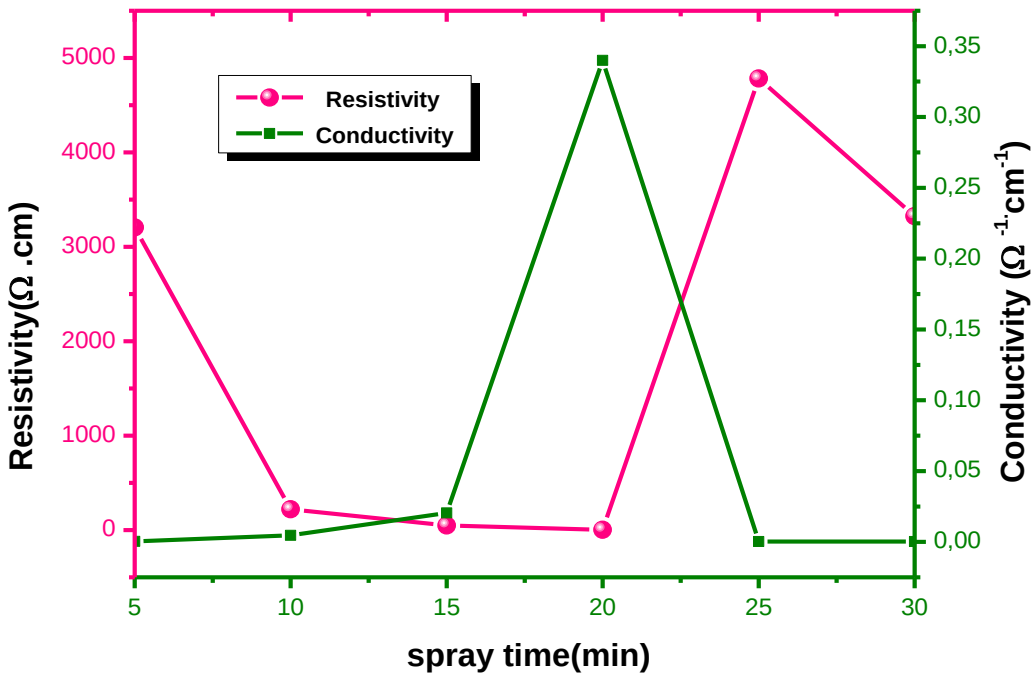

Figure III.10. Variation of conductivity and resistivity as a function of spray time.

III.7.Water contact angle

The contact angle exhibited by water droplets is contingent upon the surface structure and the nanoscale variation in droplet size. As represented in the following images.

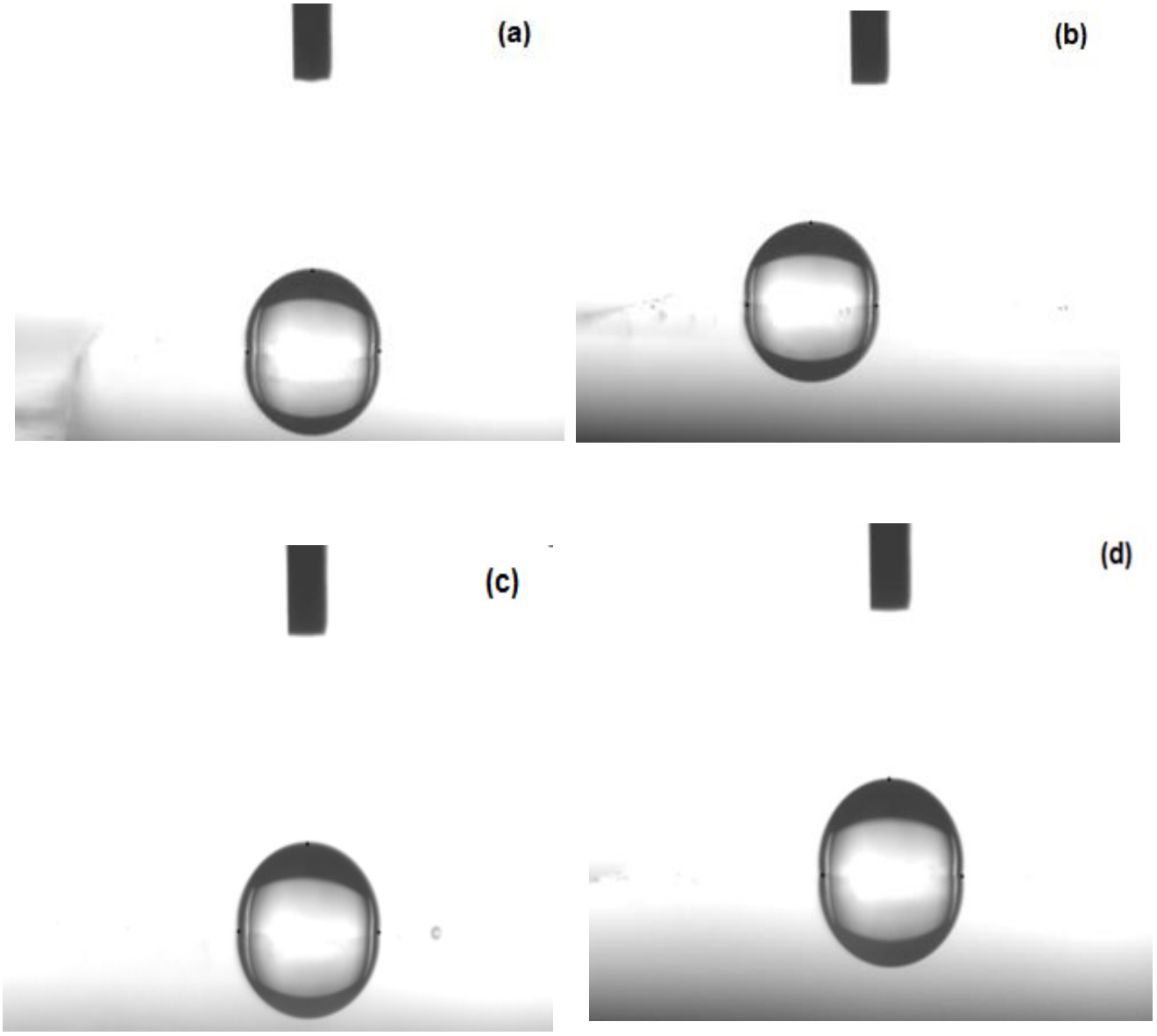

Figure III.11. Water contact angle image of various spray times of CuO (a), 5min (b),10min (c),15min (d),20min (e),25min (f),30min.

Figure III.12 illustrates the relationship between the contact angle and spray time, indicating a corresponding alteration in the thickness of the samples. We notice an increase and decrease of the contact angle such that their values in all the sample is greater than 90° and varied between 96.4°and 103.2°. The contact angle on the rough surface is greater than on the smooth surface, indicating that the roughness of the solid hydrophobic improves its hydrophobicity [168]. In general, when the contact angle between water and a solid surface is below 90°, the solid surface is classified as hydrophilic. Conversely, when the contact angle between water and a solid surface exceeds 90°, the solid surface is categorized as hydrophobic. [169].The contact angle that exhibits the smallest value is observed at the 15 minute. This phenomenon can be attributed to the heightened water adsorption on the film surface, which can be attributed to its smooth texture. The results indicate that the samples consist of hydrophobic films, which hold potential for advancements in the realm of nanotechnology, particularly in the production of water-resistant textiles.

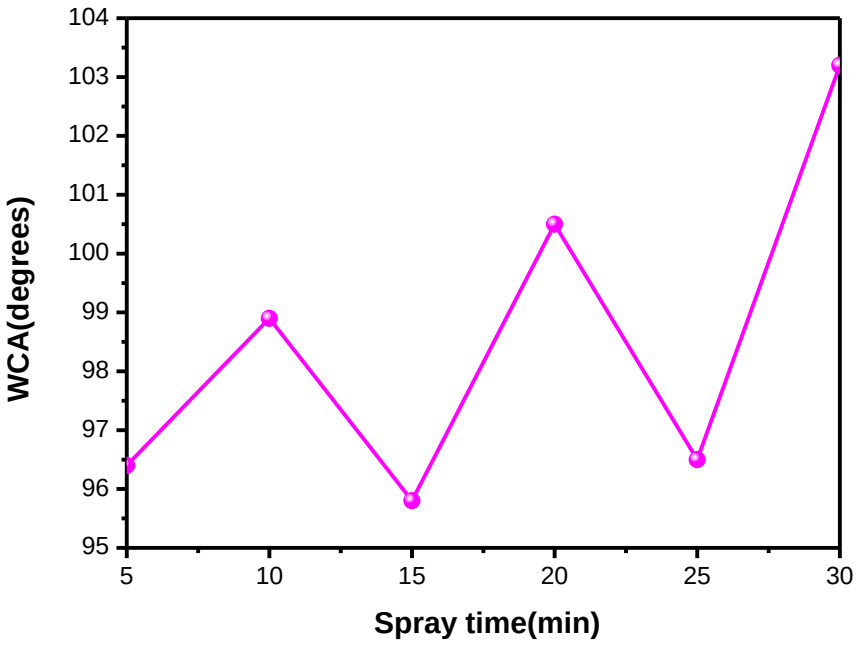

Figure III.12. Variation of water contact angle as a function of various spray times.

III.8.Conclusion

In the field of nanotechnology, self-cleaning thin films composed of varying durations of CuO spraying were employed. The films were applied onto a glass substrate using the pyrolysis spray technique. Based on the X-ray diffraction (XRD) data, the films that were generated exhibited a polycrystalline structure, characterized by a C2/c space group. Based on the findings obtained from the water contact angle measurements, it is evident that all the samples exhibit hydrophobic characteristics, as indicated by the increasing contact angle values with respect to the layer thickness. Furthermore, it is noteworthy that the contact angle on the rough surface surpasses that observed on the smooth surface. This observation suggests that the presence of roughness in hydrophobic films enhances their hydrophobic properties.

Chapter IV:

Elaboration and characterization of Al-doped copper oxide thin films for photocatalysis application

IV.1.Introduction

The initial section of this chapter focuses on the examination of the structural, morphological, optical, and electrical characteristics of copper oxide (CuO) that has been doped with varying concentrations of aluminum (Al) (x = 0%, 5%, 15%, 25%, and 50%). These films were conducted utilizing the sol-gel spin coating technique. The thin films of $Cu_{1-x}Al_xO$ were subjected to several characterization techniques, including X-ray diffraction, Fourier-transform infrared spectroscopy (FT-IR), scanning electron microscopy (SEM), energy-dispersive spectroscopy (EDS), Raman spectroscopy, UV-visible spectrophotometry, and the four-point method. The second half of the study focuses on the investigation of photocatalysis applications of these films in the degradation of Orange II dye under UV irradiation. Additionally, it examines the underlying principles and mechanisms involved in the degradation process.

IV.2. Thickness measurement

The provided diagram illustrates the variations in thickness of copper oxide (CuO) samples that have been doped with aluminum (Al) at different concentrations (x = 0%, 5%, 15%, 25%, and 50%). These samples were produced using the sol-gel spin coating technique. The films exhibited variations in thickness ranging from 106 to 798 nm.

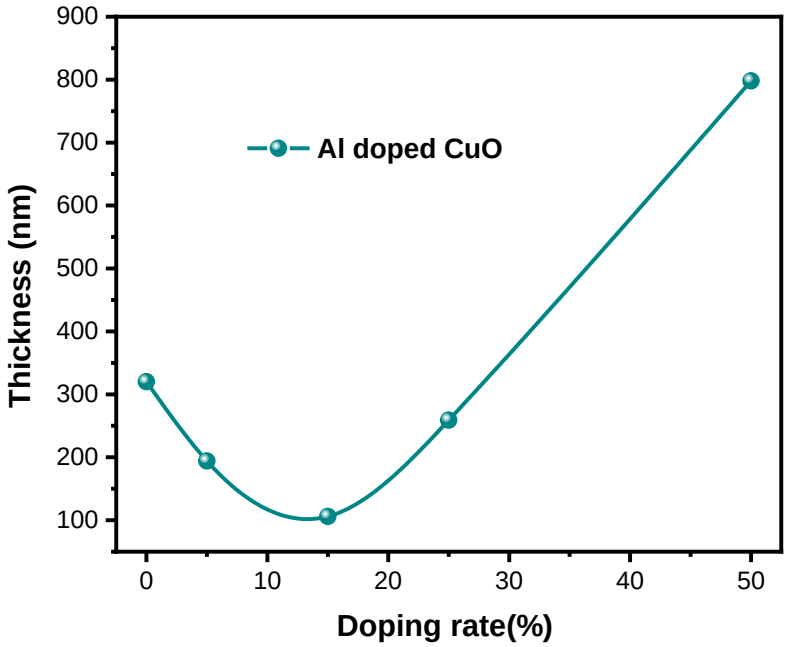

Figure IV.1. Thickness of copper oxide pure and doped with Aluminum.

IV.3. Structural properties

IV.3.1. X-Ray Diffraction

Figure IV.2 depicts the X-ray diffraction patterns obtained from the pure and Al-doped CuO thin films that were formed on a glass substrate using the spin coating technique. The identification of copper oxide as the tenorite phase, classified under the space group C2/c, is supported by the observation of distinct diffraction peaks corresponding to specific crystallographic planes (110), (-111), (200), (-202), (020), (202), (-113), (-311), and (220). These findings align with the JCPDS code sheet (00-041-0254), providing further evidence for the presence of CuO with a monoclinic structure. There is no evidence of the presence of a secondary phase like Cu_2O or Cu_4O_3.

Upon the introduction of Al doping, a noticeable displacement of the peaks is observed. This observation is substantiated by the occupation of Cu^{2+} ion sites (measuring 0.73 Å) by Al3+ ions (measuring 0.53 Å), indicating the presence of defects and vacancies within the network sites [170, 171]. Furthermore, the observation of secondary peaks provides evidence for the occurrence of a distinct phase of Al_2O_3 produced in the films that have been doped with 5%, 25%, and 50% of Aluminum.These weak peaks can be attributed to the following crystallographic planes: (104), (202), (142), (018), (214), and (300). The presence of minor peaks belonging to the Al_2O_3 phase can be attributed to the effective incorporation and favorable arrangement of Al^{3+} ions inside the CuO lattice, as described in reference [172]. In the context of doping with 15% aluminum (Al), the presence of an additional phase, namely CuAlO2, is seen. This phase is found to align well with the crystallographic planes (006), (101), (009), and (018), as indicated by the JCPDS code sheet (00-035-1401).

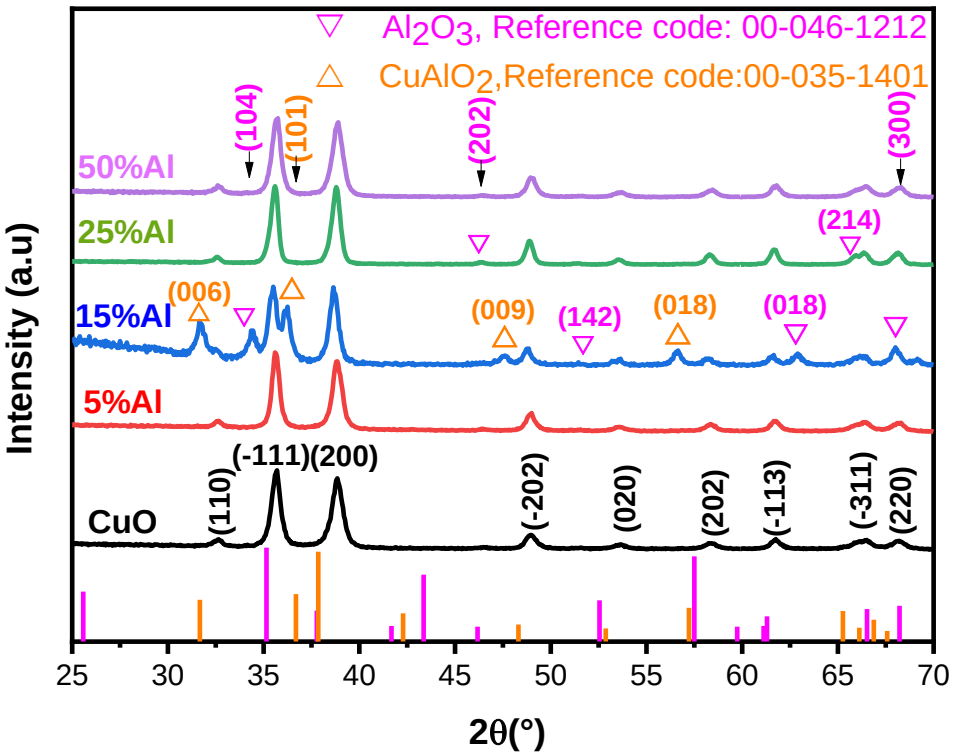

Figure IV.2. XRD spectra of Al-doped CuO thin films.

IV.3.2.Texture coefficient

Equation (II.11) is employed in the determination of the texture coefficient (Tc) and identification of the optimal orientation of these films. Figure IV.3 illustrates the texture coefficient fluctuation for two crystallographic planes, namely (-111) and (200), in both pure CuO films and CuO films doped with varying amounts of Al. It is observed that the texture coefficient, which has a value greater than 1, exhibits alignment with the crystallographic plane (-111) across all the films. The experimental results provide evidence for the presence of a preferred alignment along the (-111) crystallographic plane.

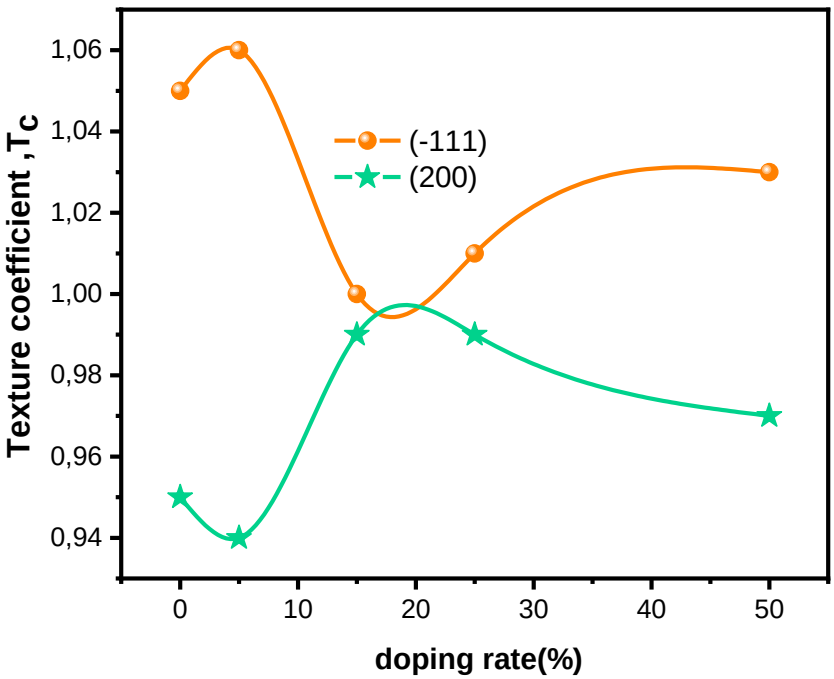

Figure IV.3. Texture coefficient as a function of the doping rate at (-111) and (200).

IV.3.3. Crystallite size and micro-strain

The determination of crystallite size and micro-strain in thin layers of pure and Al-doped CuO was performed using the Williamson-Hall relation, as described by (equation II.10). Figure IV.4 depicts the representation of the function β.cos(θ) as a function of 4.sin (θ), specifically focusing on the trace.

After doing calculations, it has been determined that the dimensions of the crystallites within the nanometer scale, precisely ranging from 21 nm to 46 nm. Moreover, empirical observations have indicated that an increase in the rate of aluminum (Al) doping results in a corresponding enlargement of the crystallite dimensions. The recrystallization events outlined above, as explained in the cited reference [173]. Can be ascribed to the increase in nucleation sites and the amalgamation of smaller crystallites, leading to the formation of bigger crystallites. An increase in the size of the crystallites has been observed. This observation presents empirical support for the heightened crystallization of these coatings. Multiple prior studies have documented a notable augmentation in the size of crystallites by the utilization of aluminum

(Al) doping [172, 174]. An independent study unveiled an inverse relationship between the doping of aluminum and the dimensions of crystallites [175].

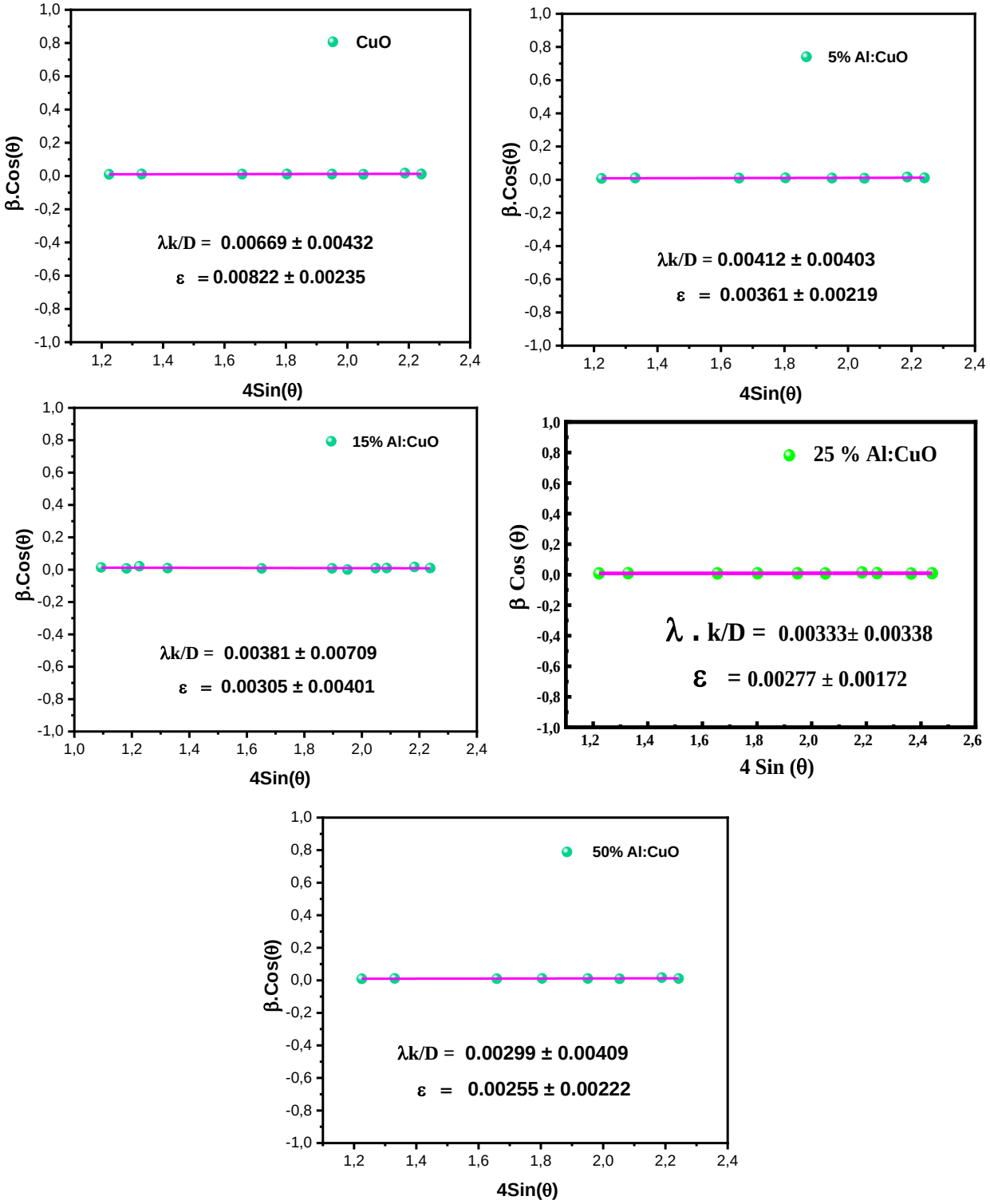

Figure IV.4. Williamson Hall plots of CuO undoped and doped with Al.

Figure IV.5 illustrates the representation of crystallite size, microstrains, and dislocation, which are determined using equations (II.8)and (II.9). The present study demonstrates a correlation between the increase in crystallites size and the decrease in microstrain and dislocation. This finding provides evidence that the introduction of Al doping reduces defects in the crystal lattice. Consequently, it can be inferred that Aluminum enhances the crystallization process of CuO-based films.

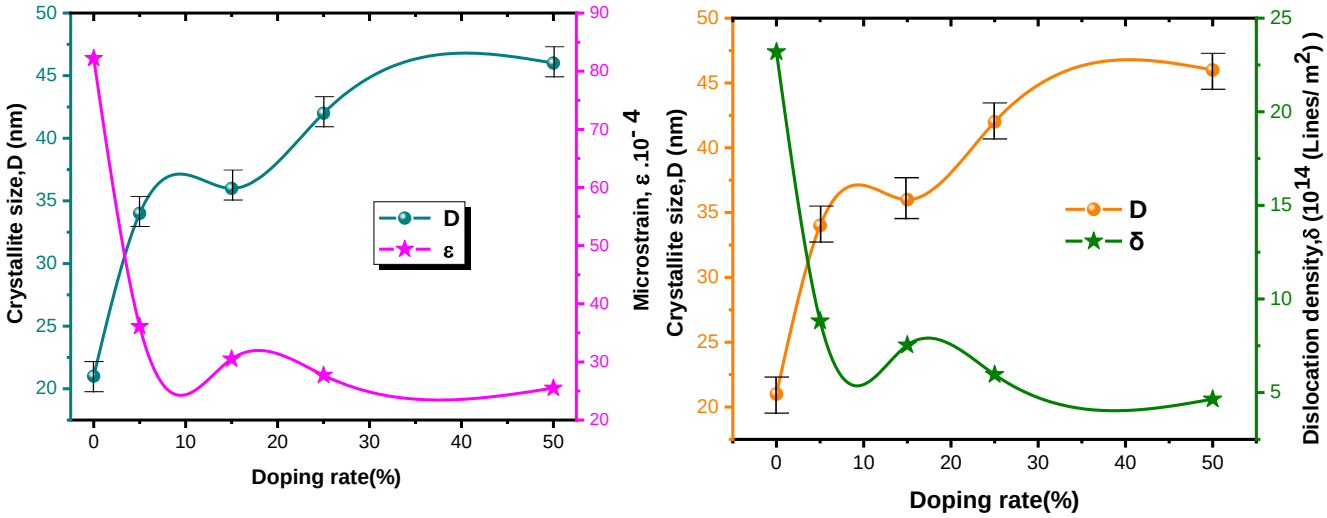

Figure IV.5. Variation of crystallite size, microstrain, and dislocation density as a function of doping with Al.

IV.3.4. Lattice parameters

Table IV.1 displays the lattice parameters and volume of the monoclinic structure. Upon examination, it is observed that the experimental lattice parameter is in agreement with the theoretical value found in the JCPDS file under code (00-041-0254). Following the introduction of doping by Al, alterations in the lattice characteristics are observed, characterized by an expansion in the volume of the lattice for doping concentrations of 5%, 15%, and 25% Al. Conversely, a compression in the volume of the lattice is observed for 50% Al doping.

Table IV.1. Crystallite size and lattice parameters for thin films of copper oxide pure and doped with Aluminum deposited by a spin coating method.

Phases	D (nm)	$\varepsilon.10^{-4}$	δ .10^{14} (Lines/ m^2)	a(Å)	b(Å)	c(Å)	β (°)	v ($Å^3$)
CuO	21±0.004	82.2	23.2	4.689	3.415	5.107	99.43	80.67
5%Al :CuO	34±0.004	36.1	8.82	4.688	3.418	5.113	99.39	81.82
15%Al :CuO	36±0.007	30.5	7.54	4.680	3.419	5.120	99.33	80.96
25%Al : CuO	42±0.003	27.7	5.96	4.680	3.419	5.122	99.38	80.88
50%Al:CuO	46±0.004	25.5	4.65	4.685	3.413	5.107	99.44	80.55

IV.4. Vibration spectroscopy investigations using FT-IR

Figure IV.6 depicts the Fourier-transform infrared (FT-IR) spectra of undoped copper oxide films and those doped with aluminum. These spectra were obtained within the wavelength range of 400-3600 nm. The technique of Fourier Transform Infrared (FT-IR) spectroscopy is commonly employed in order to analyze and ascertain the chemical characteristics of a given substance. Through the examination of the distinct vibration modes .

Multiple absorption bands have been identified in the reported spectra. Specifically, the absorption peaks detected at 472 cm^{-1}, 616 cm^{-1}, and 667 cm^{-1} can be attributed to the distinctive stretching vibrations associated with the Cu-O bond in CuO[176].Additionally, an vibration mode was detected with frequency 1742 cm^{-1}, which corresponds to the stretching vibrations of the C=O band. Another vibration mode at 1641 cm^{-1} was also identified, in connection with the H-O-H bond vibration the presence of hydroxyl groups coupled to adsorbed water [177]. The spectral bands observed at wavenumbers of 1110 cm^{-1} and 1155 cm^{-1} can be ascribed to the existence of asymmetric stretching vibrations of Si-O-Si. [178]. Following the introduction of Al doping, additional vibrations emerge, indicative of the presence of Aluminum oxide. These vibrations are observed at specific wavenumbers, namely 520 cm-1, 580 cm^{-1}, and 739 cm^{-1}, corresponding to the vibrational modes associated with the Al-O bonds. The corresponding to the Al-O-H is centered at 1011 cm^{-1} [179].

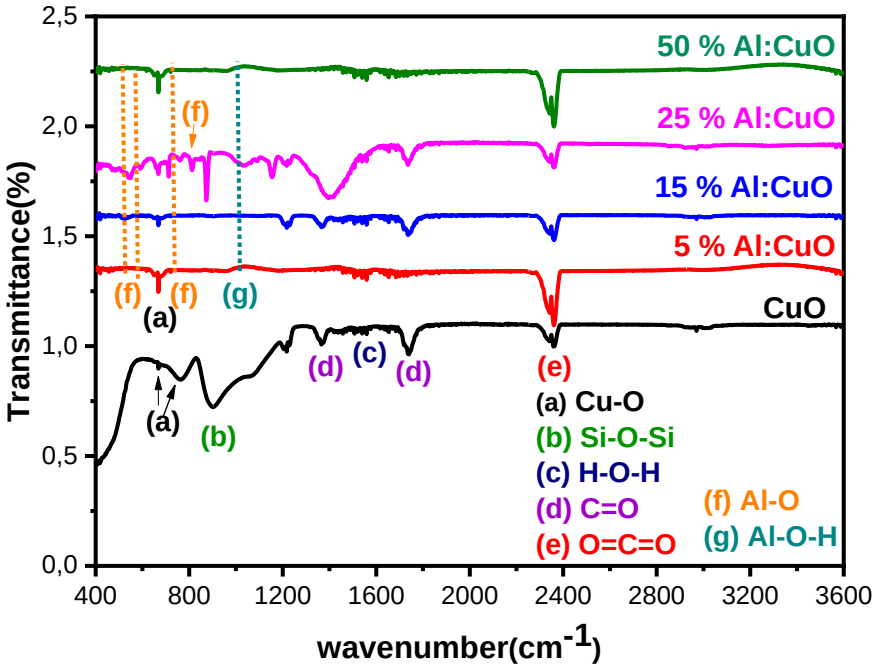

Figure IV.6. FT-IR spectra for copper oxide undoped and doped with Al.

IV.5. Scanning Electron Microscopy

Figure IV.7 displays the results of the scanning electron microscopy examination conducted on both pure and Al-doped CuO thin films. The surface of pure CuO exhibits homogeneity and a comparatively smooth texture, characterized by a reduced level of roughness. The structure is formed by the clustering of nanospheres accompanied by the presence of microcracks. Following the introduction of doping by Al, it is observed that significant alterations and enhancements occur in the surface characteristics. Specifically, the surface becomes notably smoother, denser, and more homogenous, exhibiting a nano-spherical shape. Additionally, the presence of holes is detected, which contributes to the improved degradation of photocatalysis.

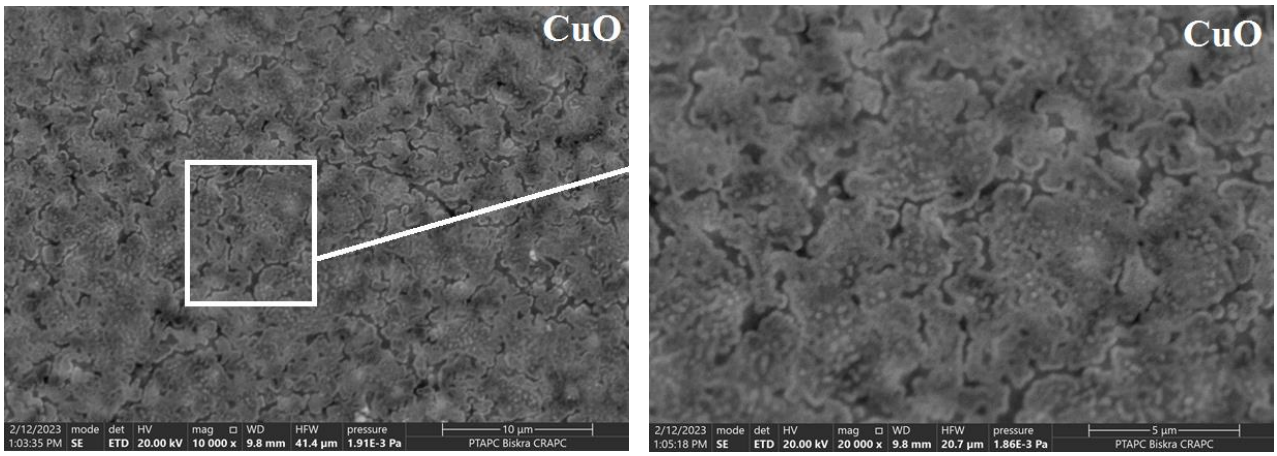

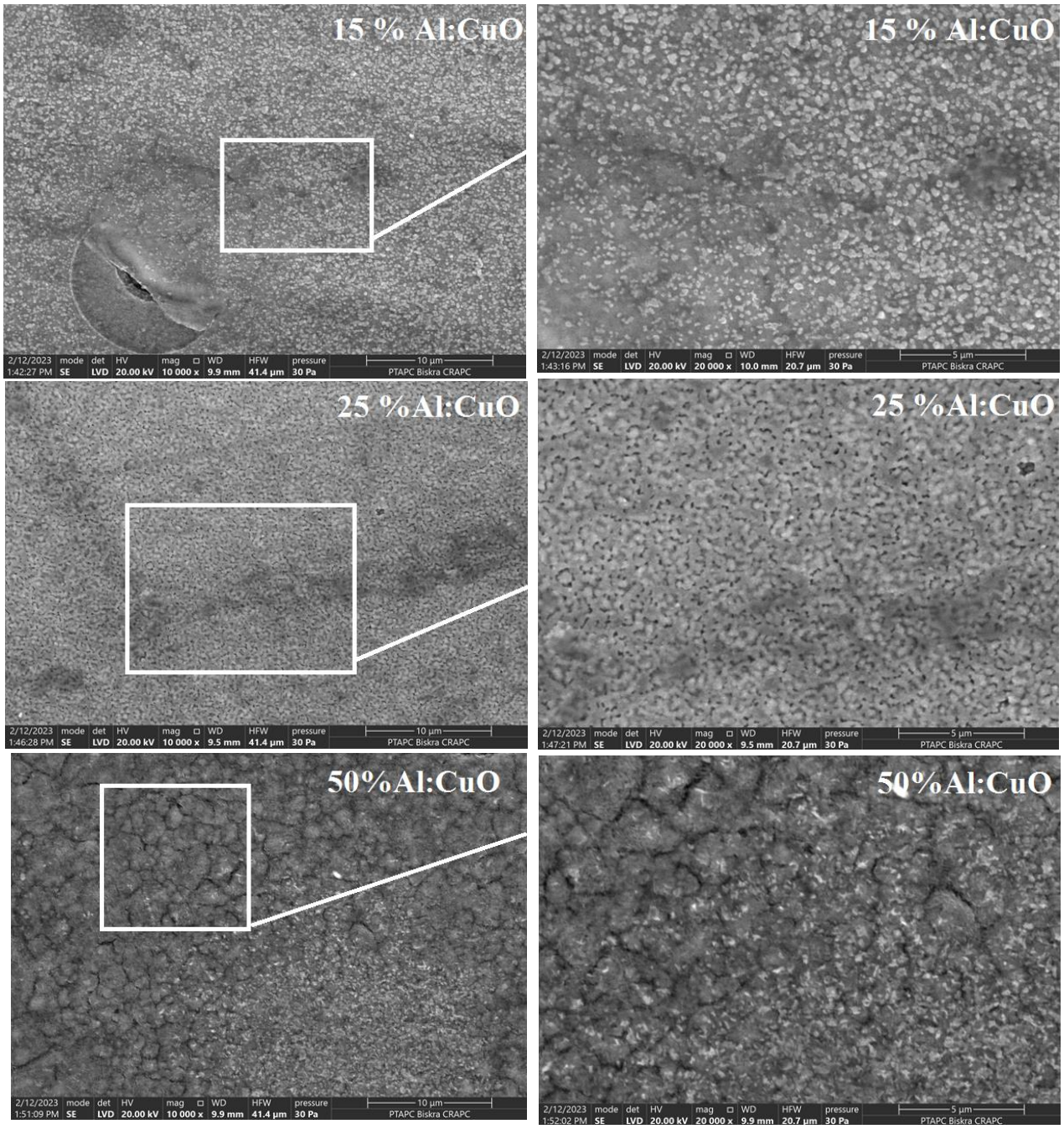

Figure IV.7. SME image for copper oxide undoped and doped with Al in 10 μm and 5 μm.

EDX analysis was conducted to investigate the chemical composition of the various samples. The atomic percentages of the key elements (oxygen, copper, and aluminum) were obtained from the EDX spectra, as depicted in Figure IV.8. The presence of the element aluminum (Al) has been verified in the context of doping. The observed trend indicates a positive correlation between the doping rate and the rise in the measured value (1.52% for a

doping rate of 15% Zn, 2% for a doping rate of 25% Zn, and 3.12% for a doping rate of 50% Zn). As seen in Table IV.2. The X-ray diffraction (XRD) analysis validates the obtained results.

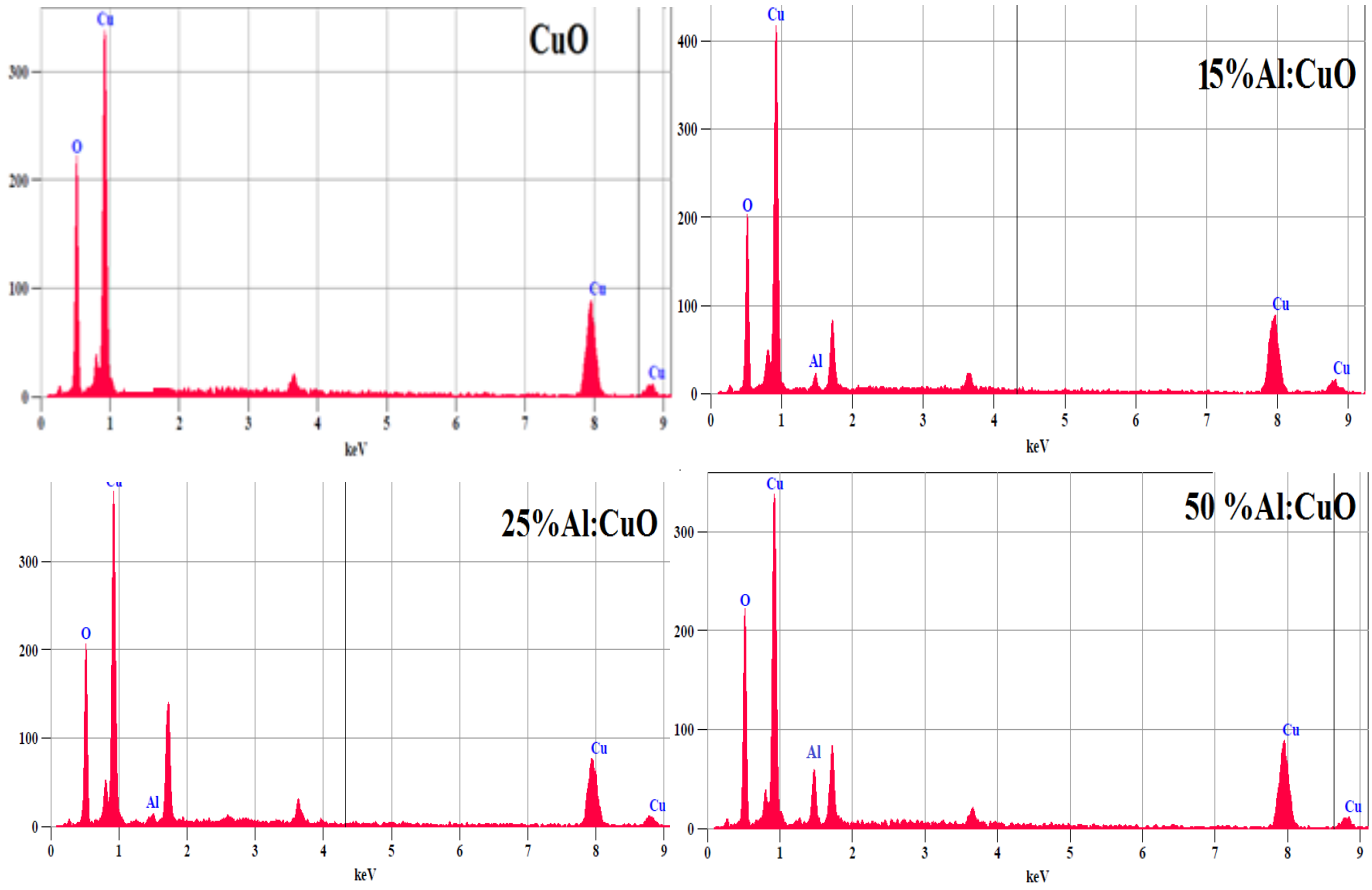

Figure IV.8. EDX spectrum of CuO undoped and doped with Al.

Table IV.2. The ratio of chemical components of CuO undoped and Al-doped.

	Weight %		
Phases	**Cu**	**O**	**Al**
CuO	84.44	15.56	0
15%Al :CuO	72.17	26.31	1.52
25%Al :CuO	70.48	27.52	2
50%Al :CuO	71.74	25.14	3.12

IV.6. Raman analysis

Figure IV.9 depicts the Raman spectra obtained from thin films consisting of pure copper oxide and copper oxide doped with varying proportions of aluminum, within the spectral range of 200-800 cm^{-1}. The latter is comprised of three primary Ag and two Bg modes, which are situated at approximately 278 cm^{-1}, 326 cm^{-1}, and 611 cm^{-1}, respectively. This study investigates the production of a tenorite phase characterized by a monoclinic structure of copper oxide [180, 181]. The observed peak shift can be elucidated by the presence of Al^{3+} ions that occupy the substitutional position within the crystal lattice of copper oxide. The experimental results indicate that the strength of the Ag peak exhibits an increase in response to doping, while concurrently displaying a drop in full width at half maximum (FWHM). This phenomenon can be attributed to the enlargement of the crystallite dimensions, resulting in a concomitant decrease in the presence of micro deformation. The Raman spectra of α-Al_2O_3 structures is given as $2A_{1g} + 2A_{1u} + 3A_{2g} + 2A_{2u} + 5E_g + 4E_u$. The presence of additional peaks of low intensity around 533 cm^{-1} and 644 cm^{-1} attributed to the Raman mode E_g and A_{1g} respectively which show the formation of a new phase of α-Al_2O_3 [182]. Based on the obtained data, it can be observed that the structural properties of the layers exhibitan enhancement with the incorporation of aluminum doping.

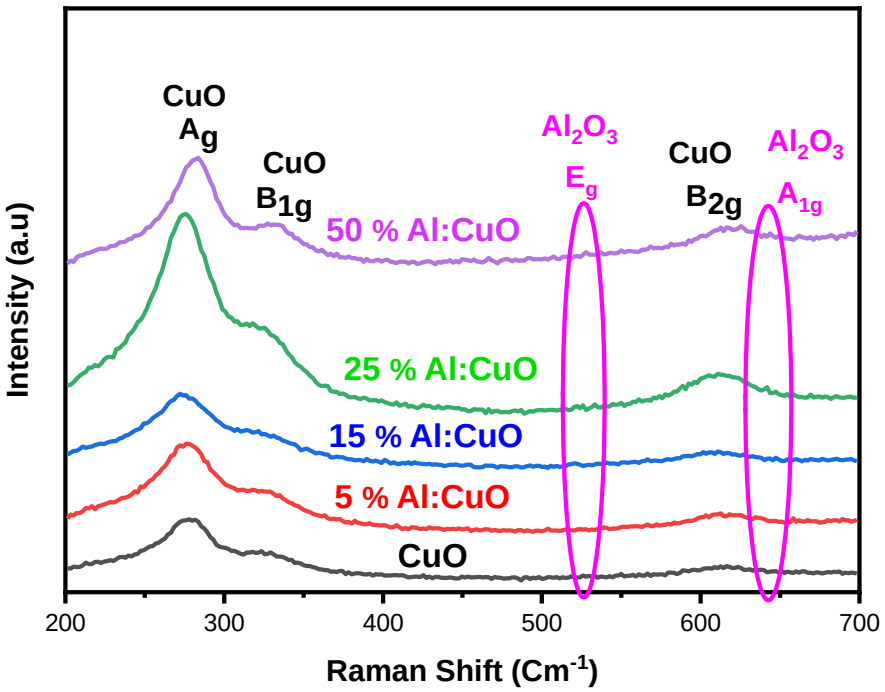

Figure IV.9. Raman spectra of Aluminum doped copper oxide.

IV.7. Optical properties

IV.7.1. Absorbance spectra

Figure IV.10 shows the absorption spectra of pure CuO and Al-doped copper oxide thin films. The absorption spectra of all films have peaks at wavelengths of 256.56 nm, 311.59 nm, and 400 nm. This observation confirms the existence of copper oxide [183]. In another study, it was observed that the layers exhibit a significant absorption around 410 nm, which is consistent with the band gap transition of the CuO [184]. It is noted that there is an influence of the Al atoms on the absorbance. All films have a higher absorbance due to the addition of aluminum compared to pure CuO. Thin film of 5%Al: CuO explain this behavior, confirming well the homogeneous and smooth surface, which prevents light. More precisely, doping by Al reduces the width of the band gap, nevertheless the absorption of these films. This allows the electron to pass through the valence band into the conduction band. A similar study shows an increase in absorption in the presence of doping [183, 185, 186].

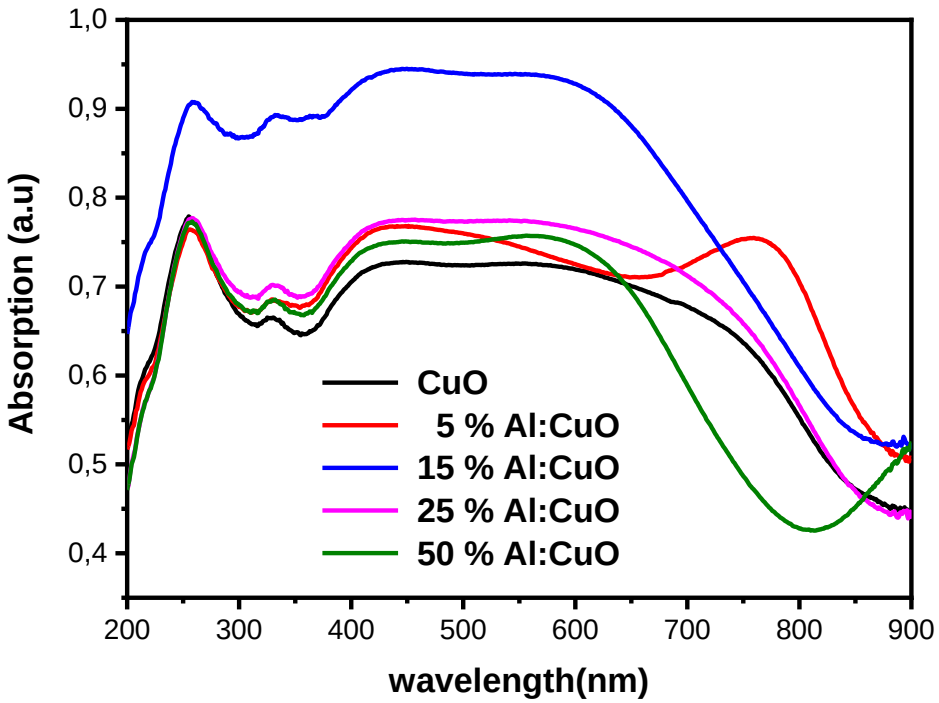

Figure IV.10. Absorbance spectra of thin films of copper oxide pure and doped with Al.

IV.7.2. Transmittance spectra

The transmittance spectra of Al-doped pure copper oxide thin films are recorded in the wavelength range of 200-900 nm as shown in Figure IV.11. It is noted that the transmittance in all films is increases at longer wavelengths in the region λ >350nm, Also in the case of pure CuO the transmittance is 4% after Al doping and the transmittance increases up to 15% at 5% Al doping rate. Then in the doping by 15% the transmittance is 18%. This increase in transmittance is explained by the smoother surface of these films reducing the scattering of light and showing lower thicknesses. In the case of 25% and 50% Al doping, the transmittance is reduced, explained by the roughness of the surface which causes the scattering of light, and also showing a increase in thickness in these films. In the region of λ<350nm we note that the transmittance is almost 0% .Also a shift towards the longest wavelengths is signing a reduction of the band gap energy with the increase in doping. A similar study shows the same variation of increase and decrease in transmittance with the existence of Al doping [172].

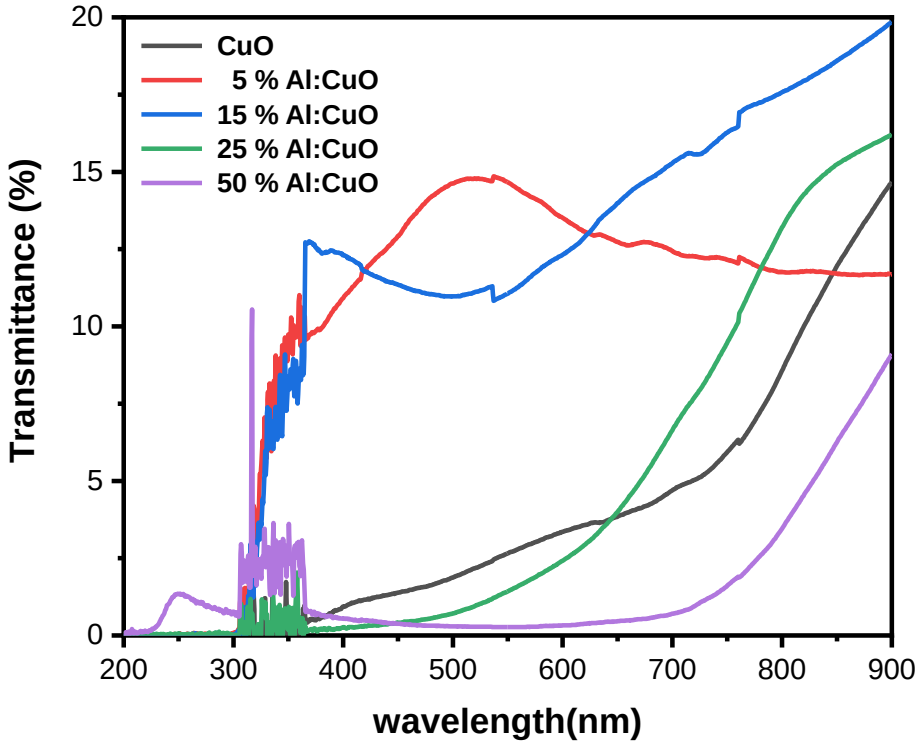

Figure IV.11. Transmittance spectra of CuO doped with Al.

IV.7.3. Energy Gap

The direct band gap of pure copper oxide and copper oxide doped with aluminum is determined using the Tauc relation, as described by Equation (II.17). The observed gap energy values, ranging from 2.62 to 1.8 eV, exhibit a reduction as the doping rate increases (see Figure IV.12). This observation suggests that the band gap energy is impacted by several variables, with the doping rate of aluminum playing a significant role. It is worth mentioning that a relationship of inverse proportionality exists between the dimensions of the crystallites and the optical band gap energy. This phenomenon can be attributed to the quantum confinement size effect [183]. Additionally, the decrease in band gap energy can be attributed to the transfer of charges between the conduction and valence band electrons of CuO and the electrons of Al^{3+} ions. The process of charge transfer in Al-doped CuO nanostructures has the potential to generate trapping levels, resulting in a reduction of the band gap of CuO [186]. According to a comparable investigation, it has been shown that there is a drop in the band gap energy as the size of the crystallite increases [185]. A recent investigation reveals that the utilization of doping agents leads to an augmentation in the gap energy as the size of the crystallite decreases [183].

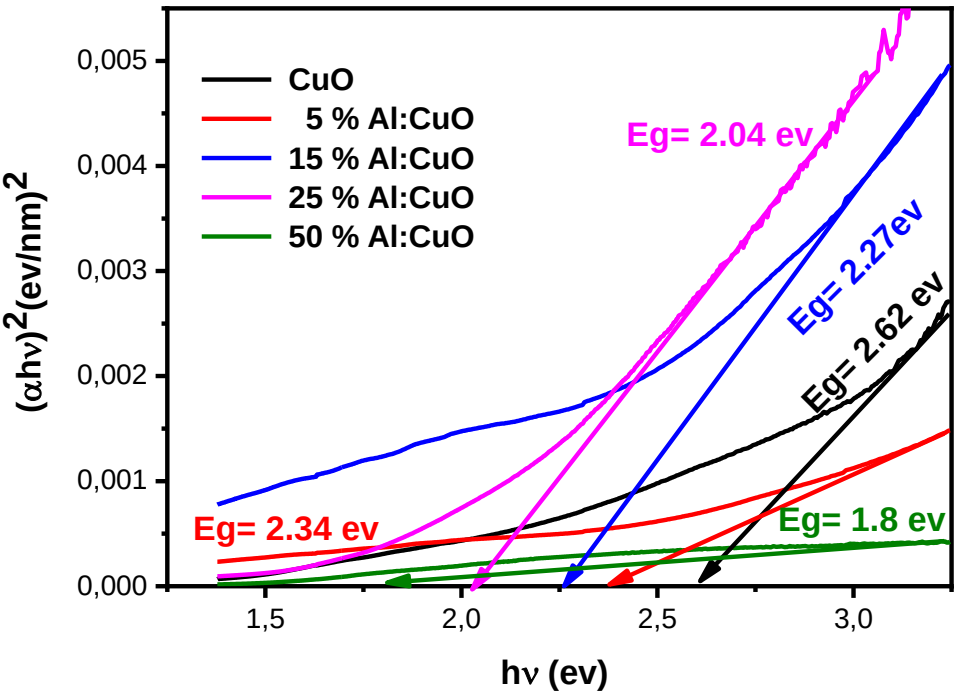

Figure IV.12. Energy gap for copper oxide pure and doped with Al.

IV.7.4. Absorption coefficient

Figure IV.13 illustrates the fluctuation of the absorption coefficient for both pure and Al-doped CuO films within a wavelength range of 350-900nm.

It has been shown that the absorption coefficient in all films exhibits a decrease as the wavelength increases. Also, the value of the absorption coefficient (α) in all films is $> 10^4$ which demonstrates direct transitions [187]. The observed increase in the absorption coefficient resulting from Al doping of 15% and 25% can be attributed to the doping effect, which enhances the generation of electron-hole pairs. These pairs are responsible for facilitating direct transitions following photon absorption. However, in the case of Al doping 50% , a reduction in absorption is observed. This can be explained by the presence of a rapid recombination phenomenon, likely due to the significantly small band gap energy value compared to other films.

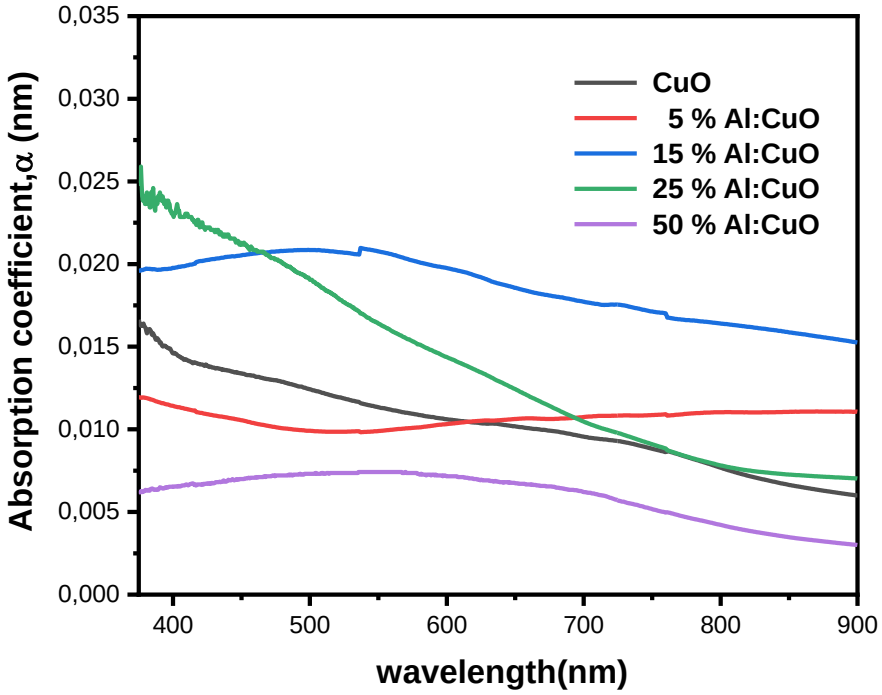

Figure IV.13. Absorption coefficient as a function of wavelength for copper oxide undoped and doped with Al.

IV.7.5. Extinction coefficient

Figure IV.14 illustrates the relationship between the extinction coefficient and wavelength for both pure and Al-doped CuO thin films.

The observed extinction coefficient in all of the films exhibits a strong correspondence with the absorption coefficient spectra, suggesting a clear correlation between these two parameters. Furthermore, the introduction of aluminum (Al) atoms significantly influences the optical properties. The films that were doped with a 15% aluminum concentration exhibited the greatest extinction coefficient. This observation can be explained by the substantial buildup of energy by the electrons within the material layer.

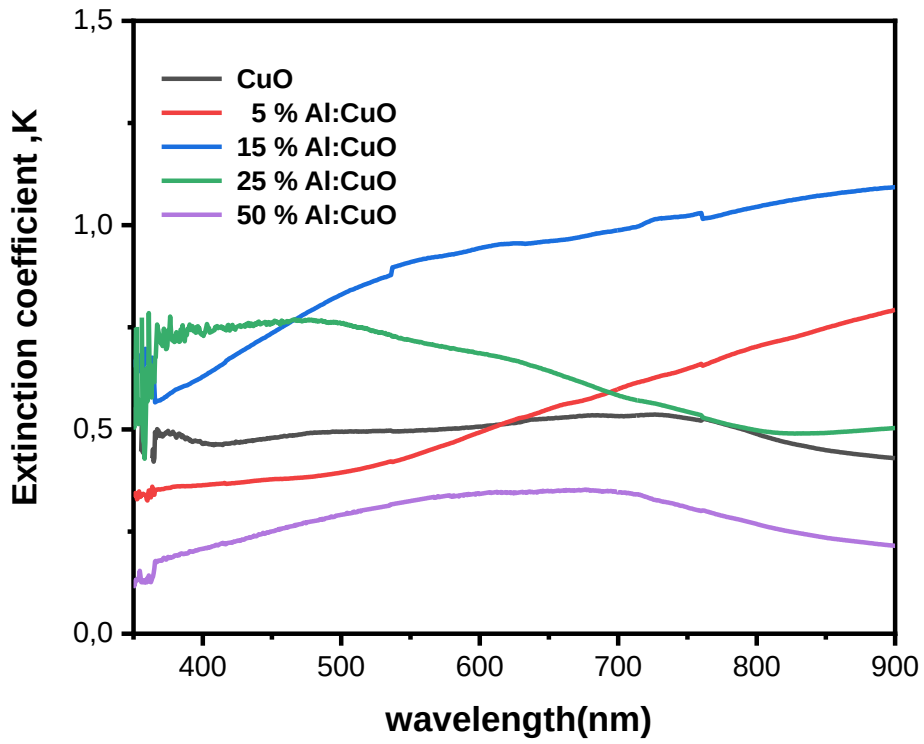

Figure IV.14. Extinction coefficient as a function of wavelength for CuO undoped and doped with Al.

IV.8. Electrical properties

Figure IV.15 depicts the fluctuations in the conductivity and electrical resistivity of both pure copper oxide films and those doped with aluminum.

As indicated by equation (II.12). There is an inverse connection between conductivity and resistivity .The observed phenomenon is that the electrical conductivity is enhanced as the rate of aluminum doping increases. This can be attributed to two factors: the increase in crystallite size, which reduces the band gap energy, and the presence of grain boundaries that serve as traps for free carriers. Consequently, the lifetime of carriers is prolonged, resulting in reduced resistance and an overall increase in conductivity. A comparable investigation yields congruent findings about conductivity [188].

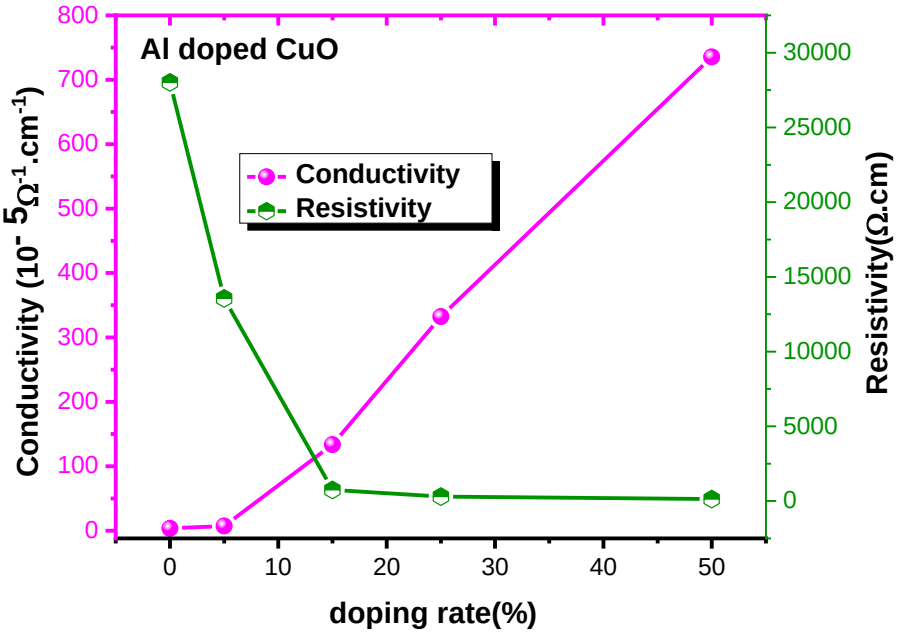

Figure IV.15. Conductivity and resistivity as a function of doping rate for CuO pure and doped with Al.

IV.9.Photocatalytic Performance

To assess the catalytic characteristics of the films that were prepared, we conducted an investigation into their potential application in photocatalysis for the degradation of the Orange II dye under UV irradiation. Figure IV.16 illustrates the spectra depicting the degradation of the dye in the presence of active films composed of pure CuO and Al-doped CuO films. All of films exhibit a peak absorption at a wavelength of λ= 485nm, which corresponds to the absorption of Orange II. Moreover, the observed reduction in absorbance as the irradiation period increases provides further evidence of the solution's deterioration in the presence of active coatings. Following a 5-hour irradiation period, it has been shown that the degradation of pure CuO is 15% when subjected to Al doping at various concentrations (5%, 15%, 25%, 50%). Notably, the degradation rate exhibits a rise to 29%, 32%, 33%, and 61%, corresponding to the aforementioned Al doping concentrations. The observed enhancement in the degradation of orange II can be attributed to the active nature of aluminum as an element and its effectiveness as a catalyst in the application of photocatalysis. Moreover, the reduction in the band gap energy leads to an increase in the number of electron-hole pairs. which are responsible for the discoloration by the generation of a large number of superoxide radicals ($O^{\bullet}$) and hydroxyl radicals ($OH^{\bullet}$), respectively.

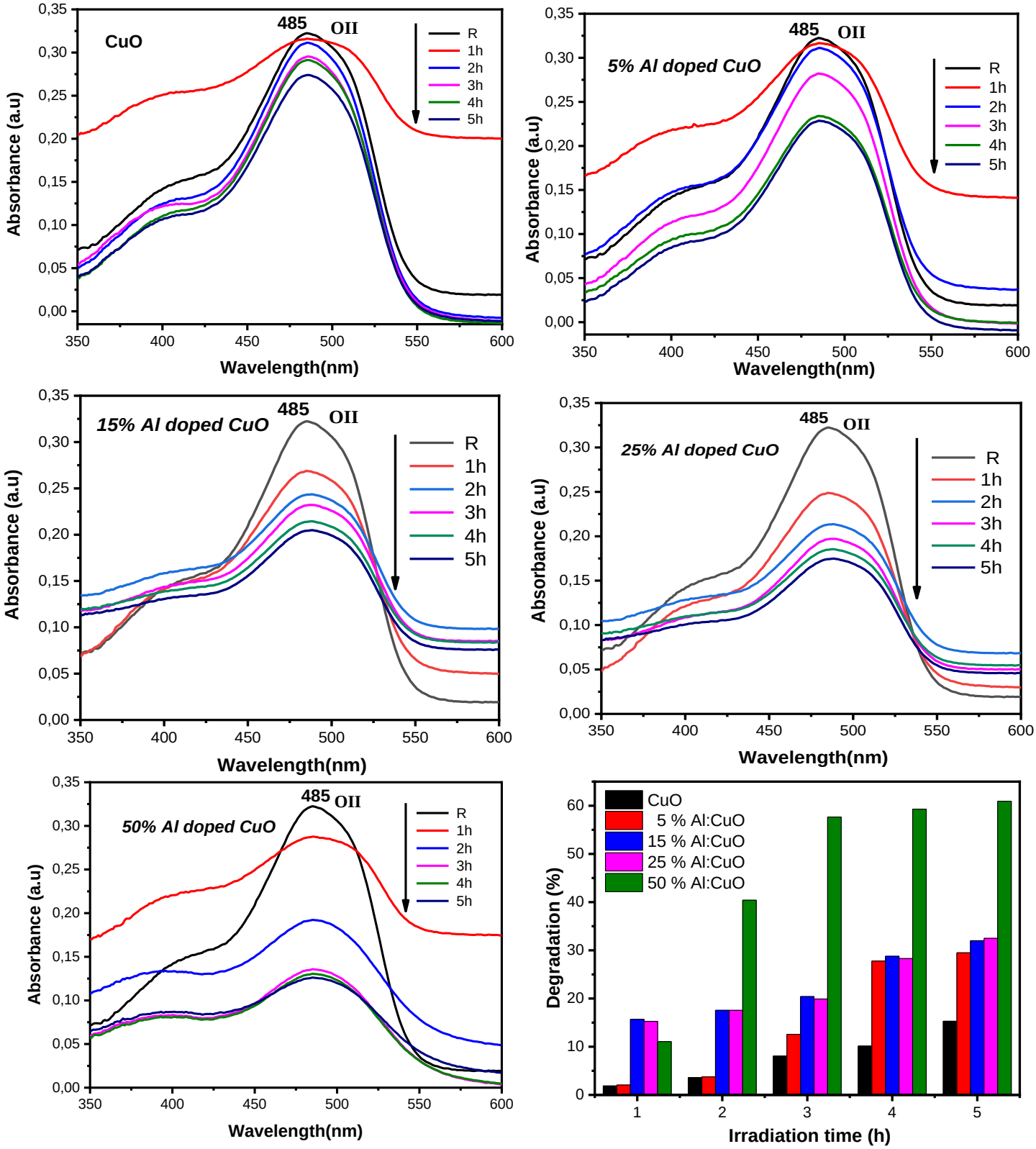

Figure IV.16. Absorption spectrum and degradation of orange II solution under UV irradiation for thin films of CuO pure and doped with Al.

In order to ascertain the degradation rate of the aforementioned films, we have constructed a plot depicting the alteration of absorption ratio in relation to irradiation duration, as illustrated in Figure IV.17. It is seen that all the films exhibit a reduction in absorption ratio with the introduction of doping. The observation reveals that the deterioration rate of pure CuO and CuO doped with 5% Al is nearly the same during the initial 3-hour period. However, a notable disparity arises thereafter, as the films doped with 5% Al exhibit a considerably accelerated degradation compared to the undoped CuO films. Moreover, this trend becomes more pronounced for films doped with 15% Al and 25% Al. The deterioration seen after a 5-hour period is nearly equivalent to the degradation found in the case of 50% aluminum doping. Notably, the coloring of the Orange II solution exhibits quick and effective degradation.

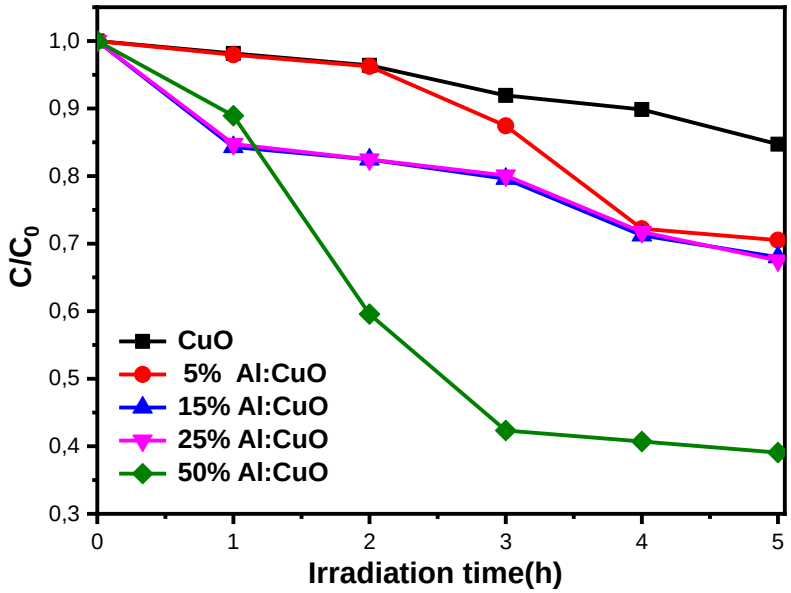

Figure IV.17. Variation of C/C_0 of orange II solution under UV irradiation as a function of irradiation time.

IV.9.1. Kinetics of degradation

In this work, we use the first-order kinetic model, see equation (I.15) to investigate the kinetics of the degradation process of the selected dye in the presence of thin films composed of pure CuO and CuO doped with Al. Figure IV.18 represents the variation of ln (C_0/C) as a function of the irradiation time, We note that all the spectra represent a straight line. The slope of this linear regression gives the first order rate constant K. It should be noted that the degradation rate exhibits a range of variability, ranging from 0.0032 cm^{-1} to 0.211 cm^{-1}.

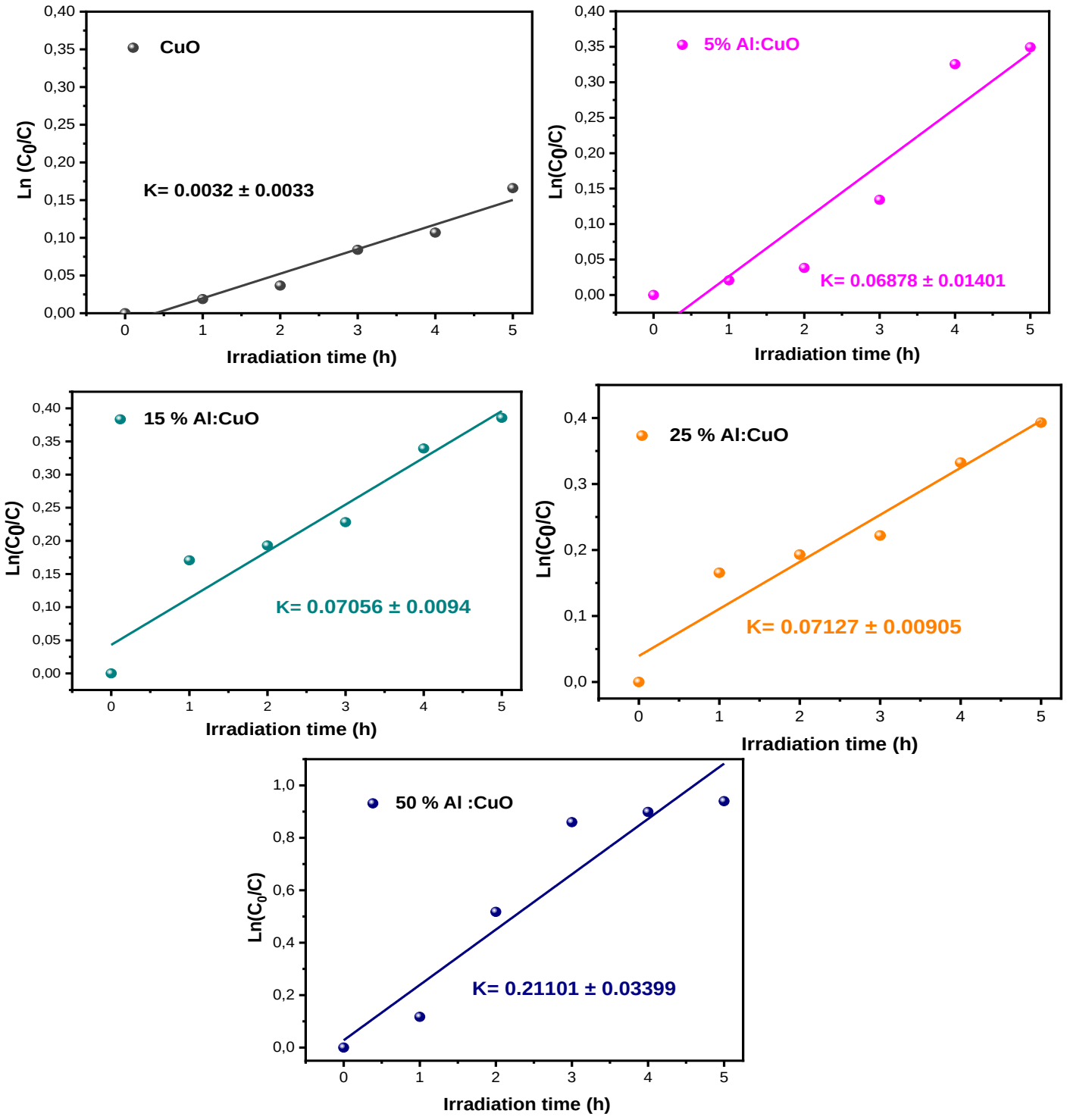

Figure IV.18. Variation of Ln (C_0/C) in the presence of CuO pure and doped with Al as a function of irradiation time.

IV.9.2. Photocatalytic Mechanism

The photocatalysis for the degradation of the Orange II solution has been studied based on active films of copper oxide undoped and doped with 5% , 15% , 25% , and 50% Aluminum. These films are excited by UV light with an energy greater than or equal to the optical band gap energy of the catalysts for the generation of electron/hole pairs,see reaction (IV.1)below. The holes in the valence band influence water to produce hydroxyl radical see reaction (IV.2). Then the electrons are involved in the reduction of O_2 to $O_2^{\cdot -}$ by reducing to give to the solution its white color (IV.6) [189,190]. The latter reacts with the Orange II dye for degradation and then produces CO_2 and H_2O. With the existence of Al doping, a large number of the pairs which is responsible for the degradation procedure. This is due to the increase in doping rate. Also, the surface of films doped with Al consists of pores enhancing degradation.

$$CuO + Al_2O_3 + h\upsilon \longrightarrow e_{CB}^{-} + h_{VB}^{+} \quad \text{(IV.1)}$$

$$O_2 + e_{CB}^{-} \longrightarrow O_2^{\cdot -} \quad \text{(IV.2)}$$

$$H_2O + h_{VB}^{+} \longrightarrow OH^{-} + H^{+} \quad \text{(IV.3)}$$

$$OH^{-} + h_{VB}^{+} \longrightarrow OH^{\cdot} \quad \text{(IV.4)}$$

$$Dye + OH^{\cdot} \longrightarrow Dye^{+} \quad \text{(IV.5)}$$

$$Dye^{+} + O_2^{\cdot -} \longrightarrow CO_2 + H_2O \quad \text{(IV.6)}$$

IV.10.Conclusion

A glass substrate was utilized to develop a thin films of undoped copper oxide and copper oxide doped with aluminum using the sol-gel spin coating technique. The aforementioned films were employed for the purpose of investigating the impact of aluminum (Al) on several features, including structural morphology, optical characteristics, electrical behavior, and photocatalysis activity. The results indicate that the samples exhibit favorable electrical conductivity following Aluminum doping. The optical characteristics of the material were improved as a result of the presence of Aluminum impurity, leading to a substantial increase in absorption within the visible spectrum. Additionally, the band gap energy decreased as the doping rate increased. The surface of the films actively doped with Al is smooth, dense, and homogeneous with nano spherical shape with the existence of pores which improve the degradation of dyes through the photocatalysis process. Photocatalysis results showed that doping with copper oxide by poor metals like (Al) improves the photocatalysis efficiency and the best degradation of a dye (Orange II) reaches 61% for the use of thin layers of CuO doped with 50% Al.

Chapter V:

Elaboration and characterization of Ag-doped copper oxide thin films for photocatalysis application

V.1.Introduction

In this work, the first part, deals with the study of the structural, morphological, optical, and electrical properties of copper oxide doped with Ag at different concentrations (x = 0%, 5%, 15%, 25%, and 50%) . The sol-gel spin coating technique was employed for the fabrication of these samples. The $Cu_{1-x}Ag_xO$ thin films underwent characterization using various techniques, including X-ray diffraction, Fourier-transform infrared spectroscopy (FT-IR), UV-visible spectrophotometry, scanning electron microscopy (SEM), energy-dispersive spectroscopy (EDS), and the four-point method. In the subsequent section, examination of the utilization of these films in the context of photocatalysis for the purpose of decomposing the Orange II dye when subjected to UV irradiation is performed. Additionally, We explore the underlying principles and mechanisms involved in the degradation process.

V.2.Thickness measurement

Using a profilometer, the thickness of CuO pure and Ag-doped copper oxide thin films was measured. The results are shown in Figure V.1. It should be noted that with increasing doping, the thickness of these films increased. It ranges from 320 nm to 670 nm.

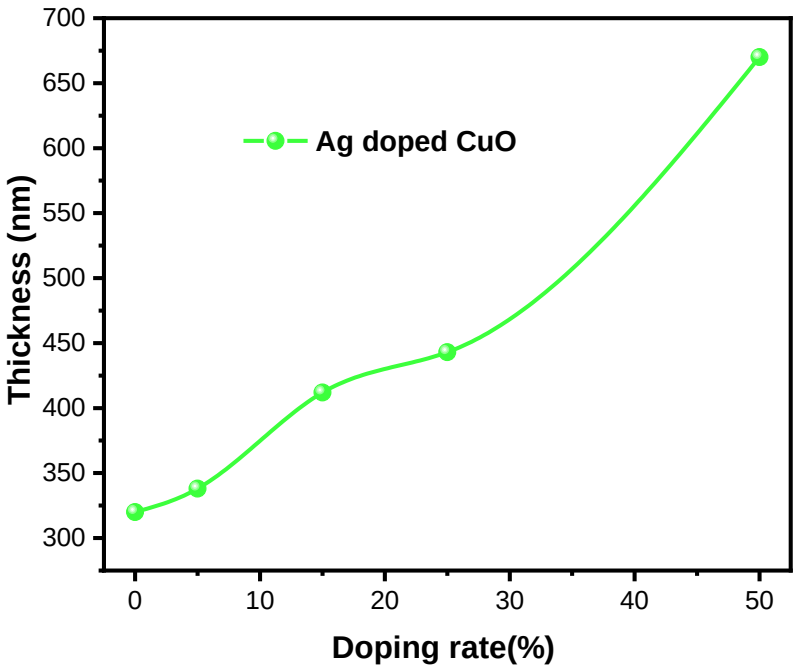

Figure V.1. Thickness of copper oxide pure and doped with Silver.

V.3.Results and discussion

V.3.1.X Ray Diffraction

Figure V.2 displays XRD spectra of Ag-doped CuO (Ag: CuO) thin layers, that were captured in the 2θ range between 25° and 70°; It displayed many crystal planes,namely (110), (-111),(200),(-202), (020), (202),(-113),(-311)and ,(220) planes .This is in good agreement with the JCPDS file code 00-041-0254 which attest to the existence of the monoclinic structure. After Ag doping and when the doping exceeds 5%, there are additional peaks corresponding the presence of the secondary phases. The existence of the phase of Ag_2O is observed through the four diffraction peaks observed at 2θ =27.77°,38.26°,54.68°,64.55°which respectively correspond to the planes (110), (200), (211), (311) in good agreement with the JCPDS file (code00-041-1104). According the JCPDS card (code00-040-0909) the (440) plane was observed indicating of the formation of Ag_2O_3 phase.

These peak positions have clearly shifted towards lower angles, and this change is evidence that ,the Cu^{2+} of ionic radius 0.73Å is occupied by Ag atoms with an ionic radius of 1.15 Å [191,192].

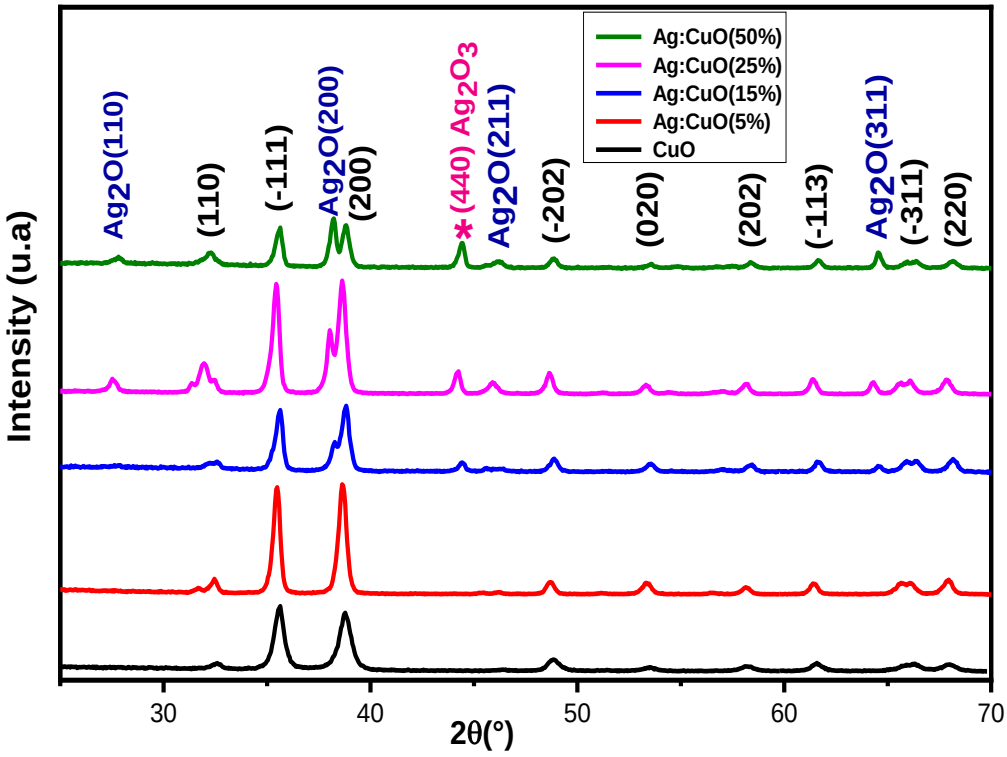

Figure V.2. XRD spectra of thin films of Ag-doped CuO.

V.3.2.Texture coefficient

When determining the texture coefficient (Tc) and finding the preferred orientation of these films, equation (II.11) is used. Figure V.3 represents the variance of the texture coefficient for the two planes (-111) and (200) for the films of CuO pure and various percentages of doping with Ag. Note that the texture coefficient (>1) in the case of pure CuO corresponds to the (-111) plane. After the doping by silver, we note that there is a change in the preferential orientation according to the (200) plane.

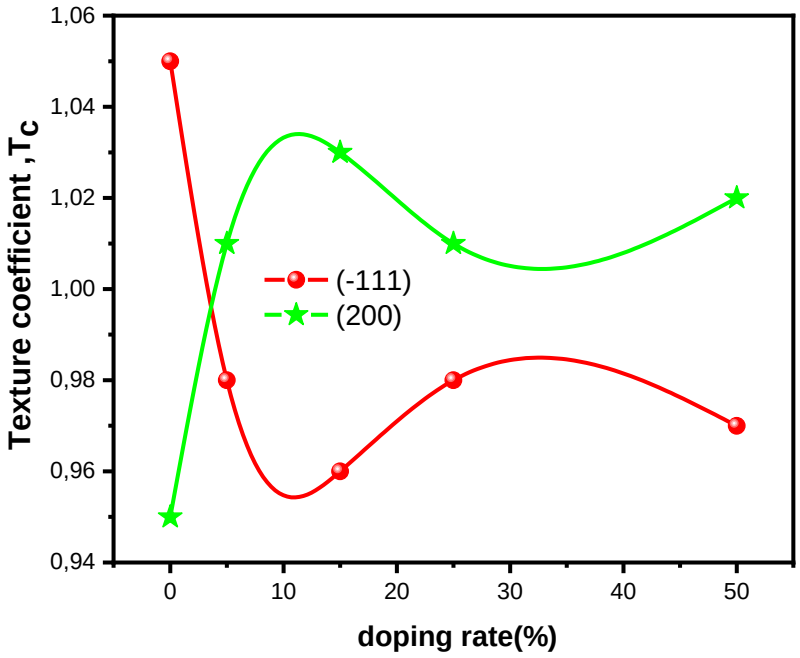

Figure V.3. Texture coefficient as a function of the doping by silver at (-111) and (200).

V.3.3.Crystallite size and micro-strain

The Williamson-Hall relationship see equation (II.10) was used to calculate the crystallite size and the microstrain of CuO pure and Ag-doped CuO thin films. The trace of β.Cos (θ) as a function of 4. Sin (θ) is shown in Figure V.4.

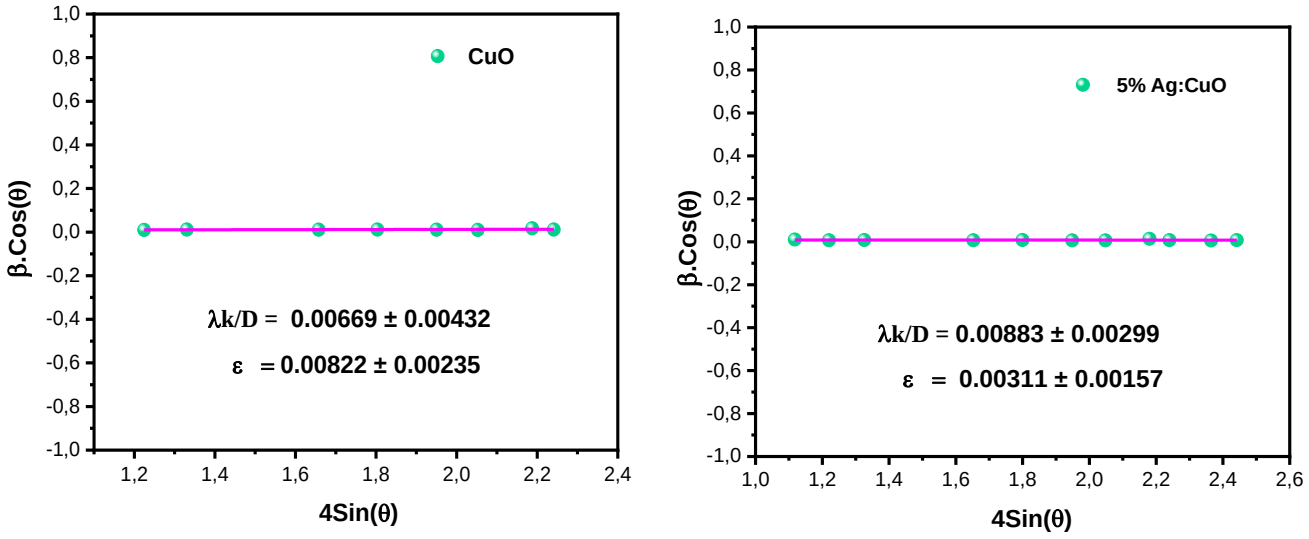

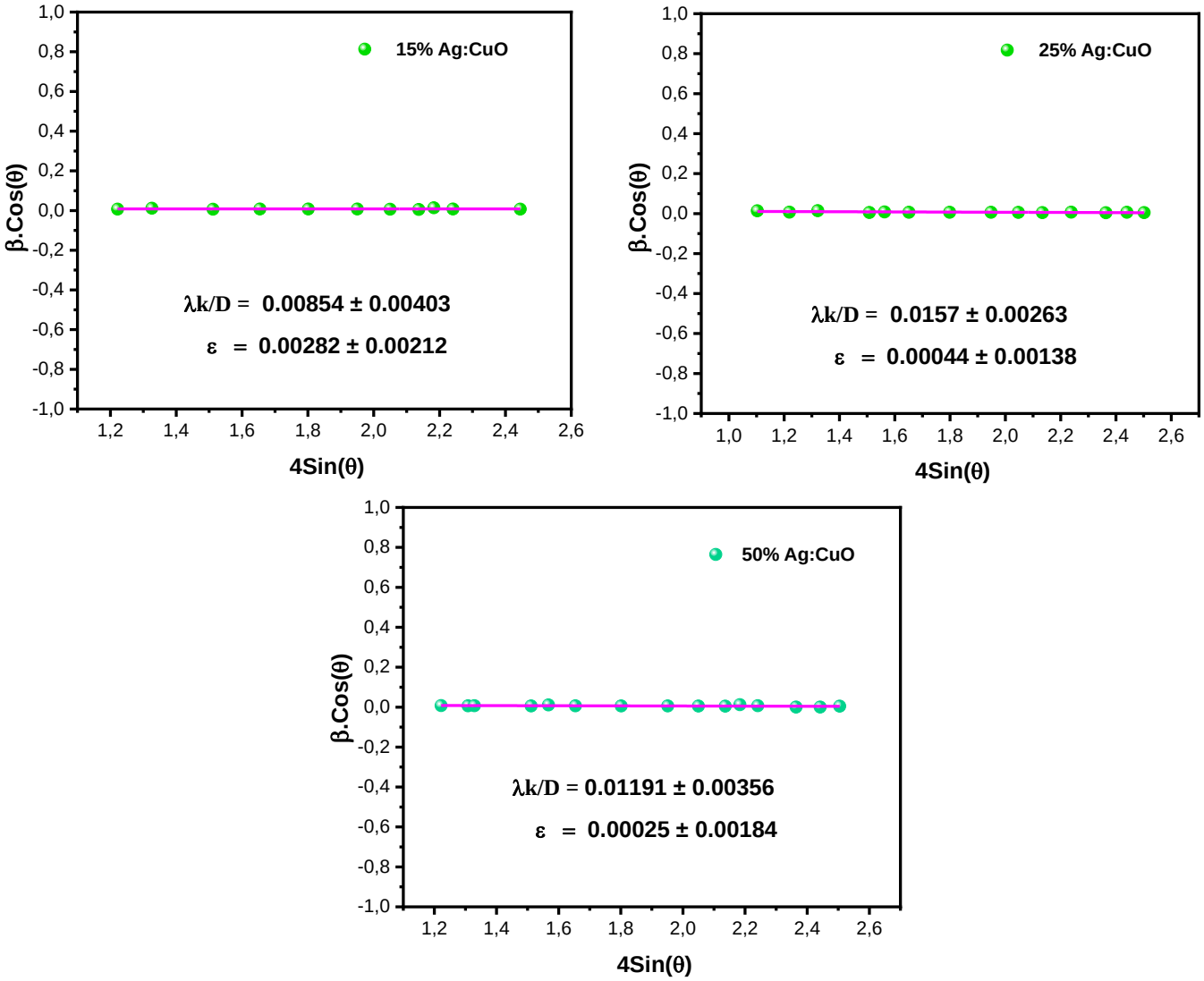

Figure V.4. Williamson Hall plots of CuO undoped and doped with Ag.

Crystallites size range from 21 nm to 33 nm and increases when the doping with Ag increases due to the ionic radius of the silver atom, see Figure (V.5). Several studies have investigated the increase of the crystallite size in case of CuO doped with Ag [193,194].Ag doping CuO improved the crystallinity of these films with an increase in crystallites size and a decrease in strain.

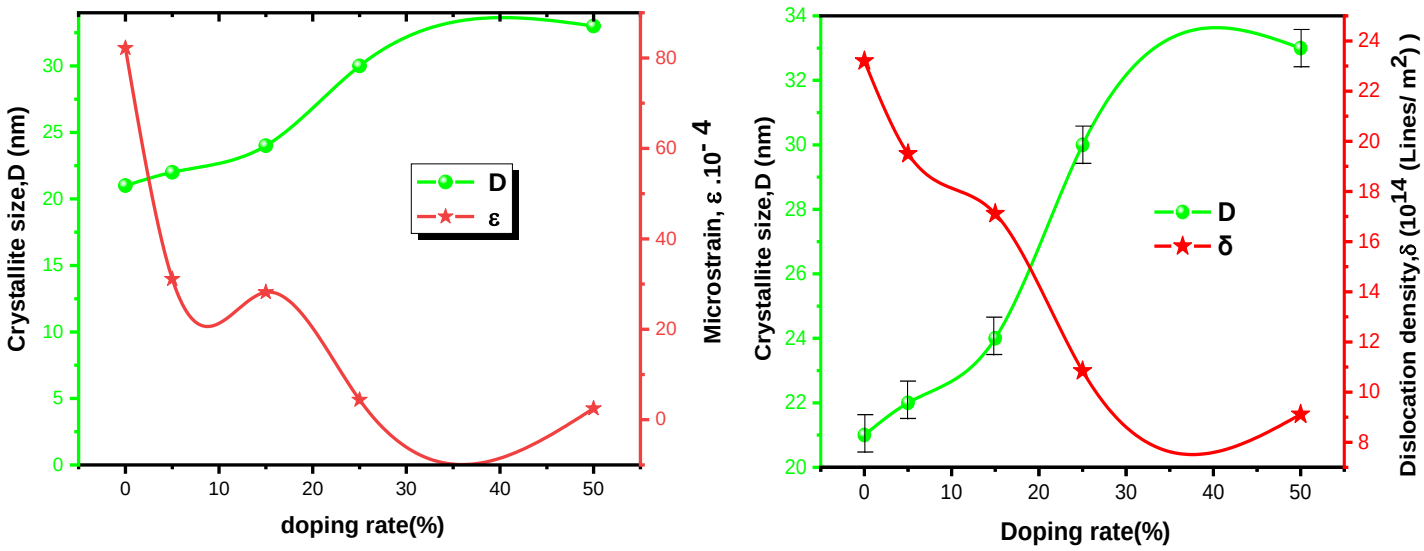

Figure V.5. Variation of crystallite size, microstrain, and dislocation density as a function of doping with Ag.

V.3.4.Lattice parameters

The values of the network parameters are displayed in Table V.1. It has been observed an increase of lattice parameters (a, b), angles β, and volumes of the crystal lattice in all of the thin films doped with silver. The obtained outcome suggests the existence of lattice dilatation effect.

Table V.1. Crystallite size and lattice parameters for thin films of copper oxide pure and doped with Ag deposited by a spin coating method.

Phases	D (nm)	$\varepsilon.10^{-4}$	$\delta.10^{14}$ (Lines/ m²)	a(Å)	b(Å)	c(Å)	β (°)	v (Å³)
CuO	21±0.004	82.2	23.2	4.689	3.415	5.107	99.43	80.67
Ag :CuO (5%)	22±0.002	31.1	19.5	4.728	3.426	5.079	99.47	81.14
Ag :CuO (15%)	24±0.004	28.2	17.11	4.709	3.426	5.075	99.44	80.94
Ag :CuO (25%)	30±0.002	4.4	10.84	4.709	3.426	5.102	99.60	81.2 3
Ag: CuO (50%)	33±0.003	2.5	9.11	4.691	3.416	5.098	99.50	80.81

V.4.Vibrational Spectroscopy

The Fourier Transform Infrared (FT-IR) spectra of thin films of Copper Oxide (CuO) and Copper Oxide doped with Silver (Ag) were obtained within the spectral range of 400-3600 cm-1. Figure V.6 illustrates the presence of multiple absorption bands, specifically at wavenumbers 472, 616, 667, and 718 cm^{-1}. These bands are attributed to the Cu-O bond vibrations and are indicative of the characteristic stretching vibrations of CuO [195].

Upon the introduction of silver at varying concentrations,namely (15%, 25%, and 50%), a substantial disparity becomes evident in the absorption spectra within the range of 400-1100 cm^{-1}. The observed peaks at 708 cm^{-1}, 804 cm^{-1}, 866 cm^{-1}, and 1147 cm^{-1} exhibit characteristics of the Ag-O bond, while the peak at 460 cm^{-1} is associated with the Ag bond Ag-O-Ag [196]. The presence of a robust chemical bond is noted to reach its maximum intensity at a wavenumber of 1742 cm^{-1}, indicating the occurrence of the C=O bond stretching vibrations. The observed peaks at 1641 cm^{-1} is indicative of the vibrational behavior of the H-O-H bond, specifically in relation to the vibration mode of hydroxyl groups that are bound to adsorbed water [197]. The spectral peaks detected at wavenumbers of 1110 cm^{-1} and 1155 cm^{-1} can be ascribed to the existence of asymmetric stretching vibrations of the Si-O-Si bond [198].

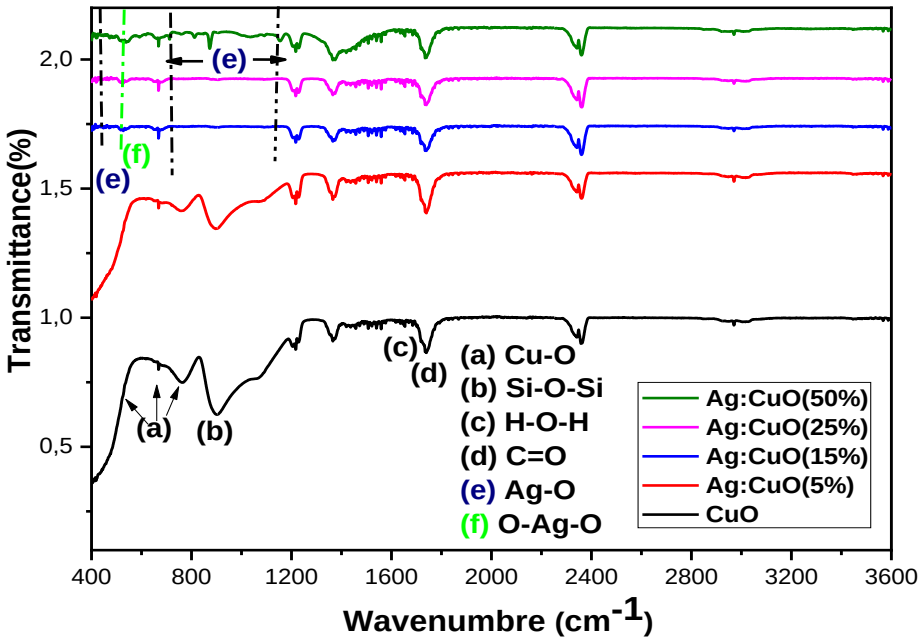

Figure V.6. Infrared spectra of the Ag-doped CuO with different percentages.

V.5. SEM Analysis

The investigation of the surface morphology was conducted using the Scanning Electron Microscope (SEM) on the thin films composed of Ag-doped copper oxide. The analysis revealed that all the films exhibited a dense deposition and uniform grain size, indicating the successful formation of a crack-free surface see Figure V.7. Previous research has demonstrated the presence of nano-spherical grains in pure copper oxide. However, a noticeable alteration in the grain morphology occurs upon the introduction of silver doping. The electron micrograph reveals that this alteration exhibits a distinct correlation with the degree of doping. Furthermore, the observation of a higher density of larger pores with an elevated doping rate provides evidence that the presence of Ag contributes to the formation of a surface with increased porosity.

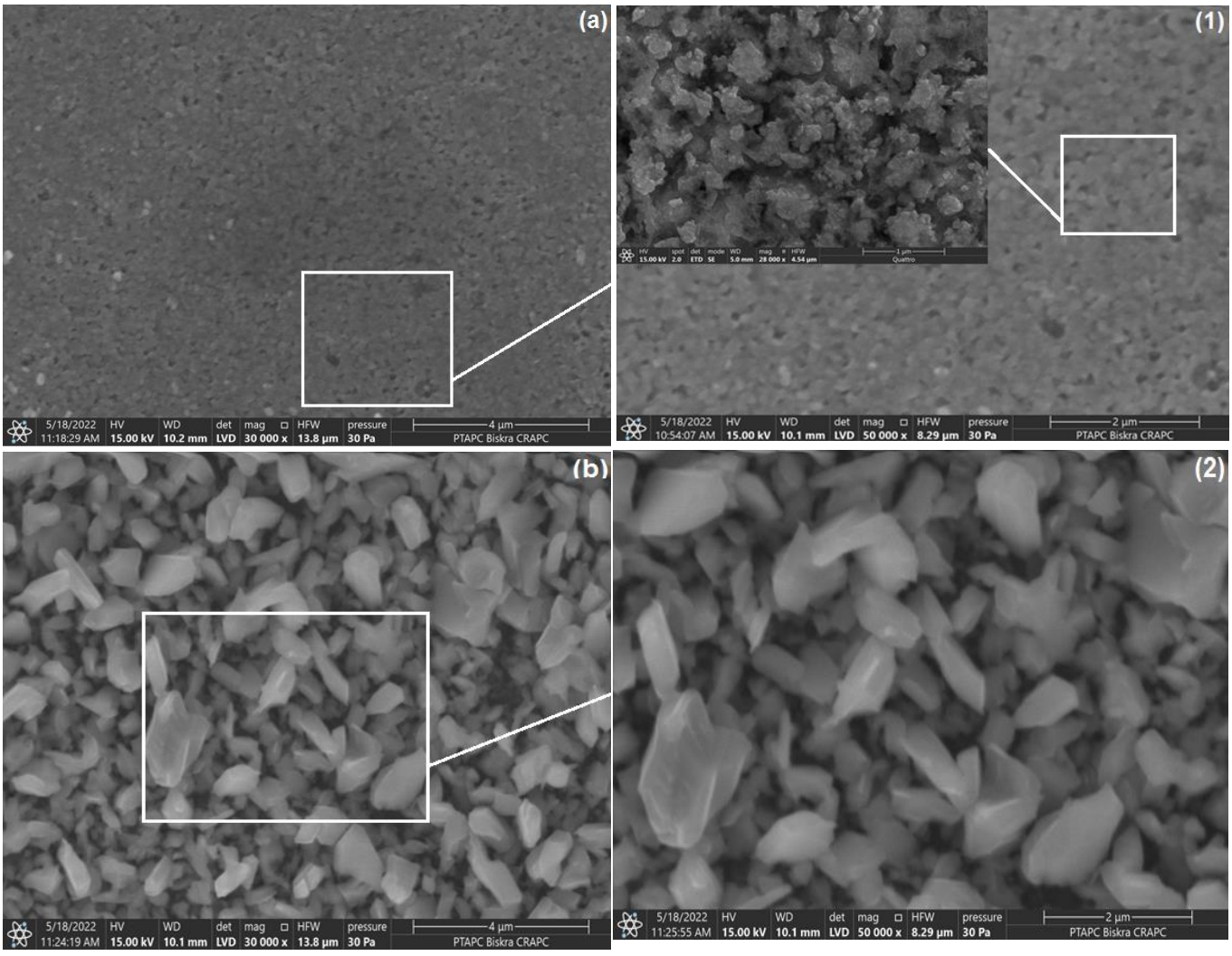

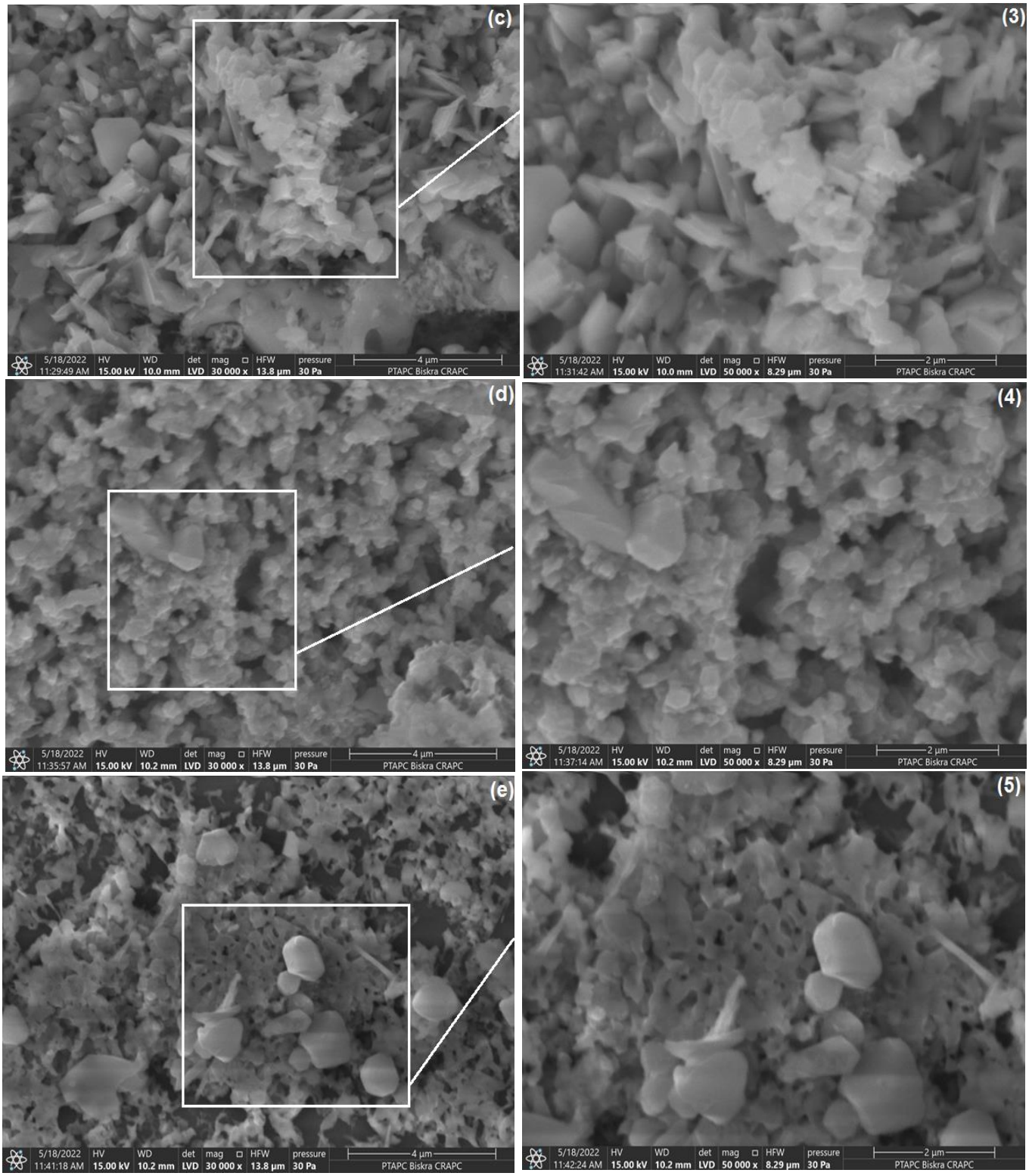

FigureV.7. SME image of various samples prepared. CuO (a), 5 % Ag:CuO (b) ,15 % Ag :CuO (c) 25 % Ag:CuO (d) , 50 % Ag:CuO (e),with zoom in 4µm and CuO (1), 5 % Ag:CuO (2) ,15 % Ag :CuO (3), 25 % Ag:CuO (4) ,50 % Ag:CuO (5), with zoom in 2µm.

V.6.EDX Analysis

The utilization of energy-dispersive X-ray (EDX) analysis was employed to validate the presence of doping in the metallic material and to determine the chemical composition of the thin layers.Figure V.8 displays the spectra of Ag: CuO thin films with varying doping ratio. The peaks corresponding to Cu and O elements are observed consistently across all samples. The occurrence of supplementary Ag peaks also increses in tandem with the augmentation of the doping rate. (0.02% for doping with 5% Ag, 1.28% for doping with 15% Ag, 33.83 % for doping with 25% Ag and 38.03% for doping with 50% Ag). This finding aligns with the XRD results and provides confirmation of the formation of CuO and Ag_2O phases.

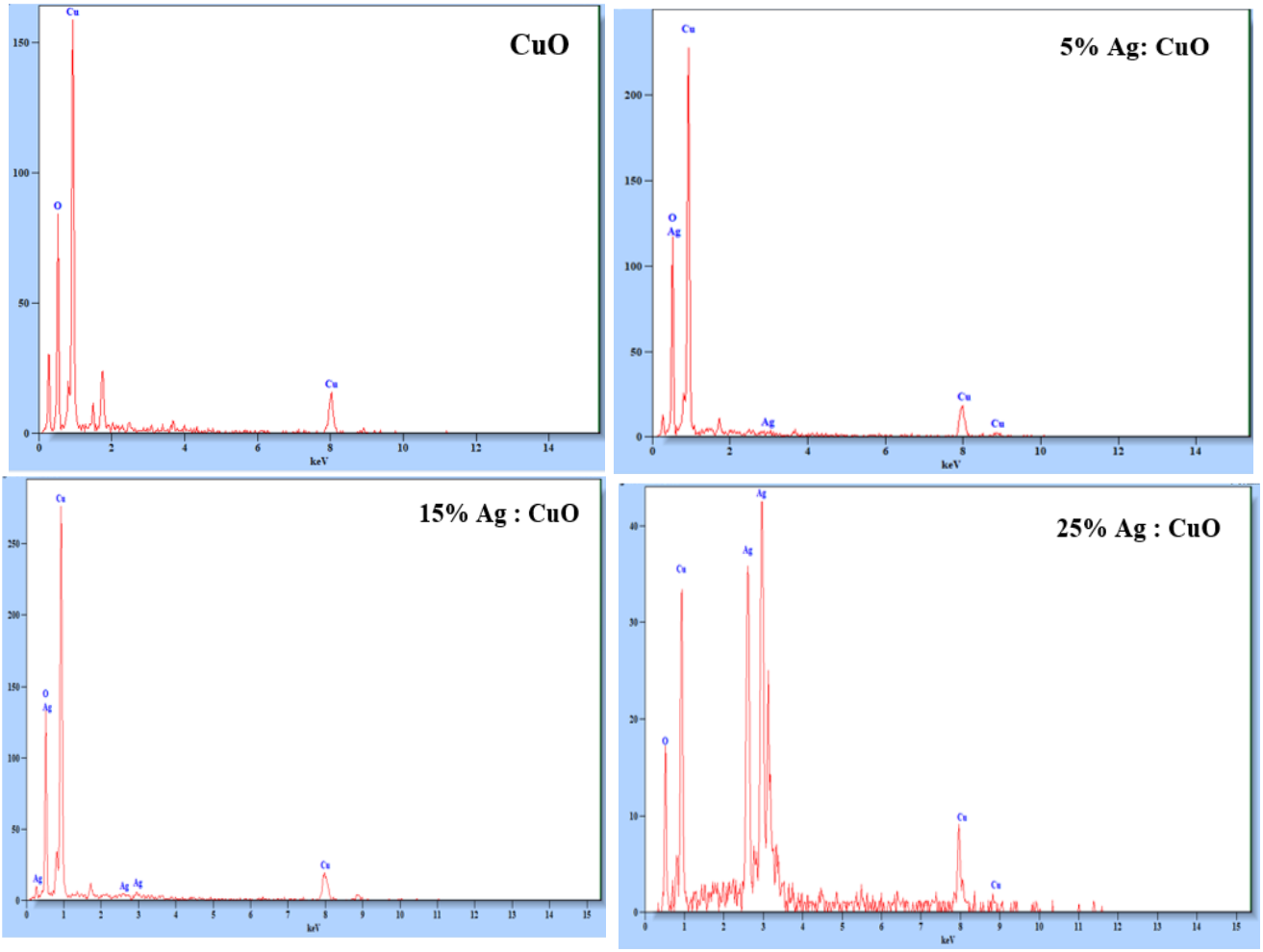

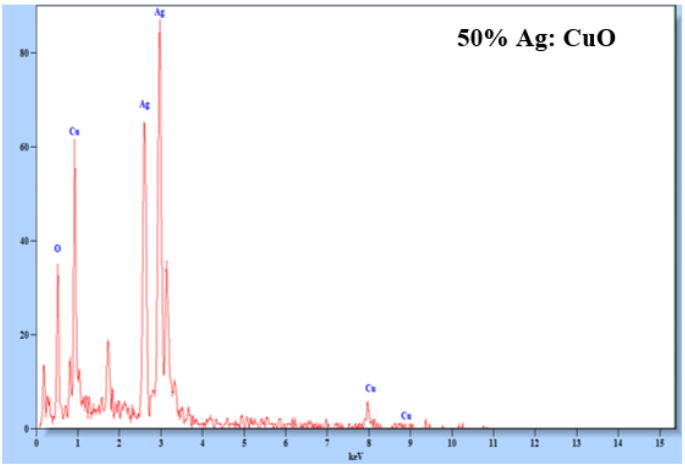

Figure V.8. EDX analysis spectrum of samples.

Table V.2. Percentage of atoms present in EDX spectrum.

Phases	Cu%	O%	Ag%
CuO	44.04	55.96	0
Ag :CuO (5%)	58.36	41.62	0.02
Ag :CuO (15%)	43.6	55.12	1.28
Ag :CuO (25%)	18.61	47.56	33.83
Ag: CuO (50%)	6.06	55.91	38.03

V.7.Optical properties

V.7.1.Absorbance spectra

The optical analysis of thin films of copper oxide, both in its pure form and doped with silver (Ag), was also conducted using a UV-Visible spectrophotometer see Figure V.9 the optical analysis of thin films of copper oxide, both in its pure form and doped with silver (Ag), was conducted using a UV-visible spectrophotometer .It is important to acknowledge that the thin layers of pure CuO exhibit the weakest absorbance when contrasted with doped samples. Different percentages of Ag were incorporated into CuO thin films, resulting in a substantial enhancement in absorption. The absorption spectrum exhibited prominent absorption bands at approximately 750 nm, which can be attributed to the band transition of CuO. These absorption bands were observed in the vicinity of 310 and 360 nm wavelengths. This implies that the films possess a crystalline structure [199,200].The decrease in band gap value of Ag: CuO thin films results in a shift of the absorption peaks towards longer wavelengths [201]. The absorption of

light is most pronounced for thin films that have been doped with silver, particularly within the visible range. In the case of pure copper oxide, the absorption reaches its peak maximum within the near infrared (IR) spectrum. This observation indicates that the absorption region, for films doped with Ag, exhibited an expansion in its spectral range from the near-infrared region to the visible spectrum.

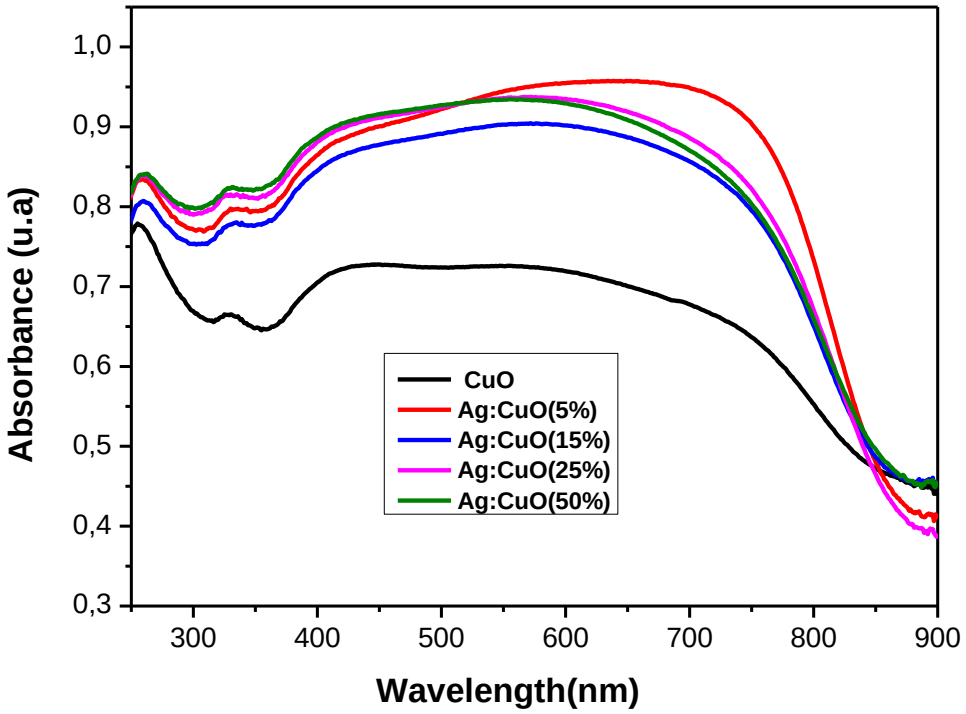

Figure V.9. Absorbance spectra of CuO thin layers doped with Silver.

V.7.2.Energy Gap

The Tauc relation (II.17) was employed to ascertain the band gap energy of the thin layers fabricated through the spin-coating technique. The band gap energy values exhibit a range ranging from 2.17 eV to 1.25 eV as the Ag doping rate increases see Figure (V.10). Doping causes the absorption edge to be displaced toward lower energies, which accounts for this decrease. The cause of this phenomenon can be attributed to the rise in energy levels surpassing those of the valence band. The obtained outcome provides confirmation that the Ag-doped CuO exhibits characteristics of a P-type semiconductor due to the displacement of the Fermi levels towards the valence band (VB). Consequently, lower energy photons are absorbed, increasing the number of transition electrons and decreasing the band gap energy values.

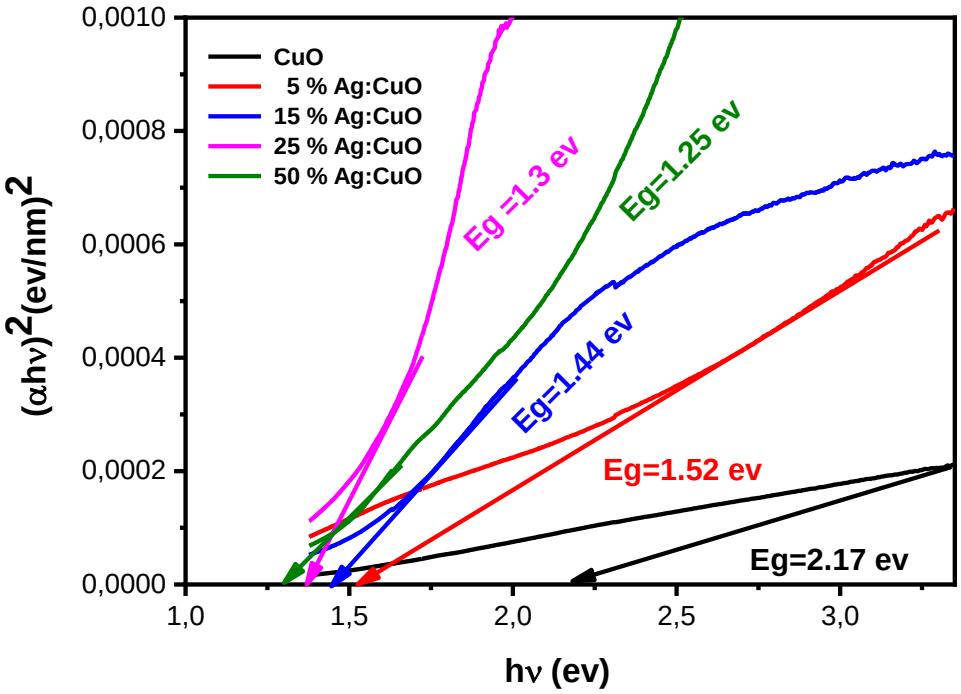

Figure V.10. Variation of $(\alpha h\nu)^2$ as a function of the photon energy of Ag-doped CuO thin layers.

V.8.Electrical properties

The four-point technique is employed for the evaluation of the electrical conductivity (σ) and electrical resistivity (ρ) of thin films of composition Ag: CuO. The conductivity value is determined by utilizing equation (II.12).The electrical conductivity of silver doped films is observed to increase with an increase in Ag doping. The conductivity of undoped CuO is measured to be $3.5.10\text{-}5\Omega^{-1}\cdot cm^{-1}$. However, when silver is introduced, the conductivity of the material increases and eventually reaches a value of $5.2.10\text{-}4\Omega^{-1}\cdot cm^{-1}$ for the 50% Ag:CuO composition. In the presence of doping, the resistance values exhibit a decreasing trend. The findings are displayed in Table V.3.

Table V.3. The electrical parameters obtained by the 4-point method.

	e(nm)	**$\rho(\Omega \cdot cm)$**	**$\sigma(\Omega^{-1}\cdot cm^{-1})$**
CuO pure	320	28016.42	$3.5.10^{-5}$
5 %Ag :CuO	338	16193.5	$6.175 .10^{-5}$
15 %Ag :CuO	412	12561.88	$7.9.10^{-5}$
25 %Ag :CuO	443	4728.45	$2.1.10^{-4}$
50 %Ag : CuO	670	1922.85	$5.2.10^{-4}$

Figure V.11 illustrates the relationship between the concentration of Ag and the conductivity and electrical resistivity of Ag:CuO films. The dissimilarity in the presence and surface shape of Cu and Ag atoms may account for the observed results, which can be attributed to the increase in resistivity due to the highest defect density at grain boundaries. The obtained electrical conductivity values were found to be consistent with the findings reported in reference [202]. Additionally, it demonstrates that as the amount of silver doping in the samples increases, so does their conductivity. The observation leads to an increase in the charge carriers responsible for electrical conduction. A reduction in the presence of grain boundaries and an augmentation in the crystallites size are both relevant factors contributing to an enhancement in electrical conductivity. These two factors together result in a reduction in energy levels and enhanced mobility of charge carriers. The size of the crystallites and the gap band gap energy are inversely correlated. A quantum confinement size effect can explain his feature [203].In addition to this effect, it was thought that a key factor in researching the impact on the electrical properties was the thickness of the copper oxide (CuO) thin films, which serve as the active component [204].

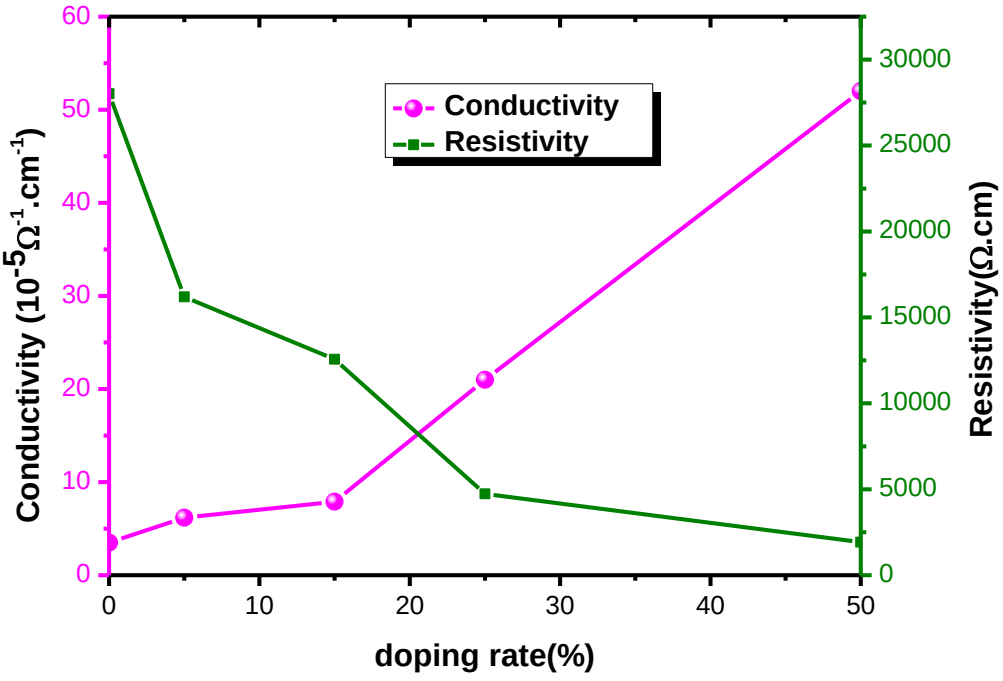

Figure V.11. Variation of conductivity and resistivity as a function of doping ratio by 4 point technique.

V.9.Photocatalytic Performance

The degradation of Orange II at a concentration of (1.78×10^{-5} mol/L) was observed during the experimental utilization of the prepared samples under UV irradiation for a duration ranging from one hour to five hours see Figure V.12. The absorption spectra exhibited are indicative of photocatalysis and encompass wavelengths ranging from 350 to 600 nm. The entirety of the spectra represent an identical decoy with an absorption maximum at λ = 485 nm, which corresponds to the absorption band wavelength of the Orange II dye. The spectra showed a decrease in absorption during radiation exposure. The dye changes from light to transparent color, demonstrating the effectiveness of these thin films as active catalysts in photocatalysis applications. The Ag: CuO, at various doping concentrations, exhibited notable degradation efficiency within the initial three-hour period. Notably, the film doped with 50% Ag consistently demonstrated the highest catalytic activity throughout the entire duration. This data demonstrates that the degradation of the dye is most effective when the degradation rate reaches approximately 43% after 5 hours see Figure (V.12). Furthermore, this degradation rate is nearly twice as high as the degradation rate of pure CuO, which is 27% for the same duration.

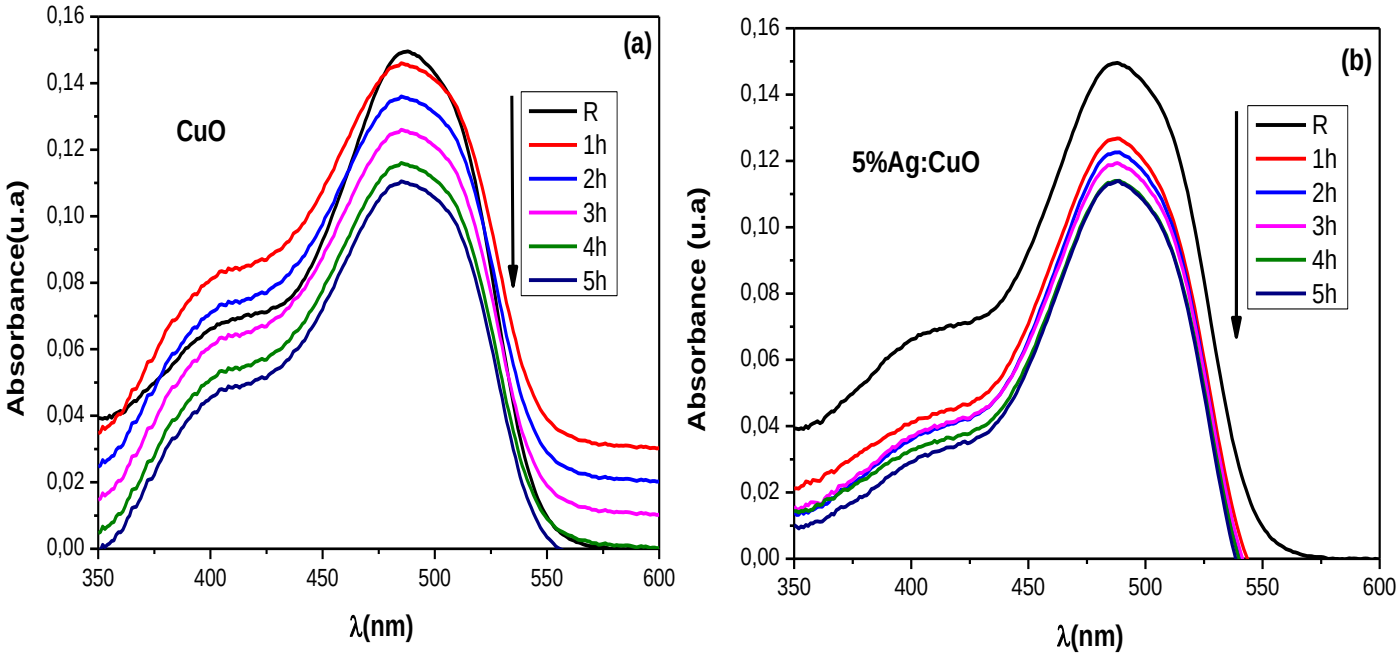

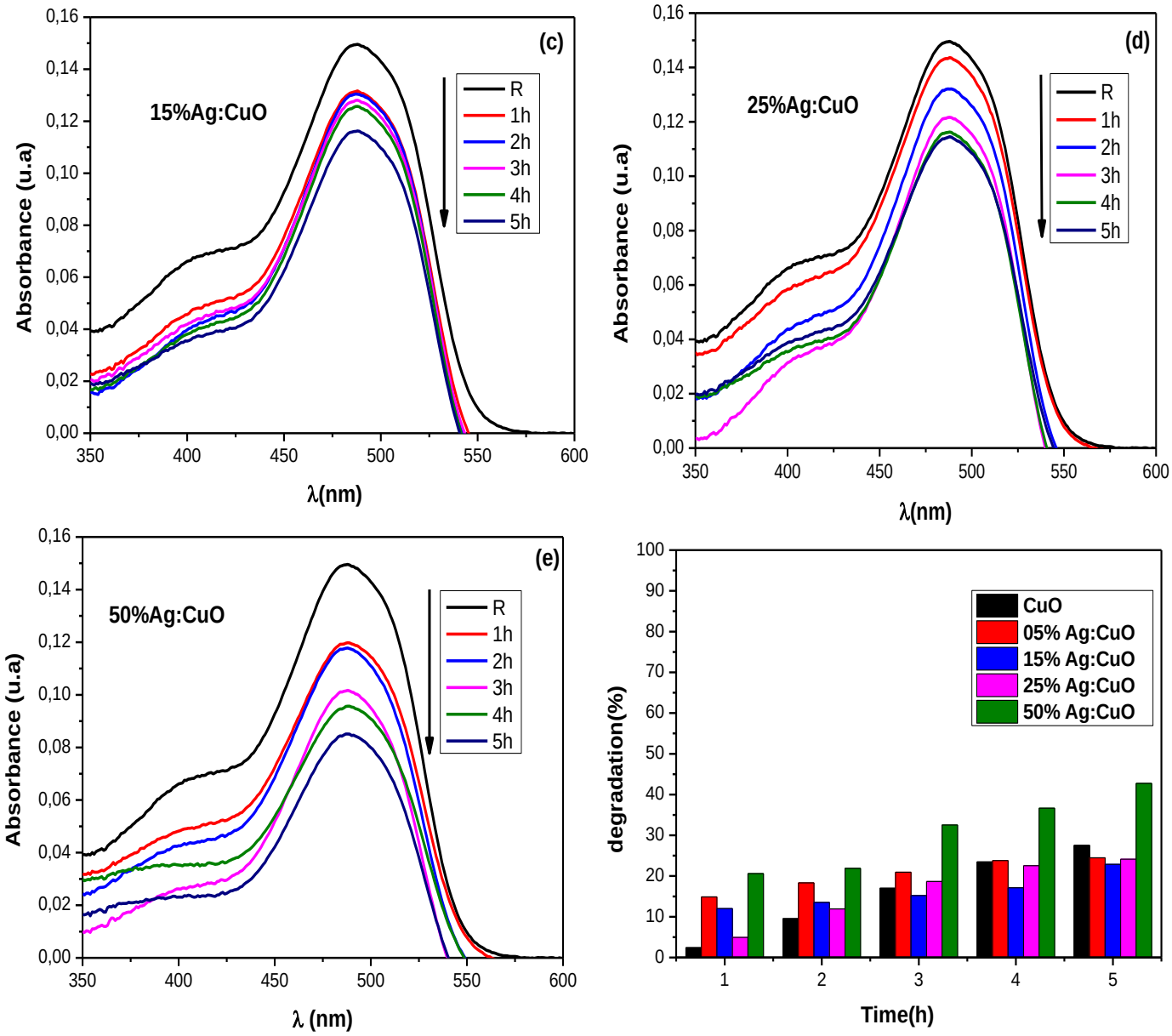

Figure V.12. Evolution of absorption spectra of orange II(OII) and their degradation as a function of irradiation time with UV light in the presence of thin layers (a) :CuO , (b) : 5% Ag :CuO, (c) :15 %Ag :CuO, (d) : 25%Ag :CuO, and (e) : 50% Ag :CuO.

The rate constants for Orange II dye degradation using pure and 5% doped CuO thin film catalysts up to 50% are respectively $6.69.10^{-3}$ min^{-1}, $7.03.10^{-3}$ min^{-1}, $6.55 .10^{-3}$ min^{-1}, $6.83.10^{-3}$ min^{-1} and $8.23.10^{-3}$ min^{-1}. These results illustrate the photocatalysis properties of these layers in the decomposition reaction of Orange II. For instance, the degradation rate is observed to be faster in the case of 50% silver (Ag) doping as compared to the other doping concentrations.

This observation indicates that the film in question serves as a highly potent catalyst, primarily attributed to the incorporation of the Ag element.

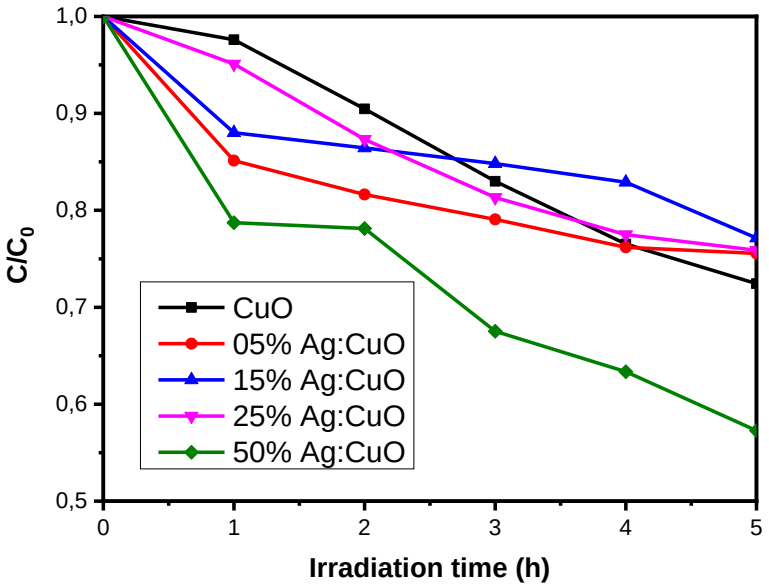

Figure V.13. Variation of (C/C_0) as a function of the irradiation time in the presence of thin layers of the Ag: CuO.

V.9.1.Kinetics of degradation

To understand the degradation reaction kinetics of the chosen dye, we studied the first-order kinetic model see equation (I.15) in the presence of pure CuO and Ag-doped thin films. Figure V.14 represents the variation of Ln (C**0**/C) in accordance with the duration of exposure to radiation, we note that all spectra present a straight line. The first-order rate constant k can be determined by calculating the slope of the linear regression.Note that the degradation rate varies between 0.064 cm^{-1} and 0.111 cm^{-1}.

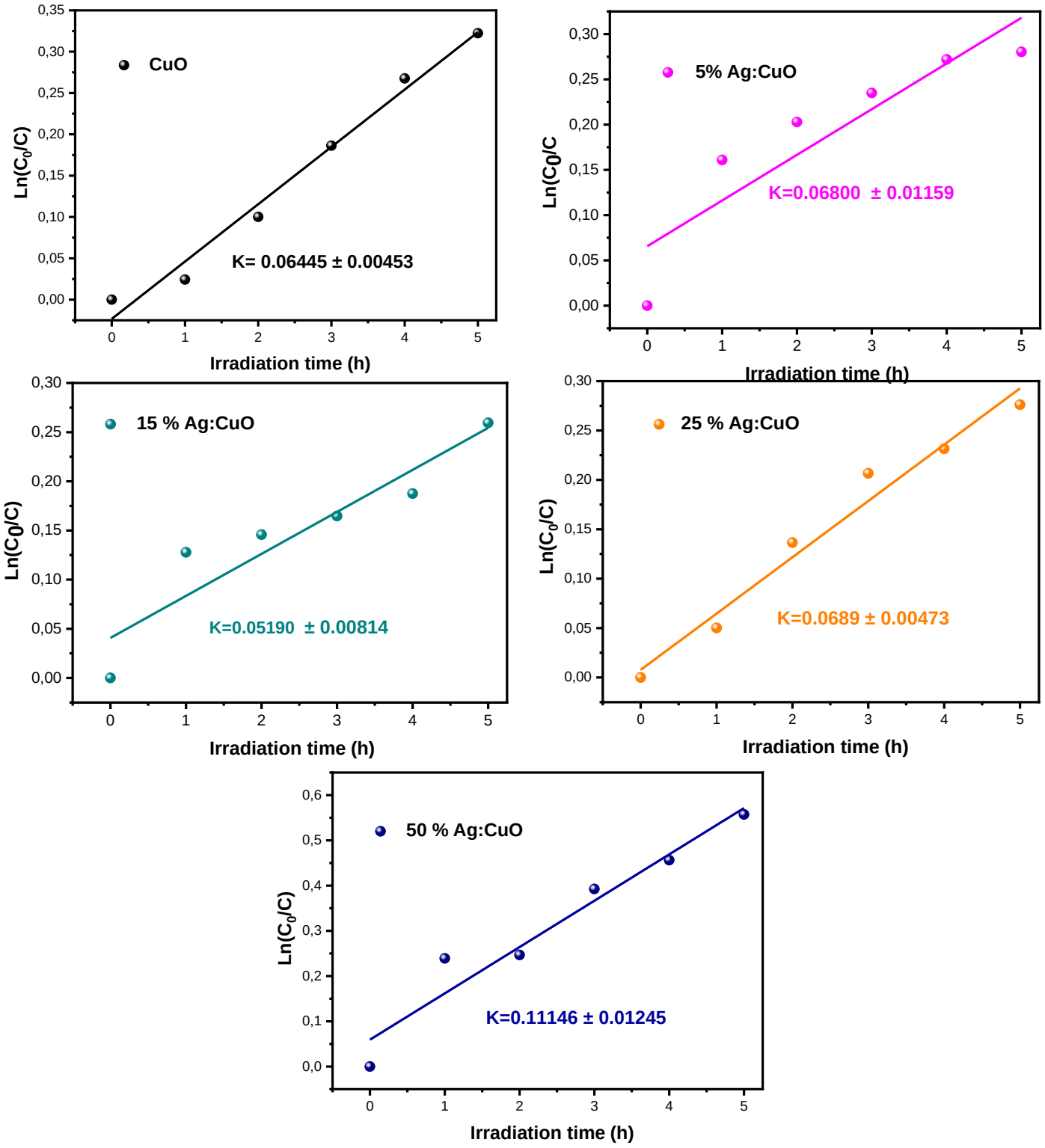

Figure V.14. Variation of Ln (C_0/C) in the presence of CuO pure and doped with Ag as a function of irradiation time.

V.9.2.Photocatalytic mechanism

The present study investigates the optical, structural, and morphological properties of thin films. The samples under investigation consist of copper oxide (CuO) with varying percentages of silver (Ag), specifically 5%, 15%, 25%, and 50% Ag.Copper (II) oxide (CuO) exerts a substantial impact on the photocatalysis capabilities. The properties of the samples are influenced by factors such as band gap energy, light absorption, crystallinity, and surface characteristics [205].

Heterogeneous photocatalysis relies on the absorption of photons with energy equal to or greater than the width of the semiconductor forbidden band gap ($h\nu \geq Eg$)[206].The transfer of electrons from the valence band to the conduction band results in the formation of a hole in the valence band, facilitating the creation of an electron-hole pair (e-/h+). In the goal to generate hydroxyl radicals ($OH^{\bullet}$), holes in the valence band interact with anions (OH^-). Superoxide radicals $^{\bullet}O_2^-$ are formed when electrons in the conduction band interact with oxygen molecules O_2, and gives the transparent solution see equation(V.2) which increased when active layers were deposited with low gaps.

$$CuO + Ag_2O + h\upsilon \longrightarrow e_{CB}^- + h_{VB}^+ \quad (V.1)$$

$$O_2 + e_{CB}^- \longrightarrow O_2^{\cdot -} \quad (V.2)$$

$$H_2O + h_{VB}^+ \longrightarrow OH^- + H^+ \quad (V.3)$$

$$OH^- + h_{VB}^+ \longrightarrow OH^{\cdot} \quad (V.4)$$

$$Dye + OH^{\cdot} \longrightarrow Dye^+ \quad (V.5)$$

$$Dye^+ + O_2^{\cdot -} \longrightarrow CO_2 + H_2O \quad (V.6)$$

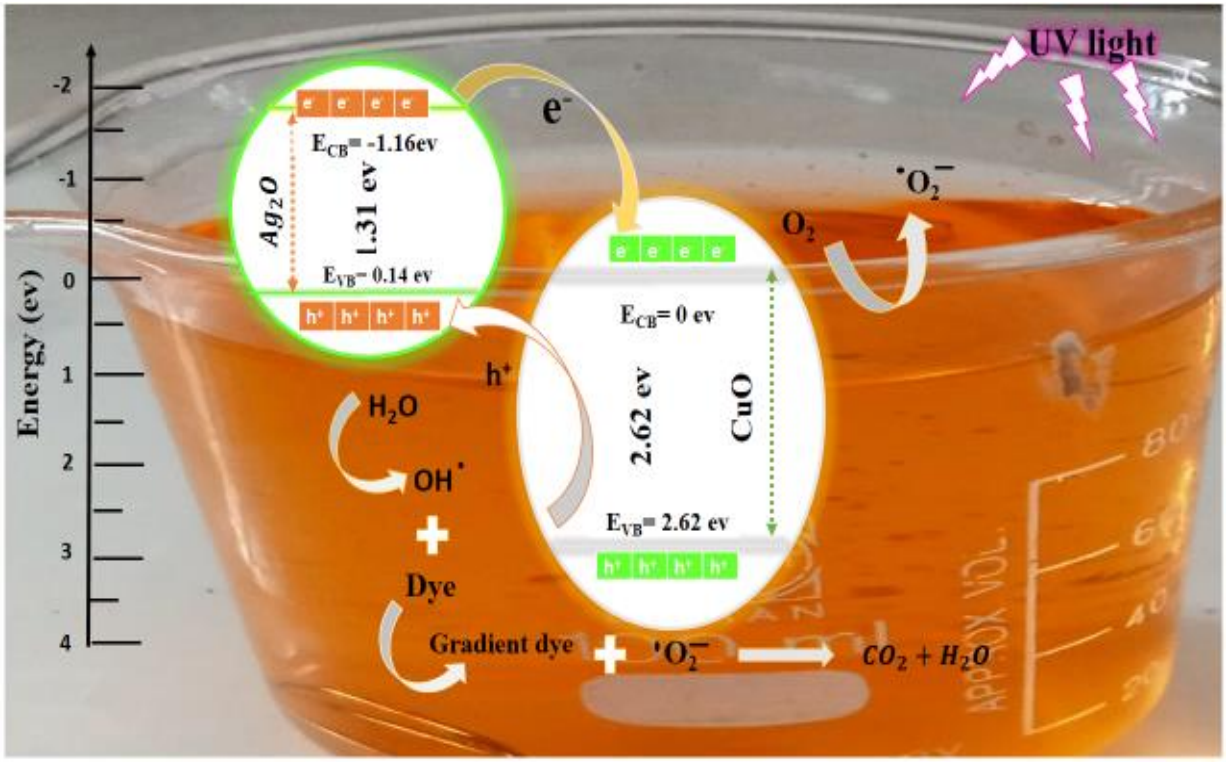

Figure V.15. The photocatalytic mechanism of Ag-doped CuO thin layers under UV light.

V.10.Conclusion

A thin films of copper oxide pure and doped with Ag was deposited by the sol-gel spin coating method on a glass substrate. These films were used to study the effect of silver on the structural morphological, optical, electrical, and photocatalysis properties of these films. Results show that these samples have a good electrical conductivity in the case of silver-doped CuO. Their optical behavior was ameliorated due to the silver impurity which significantly enhanced the absorption in the visible range. The scanning electron microscopy (SEM) analysis revealed the presence of pores in the case of silver (Ag) doping. Photocatalysis results showed that doping with copper oxide by transition metals (Ag) improves the photocatalysis efficiency and the best degradation of the dye (Orange II) reaches 43 % for the utilization of thin layers of copper oxide (CuO) doped with a 50% concentration of silver (Ag).

General conclusion

General conclusion

The thin layers based on copper oxide, prepared by pneumatic spray pyrolysis method and by sol-gel spin coating method , were used in the self-cleaning and photocatalysis applications to degrade orange II dye under UV irradiation, respectively.

Copper oxide thin films were deposited by pneumatic spray pyrolysis method on a glass substrate, heated at 400°C for different spraying times (5min, 10min, 15min, 20min,25min, and 30min) with a flow rate of 20ml/h using solution copper nitrate $Cu(NO_3)_2$.with a 0.1M of precursor concentration. These films are characterized by X-ray diffraction (XRD), Fourier-transform infrared (FT-IR), UV-visible spectroscopy, four point method, and water contact angle. To study the effect of spraying time on structural, optical, and electrical and the technique of self-cleaning to test the surfaces of our films and their industrial and environmental importance.

The main results obtained are as follows:

- ✓ The thickness of these films changes between 102-650 nm. Are increases with the increase of spraying time.
- ✓ According to the XRD results, all peaks confirm the formation of the phase tenorite phase of monoclinic structure; the deposited of copper oxide (CuO) were polycrystalline with directions along the (111) plane.
- ✓ The crystallite size variated between 14 and 23nm.
- ✓ FT-IR spectroscopy confirms the presence of the CuO phase and agrees will the results of XRD.
- ✓ The average transmission between 400 and 800nm is 65% to 50%, and the gap energy is 2.65eV to 1.09eV.
- ✓ A maximum value of the electrical conductivity at 0.34 $\Omega^{-1}.Cm^{-1}$ corresponds to a spraying time of 20 min.
- ✓ All samples' water contact angle values are greater than 90° and range from 96.4° to 103.2°.
- ✓ As we can see from these results that all the samples are hydrophobic films.

The heterogeneous photocatalysis of metal oxide for the degradation of organic pollutant orange II is the subject of this study. The preparation of thin layers of CuO, pure and doped with Al and Ag at different concentrations (x = 5%, 15%, 25%, and 50%) by the sol-gel (spin-

coating) method on glass substrate, makes it possible to see the effect of doping elements of different ionic radius on the CuO in the photocatalysis application. The structural, morphological, optical, and electrical properties of these layers. They were studied by XRD, FT-IR, Raman, MEB, and UV-Visible spectrophotometry, for the degradation of orange II dye.

The main results obtained are as follows:

- **Al-doped copper oxide**

✓ The thickness of these films changes between 106-798 nm.

✓ According to XRD results, all peaks confirm the existence of a preferential orientation along the (-111) plane.

✓ The crystallite size varies between 21 nm and 46 nm and increases with the Al doping rate.

✓ The FT-IR and Raman spectra confirm the presence of CuO and Al_2O_3 phase agrees will the results of XRD.

✓ The gap energy variated between 2.62eV and 1.8eV decreases with increased electrical conductivity.

✓ In MEB results, after the doping by Al, we note that there is a change and improvement in the surface being smooth, dense, and homogeneous with the shape of nano spherical and the existence of the pores, which improves the degradation of photocatalysis.

✓ According to the photocatalysis application, all the films represent a maximum absorption with a wavelength λ= 485nm representing the wavelength of orange II.

✓ The degradation in CuO is 15%, and with Al doping (5%, 15%, 25%, 50%), we note an increase in the degradation rate to (29%, 32%, 33%, and 61%), respectively.

✓ Photocatalysis results showed that doping copper oxide by (Al) improves the photocatalysis efficiency, and the best degradation of a dye (orange II) reaches 61% for using thin layers of CuO doped with 50% Al.

- **Ag-doped copper oxide**

✓ With increasing doping, the thickness of these films increased. It ranges from 320 nm to 670 nm.

✓ The crystallite sizes are nanometric variated from 21 nm to 33 nm and increase with the increase of doping.

✓ Large pores and more significant numbers with increased doping rates confirm that Ag gives a more porous surface.

- ✓ The FT-IR spectra confirm the presence of CuO and Ag_2O phase agrees will the results of XRD.
- ✓ With an increasing Ag doping rate, the energy gap values range from 2.17 eV to 1.25 eV.
- ✓ The electrical conductivity increases with an increase in the case of doped with silver, as the conductivity of the CuO pure is $3.5.10^{-5}\ \Omega^{-1}\cdot cm^{-1}$, while in the presence of silver, it increases until they reach a value of $5.2.10^{-4}\ \Omega^{-1}\cdot cm^{-1}$for the 50 % Ag: CuO.
- ✓ All spectra represent an absorption maximum of 485 nm, representing the wavelength of dye orange II.
- ✓ Photocatalysis results showed that doping with copper oxide by transition metals (Ag) improves the photocatalysis efficiency, and the best degradation of a dye (orange II) reaches 43% for the use of thin CuO doped with 50% Ag.

At the end of this study, the thin films based on copper oxide are excellent in self-cleaning and in photocatalysis application for degrading dyes due to the better crystalline quality, morphology, and electrical properties. This is what drives us to choose this metal oxide with doping and co-doping by metals for the application of toxic gas sensors and in the antibacterial application as perspectives of this work.

References

References

[1] S. M. Ali et al., "Structural and optical properties of pure and Ag doped ZnO thin films obtained by sol gel spin coating technique," Mater. Sci. Pol., vol. 33, no. 3, pp. 601–605, 2015.

[2] A . Habib, N.Jewena , A K M. Shahabuddin , S. K. Das , J.l I. Khandaker , F .Ahmed "hydrothermal synthesis of CuO nanoparticles and a study on Property variation with synthesis temperature ," J. Appl. Fundam. Sci., vol. 6(2), no. 2395–5562, 2020.

[3] K. Hossain and C. Collins, « Potential Applications of Self-Cleansing Nano Lotus Leaf Biomimicked Coating in Different Construction Sectors», Build. Tomorrow's Soc. June, 2018.

[4] P. Ragesh, V. A. Ganesh, S. V Nair, and A. S. Nair, "A review on 'self-cleaning and multifunctional materials,'" J. Mater. Chem. A Mater. energy Sustain., vol. 2, no. August, pp. 14773–14797, 2014.

[5] N. Ezzatahmadi et al., «Catalytic degradation of Orange II in aqueous solution using diatomite-supported bimetallic Fe/Ni nanoparticles », p. 7687 7696, 2018.2014.

[6] U. G. Akpan et B. H. Hameed, « The advancements in sol – gel method of doped-TiO_2 photocatalysts », vol. 375, p. 1 11, 2010.

[7] M. Maraj, A. Raza, X. Wang, J. Chen, K. N. Riaz, et W. Sun, « Mo-doped CuO Nanomaterial for Photocatalytic Degradation of Water Pollutants Under Visible Light », p. 1 11, 2021.

[8] R. D. Prabu et al., « An effect of temperature on structural , optical , photoluminescence and electrical properties of copper oxide thin fi lms deposited by nebulizer spray pyrolysis technique », Mater. Sci. Semicond. Process., vol. 74, no October 2017, p. 129-135, 2018.

[9] A. O. Ibhadon et P. Fitzpatrick, « Heterogeneous Photocatalysis: Recent Advances and Applications », p. 189 218, 2013.

[10] F. Bayansal et T. Tas, « Effect of Cobalt Doping on Nanostructured CuO Thin Films », Metallurgical and materials transaction A, vol 45, 2014.

[11] L. Sun et al., « Nitrogen-Doped Carbon-Coated CuO-In_2O_3 p–n Heterojunction for Remarkable Photocatalytic Hydrogen Evolution », Adv. Energy Mater., vol. 9, no 48, p. 1-11, 2019.

[12] H. Search, C. Journals, A. Contact, M. Iopscience, et I. P. Address, « Sputtered copper oxide (CuO) thin films for gas sensor », vol. 2417, p. 0 4, 2006.

[13] D. Rania, A. Rabah, T. Mamadou, et M. Christine, « Elaboration de nanomatériaux fonctionnels pour des applications biomédicales », Récents progrès en génie des procédés,no110, 2017.

[14] T. Oku, R. Motoyoshi, K. Fujimoto, T. Akiyama, B. Jeyadevan, et J. Cuya, « Structures and photovoltaic properties of copper oxides / fullerene solar cells », J. Phys. Chem. Solids, vol. 72, no 11, p. 1206 1211, 2011.

[15] M. F. A. Aboud, S. Haider, et M. F. Warsi, « Fabrication of Binary Metal Doped CuO Nanocatalyst and Their Application for the Industrial Effluents Treatmen », Ceram. Int., 2020.

[16] S. S. Akarmazyan, P. Panagiotopoulou, A. Kambolis, C. Papadopoulou, et D. I. Kondarides, « Applied Catalysis B : Environmental Methanol dehydration to dimethylether over Al_2O_3 catalysts », "Applied Catal. B, Environ., vol. 145, p. 136 148, 2014.

[17] A. S. Ivanova et al., « Environmental Metal – support interactions in Pt / Al_2O_3 and Pd / Al_2O_3 catalysts for CO oxidation », Applied Catalysis B: Environmental,vol. 97, p. 57 71, 2010.

[18] S. Benramache « Elaboration et caractérisation des couches minces de ZnO dopées cobalt et indium », thèse doctorat, université Mohamed Kheider-Biskra, 2012, page 6.

[19] K.Kamli « Elaboration et caractérisations physico-chimique des couches minces de sulfure d'étain par spray ultrasonique : Effet des sources d'étain », mémoire magister, université Mohamed Kheider-Biskra, 2013, page4, 16,17.

[20] R.Azizi «The effect of doping on the properties of thin films of Indium oxide(In_2O_3) deposited by ultrasonic spray for optoelectronic application »,doctoral thesis, university Mohamed Kheider- Biskra, 2020, page1.

[21] H. Moualkia « Elaboration et Caractérisation de Couches Minces de Sulfure de Cadmium (CdS) » , thèse doctorat, université Mentouri –Constantine, 2010, page 4.

[22] O.Daranfad «Elaboration et caractérisation des couches minces de Sulfure de Zinc préparées par spray ultrasonique »,mémoire magister, université Mentouri –Constantine, page12.

[23] L. Herissi « Élaboration et caractérisation de couches minces d'oxydes métalliques destinées à des applications optoélectroniques » thèse doctorat, Université Larbi Ben M'hidi -Oum El Bouaghi, 2016, page 4.

[24] M.Ayachi «Elaboration par la méthode sol gel spin coating et caractérisations des couches minces de ZnO »mémoire magistère, université Jijel, 2012, page6.

[25] M.Khechba « Caractérisation de la réaction interfaciale entre une couche mince de tungstène et un substrat d'acier » mémoire magister, université Mentouri –Constantine, 2008, page 12.

[26] J.E. Greene « Thin Film Nucleation, Growth,and Microstructural Evolution: An Atomic Scale View » 1er édition, university of Illinois, Urbana, USA, 2006, page557.

[27]W. Wei « Electrical and Optical Properties of Ga-Doped $Mg_{1-x}Zn_xO$ System», doctoral thesis, university North Carolina State, 2010, page 79.

[28] B.Plujat « Étude des interactions plasma/surface pour la compréhension de la croissance de couches minces SiCN : H et de leur interface film/substrat : répercussions sur leurs propriétés »thèse doctorat, Université perpignan via domitia, 2017, page25.

[29] S. N. Ogugua, O. M. Ntwaeaborwa, et H. C. Swart, « Latest development on pulsed laser deposited thin films for advanced luminescence applications », Coatings, vol. 10, no 11, p. 1-22, 2020.

[30] A. Marty et S. Andrieu, « Croissance et structure des couches minces », J. Phys. IV JP, vol. 6, no 7, 1996.

[31] F. Ynineb «Contribution à l'élaboration de couches minces d'Oxydes Transparents Conducteurs (TCO) », mémoire magister, université Mentouri –Constantine, 2010, page4 ,5.

[32] E. C. Nwanna, P. E. Imoisili, S. O. Bitire, et T. Jen, « Biosynthesis and Fabrication of Coppe Oxide Thin Films as a P-Type Semiconductor for Solar Cell Applications », Coatings, vol.11, 2021.

[33] S. Using et S. Pyrolysis, « Structural and Optical Properties of CuO Thin Films Synthesized Using Spray Pyrolysis Method », , Coatings, vol.11, 2021.

[34] R. U. Osuji, F. I. Ezema, D. S. Polytechnic, et D. State, « Synthesis and Characterisation of Copper Oxide Thin Films Using Successive Ionic Layer Adsorption Reaction (SILAR) Method », p. 68-76, 2016.

[35]A.Kerour «Synthèse écologique des nanoparticules des oxydes de cuivre et application photocatalytique »,thèse doctorat, université Mentouri -Constantine,2018,page13.

[36] N. A. Raship, M. Z. Sahdan, F. Adriyanto, M. F. Nurfazliana, et A. S. Bakri, « Effect of annealing temperature on the properties of copper oxide films prepared by dip coating technique », AIP Conf. Proc., vol. 1788, no January 2017,2017.

[37] A. Chapelle, « Elaboration et caractérisation de films minces nano composites obtenus par pulvérisation cathodique radiofréquence en vue de leur application dans le domaine des capteurs de CO_2 », thèse doctorat, université Toulouse, 2012, page 40.

[38] S.Addala, «Elaboration et caractérisation de matériaux composites à base de nanoparticules du semi-conducteur CuO et de l'oxyde de terre rare Dy_2O_3 dispersées dans les matrices diélectriques KBr, KCl et NaCl », thèse doctorat, université Mentouri -Constantine, 2015, page13,14,16.

[39] F.Z.Chafi, «Deposition of undoped and doped Copper Oxide thin films by Spray Pyrolysis technique: Experiment and Theory », doctoral thesis, University Mohammed V, Rabat, 2017,page22.

[40] R.Bacha, « La synthèse des nano particules de CuO avec la méthode de précipitation sol_ gel, en utilisant le précurseur CuCl2 et l'étude de leurs propriétés structurales et optiques », mémoire magister, université Mentouri –Constantine, 2015, page23, 35.

[41] A.Bejaoui, « Capteurs à base des couches minces d'oxyde de cuivre (II) (CuO) : Optimisation et modélisation en vue de la détection de gaz », thèse doctorat, université de Carthage, 2013, page 26 ,27.

[42] S.Mechdjebi, «La synthèse des nano poudres de CuO avec la méthode précipitation Sol-Gel en utilisant le précurseur$CuSO_4$ et l'étude de leurs propriétés structurales et optiques », mémoire magister, université Mentouri –Constantine, 2015, page29, 30.

[43] M.Zeggar, «Cupric Oxide thin films deposition for gas sensor application », doctoral thesis, university Mentouri –Constantine, 2016, page14, 28.

[44] I. El Younsi, « Elaboration et caractérisation de nouvelles couches sensibles pour la réalisation de capteurs de CO2 », thèse doctorat, Université de Toulouse, 2015, page38.

[45] A.Altaweel, «Synthèse de nanostructures d'oxyde de cuivre par micro-post-décharge microondes à pression atmosphérique», thèse doctorat, Université Lorraine, France, 2014. page17.

[46] J.Toupin , « Photo électrolyse de l'eau :Etude de matériaux semi-conducteurs de type p comme photocathode pour la réduction de protons en H_2 »,thèse doctorat ,université Pierre et Marie Curie,2016,page40 ,42.

[47] L.Martin, « Etude de l'oxyde de cuivre CuO, matériau de conversion en film mince pour microbatteries au lithium : caractérisation des processus électrochimiques et chimiques en cyclage », thèse doctorat, université de Pau et des pays de l'Adour, 2013, page201.

[48] S. Choudhary et al., « Oxidation mechanism of thin Cu films: A gateway towards the formation of single oxide phase », AIP Adv., vol. 8, no 5, 2018.

[49] M.Berrahal « Élaboration et caractérisation d'un composite oxyde de fer/pyrochlore de formule Fe_2O_3- $Bi_{15}.Sb_{1.5}.CuO_7$: Application catalytique », mémoire magister ,université Mohamed Boudiaf Oran,2017,page29.

[50] G. Papadimitropoulos, N. Vourdas, V. E. Vamvakas, et D. Davazoglou, « Optical and structural properties of copper oxide thin films grown by oxidation of metal layers », Thin Solid Films, vol. 515, no 4, p. 2428-2432, 2006.

[51] K. Han et M. Tao, « Electrochemically deposited p-n homojunction cuprous oxide solar cells », Sol. Energy Mater. Sol. Cells, vol. 93, no 1, p. 153-157, 2009.

[52] S. T.c and A. B. Saptarshi De a, N. Venkataramani a, Shiva Prasad b, R. O. Dusane a, Lionel Presmanes c, Y. Thimont c, P. Tailhades c, Valérie Baco-Carles c, Corine Bonningue c, « Ethanol and

Hydrogen gas-sensing properties of CuO–$CuFe_2O_4$ nanostructured thin films », Power Eng., no July, 2003.

[53] L. Presmanes et al., « Integration of P-Cuo thin sputtered layers onto microsensor platforms forgas sensing », Sensors (Switzerland), vol. 17, no 6, 2017.

[54] A. Sharma, Y. Kumar, et P. M. Shirage, « Structural, optical and excellent humidity sensing behaviour of $ZnSnO_3$ nanoparticles: effect of annealing », J. Mater. Sci. Mater. Electron., vol. 29, no 13, p. 10769-10783, 2018.

[55] N. D. Khiavi, R. Katal, S. K. Eshkalak, S. Masudy-Panah, S. Ramakrishna, et H. Jiangyong, « Visible light driven heterojunction photocatalyst of CuO-Cu_2O thin films for photocatalytic degradation of organic pollutants », Nanomaterials, vol. 9, no 7, 2019.

[56] L. Sun et al., « Nitrogen-Doped Carbon-Coated CuO-In_2O_3 p–n Heterojunction for Remarkable Photocatalytic Hydrogen Evolution », Adv. Energy Mater., vol. 9, no 48, p. 1-11, 2019.

[57] W. Mohsen, M. A. Sadek, et H. A. Elazab, « Green synthesis of copper oxide nanoparticles in aqueous medium as a potential efficient catalyst for catalysis applications », Int. J. Appl. Eng. Res., vol. 12, no 24, p. 14927-14930, 2017.

[58] A. A. Al-Ghamdi, M. H. Khedr, M. Shahnawaze Ansari, P. M. Z. Hasan, M. S. Abdel-Wahab, et A. A. Farghali, « RF sputtered CuO thin films: Structural, optical and photo-catalytic behavior », Phys. E Low-Dimensional Syst. Nanostructures, vol. 81, p. 83-90, 2016.

[59] K. Sahu, A. Bisht, A. Dutta, T. Som, et S. Mohapatra, « Morphological, optical, catalytic and photocatalytic properties of RF magnetron sputtered Au-Cu_2O-CuO nanocomposite thin films », Surfaces and Interfaces, vol. 26, no July, p. 101436, 2021.

[60] S. S. Akarmazyan, P. Panagiotopoulou, A. Kambolis, C. Papadopoulou, et D. I. Kondarides, « Environmental Methanol dehydration to dimethylether over Al_2O_3 catalysts », "Applied Catal. B, Environ., vol. 145, p. 136 148, 2014.

[61] A. S. Ivanova et al., « Environmental Metal – support interactions in Pt / Al_2O_3 and Pd / Al_2O_3 catalysts for CO oxidation », vol. 97, p. 57 71, 2010.

[62] A. Kabir, « A DFT + U Study on the Structural , Electronic , Magnetic , and Optical Properties A DFT + U Study on the Structural , Electronic , Magnetic , and Optical Properties of Fe and Co co-doped CuO . », no February, 2022.

[63] C. Ronning, « Binary copper oxide semiconductors: From materials towards devices ,1 », vol. 1509, no 8, p. 1487-1509, 2012.

[64] N.Nait Merzoug « application des tiges de dattes dans l'adsorption de polluants organiques », mémoire magistère, université Mohamed Cherif Massaadia Souk-Ahras, 2014, page3.

[65] R.Cherrak «valorisation d'un catalyseur nano composite et son application pour la dégradation photo catalytique des polluants organiques » thèse doctorat, université Abdelhamid ibn Badis-Mostaganem, 2018, page26.

[66] S. Hammami «Étude de dégradation des colorants de textile par les procédés d'oxydation avancée. Application à la dépollution des rejets industriels », thèse doctorat, Université Paris-Est et Tunis El Manar, 2008, page08.

[67] D.Chebli «Traitement des eaux usées industrielles: Dégradation des colorants azoïques par un procédé intégré couplant un procédé d'oxydation avancée et un traitement biologique »,thèse doctorat ,université doctorat, université Ferhat Abbas-Sétif,2012,page06.

[68] L. Naidja «élimination du coloration organe II en solution aqueuse, par vois photochimique et par adsorption »mémoire magister, université Mentouri-constantine,2010,page 08.

[69] J.R.Merouni « Traitement de coloration azoïque et anthraquinonique par procèdes d'oxydation avancée(POA) » thèse doctorat, université Abdelhamid ibn Badis- Mostaganem, 2011, page01.

[70] N. Benselka « Synthèses d'argiles anioniques ($MgFeCO_3$)par coprécipitation et dégradation thermique de l'urée et applications à l'élimination de colorants anioniques dans les effluents textiles »,thèse doctorat, université Mohamed Boudiaf –Oran,2015,page 60.

[71] S.Oukil « matériaux méso poreux à base de Ni/Co : Application à la réaction d'élimination du bleu de méthylène », thèse doctorat, université houari boumadiane-Alger,2020,page07.

[72] N .Bouanimba « Etude comparative de la dégradation photochimique et photo catalytique de quatre colorants : Impact de la structure chimique et corrélation entre l'adsorption et l'activité photo catalytique de TiO2 », thèse doctorat, université Mentouri-Constantine, 2014, page 08.

[73] F .Ouadjenia «cinétique et modélisation de carbone et adsorption de métaux lourds et de colorants par la vase de chorfa », thèse doctorat, université Djilali Liabes –Sidi Bel Abbes, 2015, page43.

[74] N.Laid «dégradation photo catalytique de mordant bleu13 en milieu hétérogène ».mémoire magister, université Mentouri-Constantine, 2010, page 07.

[75] D.Bouras «Élaboration et caractérisation des céramiques à base de mullite et du zircon et leurs applications à la photocatalyse», thèse doctorat, Université Larbi Ben M'hidi -Oum El Bouaghi, 2018, page 109.

[76] S. Esmaeili, M. Dehvari, et A. Babaei, « Degradation of Acid Orange 7 Dye with PMS and H_2O_2 Activated by $CoFe_2O_4$/PAC Nanocomposite », Arch. Hyg. Sci., vol. 8, no 1, p. 35-45, 2019.

[77] S.Aga « Etude cinétique et thermodynamique de l'adsorption de quelques colorants textiles par des résidus issus de l'industrie agroalimentaire », mémoire magister, université Ferhat Abbas-Sétif,2015,page12.

[78] V.I.Merupo, «Synthèse et caractérisation de matériaux nanostructures $BiVO_4$ dopés par des métaux pour des applications en Photo catalyse », thèse doctorat, Université du Maine-France, 2016, page 02.

[79] I. Bousniubra «Contribution à l'élimination de colorants (Vert de méthyle et Bromocrésol pourpre) par procédés photochimiques en phase homogène (séparés et mélangés), en phase hétérogène en milieu aqueux et par adsorption (Vert de méthyle) sur ZnO »,thèse doctorat, université Mentouri –Constantine,2017,page54.

[80] S. Bouhadoun , « Synthèse de nanoparticules de dioxyde de titane par pyrolyse laser et leur application en photo catalyse »,thèse doctorat, université Paris Saclay-France, 2015,page40.

[81] O.Lakbita «Photocatalyseurs à base de Ag_2CO_3 et TiO_2 déposés par voie humide

(sol-gel, précipitation) et sèche (mécanosynthèse) sur des supports argileux d'origine naturelle », thèse doctorat, université toulouse -France, 2016, page21.

[82] N.Koriche « synthése de nouveaux oxydes $CuLaO_2$+X, $AgMnO_2$et WO_3dopé par cuivre Application à la photocatalyse hétérogéne »,thése doctorat,université houari boumadiane-Alger ,2012 ,page 27.

[83] I.Sayah, «Etude de revêtements photo catalytiques à base de dioxyde de titane nano structuré élaborés par pulvérisation cathodique magnétron en condition réactive », thèse doctorat , université toulouse -France, 2017, page9.

[84] A.Jezzini « $ZnFe_2O_4$ pour des applications en photo catalyse hétérogène dans le visible », thèse doctorat, université Libanaise, 2020, page 21.

[85] S.Kaiza « elaboration par voie chimique et électrochimique des oxydes métallique distinés à la protuction des métaux,application à l'envéronnement »,thése doctorat ,université Houari boumadiane-Algie ,2018 ,page 36.

[86] W.Ravisy «Croissance et propriétés photo catalytiques de couches minces de TiO_2 et W-TiO_2 déposées par PECVD sur polymère », thèse doctorat, université Nantes-France, 2021, page29.

[87] H.Sihem « Application de la photocatalyse pour la dégradation des polluants chimiques et bactériologiques dans l'eau en utilisant des catalyseurs irradiés par des photons de lumière naturelle ou artificielle (UV-A /UV-B) », thèse doctorat, université claude bernard Lyon1, 2012, page38.

[88] N.H.Salah «Etude de la dégradation photo catalytique de polluants organiques en présence de dioxyde de titane, en suspension aqueuse et en lit fixe », thèse doctorat, université de Grenoble- France et Mentouri -Constantine, 2012, page17.

[89] W. Halim, «Synthèse contrôlée par additifs latex de nanoparticules mésoporeuses à base de TiO_2 : M (M=Pd, Ag, Cu, Ni...) : caractérisation et applications en photocatalyse »,thése doctorat,thése doctorat, université Hassan II –Maroc ,2021,page10,11.

[90] C.S.Miyashiro « Développement de catalyseurs hétérogènes pour la photodégradation du néonicotinoïde acétamipride dans l'eau »,thèse doctorat ,université Laval-canada,2021,page13.

[91] N.Khelloul « dégradation d'un mélange de coloration par plasma glidarc. études de l'influence de différentes substances », mémoire de magister, université Abdelhamid ibn Badis- Mostaganem, 2012, page44.

[92] M. Mansour « synthèse et caractérisations de matériaux a base d'oxyde de bismuth. Application à l'adsorption et la photo-catalyse », thèse doctorat, université Abdelhamid ibn Badis- Mostaganem, 2020, page14.

[93] K. Kouadio Dobi-Brice, L. Ekou, T. Ekou, et Y. Zoungranan, « Biosorption du Bleu de Méthylène et de l'Orange II sur le Lichen Parmotrema Dilatatum Désactivé », Eur. J. Sci. Res., vol. 149, no 4, p. 473-363, 2018.

[94] S.bouhadoun «Synthèse de nanoparticules de dioxyde de titane par pyrolyse laser et leur application en photocatalyse », thèse doctorat, université paris-Sub, 2015, page 42.

[95] M.N.Ghazzal «Développement et validation d'un test pour déterminer les propriétés photocatalytiques de surfaces autonettoyantes : application aux couches minces de TiO_2 »,thèse doctorat,université Paul Verlaine de Metz-France, 2008, page19.

[96] S. Lacombe et al. « La photocatalyse pour l'élimination des polluants », Actual. Chim., no 308-309, p. 79-93, 2007.

[97] M.Ismail « Préparation et caractérisation de nouveaux matériaux pour les réactions de dépollution photo catalytique de l'eau dans le visible » thése doctorat , institut national des sciences appliquees et de technologie -Tunisie ,2011 ,page 96.

[98] I. El Saliby, A. McDonagh, L. Erdei, et H. K. Shon, « Water reclamation by heterogeneous photocatalysis over titanium dioxide », Green Technol. Sustain. Water Manag., p. 679-704, 2016.

[99] A.Grine, « Elaboration et caractérisation par RX d'oxydes sous forme de couches minces », mémoire magister, université Mentouri –Constantine, 2015, page16.

[100] S.Rahmane « Elaboration et caractérisations des couches minces par spray pyrolyse et pulvérisation magnétron », thèse de doctorat, université Mohamed Kheider- Biskra, 2008, page21, 22, 45,46.

[101] J. P. & L. Ludwig, « Thin Film Deposition Using Spray Pyrolysis », vol. 14, no 2, 2005.

[102] J. Garnier, «Elaboration de couches minces d'oxydes transparents et conducteurs par spray CVD assiste par radiation infrarouge pour applications photovoltaïques », thèse doctorat, université d'Arts et Métiers, 2009, page 33,34,87.

[103] N. Boubrik « Comparaison des effets antireflets du SnO_2 et ZnO utilisés comme couches antireflet sur les propriétés de la cellule solaire à homo-jonction », mémoire magister, université Mouloud Mammeri Tizi-Ouzou, 2013, page 34.

[104] S. Iaiche « Etude des couches minces $Zn(Al)_2O_4$, corrélation élaboration-propriétés et application ».Thèse de doctorat en sciences, université Larbi ben M'hidi Oum EL Bouaghi, 2016, page34.

[105] V. K. Singh, « Thin Film Deposition by Spray Pyroysis Techniques », Emerg. Technol. Innov. Res., vol. 4, no 11, p. 1-9, 2017.

[106] A. Derbali, « Élaboration et Caractérisations Physico-chimiques des Couches Minces de Sulfure de Zinc (ZnS) En Vue d'applications Photovoltaïques », thèse de doctorat, université Mohamed Kheider Biskra, 2018, page 17,18.

[107] H.Guendouz , «Elaboration et caractérisation des couches minces d'oxyde de zinc co-dopé aluminium-étain par la technique sol-gel spin coating »,thèse doctorat, université Jijel,2019,page16.

[108] S.Khodja «Elaboration et caractérisation de couches minces de ZnO pour des applications optoélectroniques » thèse doctorat, université Badji Mokhtar –annaba, 2017, page 56.

[109] A.P. Magalhaes « Développement d'un procédé couplé sol-gel électrophorèse pour des applications en anti-corrosion »thèse doctorat, université de Toulouse-France, 2016, page 51.

[110] M.Khechba, «Elaboration et étude des couches minces d'oxyde d'étain », thèse doctorat, université Mentouri –Constantine, 2018, page27.

[111] H.Trir « Conception des dispositifs optoélectroniques à base d'oxyde de cuivre », thèse de doctorat, université Mohamed Kheider Biskra, 2020, page10.

[112] M.Dahnoun, « Preparation and characterization of Titanium dioxide and Zinc oxide thin films via Sol-Gel (spin coating) technique for optoelectronic applications », thèse de doctorat, université Mohamed Kheider Biskra, 2020, page22.

[113] Malika Medjaldi, « Elaborations et caractérisations des couches minces », thèse de doctorat, université Larbi ben M'hidi Oum EL Bouaghi, 2018, page 29.

[114] M.C.Benachour, « Elaboration et caractérisation des couches minces de TiO_2 dopées à l'erbium, à différentes températures et épaisseurs », mémoire magistère, université Mentouri -Constantine, 2011, page40, 61.

[115] L. Yahia-Cherif «Conception d'un réacteur photo catalytique en vue de la dégradation de polluants organiques en phase aqueuse », mémoire magister, université A. Mira –Bejaia, 2010, page22, 23.

[116] S. Houyem, « Élaboration et caractérisation de couches minces co-dopées In, Co, préparées par la pulvérisation cathodique, applications aux cellules photovoltaïques », thèse doctorat, Université du Littoral Côte d'Opale, 2019, page19.

[117] E. Tranquillo et F. Bollino, « Surface Modifications for Implants Lifetime Extension : An Overview of Sol-Gel Coatings », p. 1-21, 2020.

[118] P. Gravereau, « Introduction à la pratique de la diffraction des rayons X par les poudres ». 3éme édition, Masson, France, 2012, page 42et 57.

[119] L .Bergerot, « Etude de l'élaboration d'oxyde transparent conducteur de type-p en couches minces pour des applications à l'électronique transparente ou au photovoltaïque », thèse doctorat, université Grenoble Alpes Français, 2016, page 71.

[120] C.Zahla, « Etude expérimentale et théorique de l'interaction métal-oxyde de cérium », thèse doctorat, université Mentouri – Constantine, 2009, page 21,22.

[121] F. Serna, J. Lagneau, et J.-M. Carpentier, « La diffraction des rayons X : une technique puissante pour résoudre certains problèmes industriels et technologiques », Diffr. des rayons X Catal., no 1, p. 1-11, 2014.

[122] A. Moustaghfire « Élaboration et caractérisation de couches minces d'oxyde de zinc Application à la photo protection du polycarbonate ».Thèse de doctorat, Université Blaise Pascal, 2004, page 58.

[123] R. Djebian, B. Boudjema, A. Kabir, et C. Sedrati, « Physical characterization of CuO thin films obtained by thermal oxidation of vacuum evaporated Cu », Solid State Sci., vol. 101, no February, p. 106147, 2020.

[124] A.Hafdallah, « Dépôt et caractérisation des électrodes en couches minces transparentes et conductrices », thèse de doctorat, université Mentouri –Constantine, 2016, page 32.

[125] Sarra Dridi 1,2, Eric Aubry 3, Nabila Bitri 1, Fatma Chaabouni 1 and Pascal Briois 3, "Growth and Characterization of Cu2MnSnS4 Thin Films Synthesized by Spray Pyrolysis under Air Atmosphere Sarra," pp. 1–10, 2020.

[126] Y. T. Prabhu, K. V. Rao, V. S. S. Kumar, and B. S. Kumari, "X-Ray Analysis by Williamson-Hall and Size-Strain Plot Methods of ZnO Nanoparticles with Fuel Variation," World J. Nano Sci. Eng., vol. 04, no. 01, pp. 21–28, 2014.

[127] D. Kumar, N. K. Verma, C. B. Singh, and A. K. Singh, "Crystallite size strain analysis of nanocrystalline La $_{0.7}$ Sr $_{0.3}$ MnO_3 perovskite by Williamson-Hall plot method," AIP Conf. Proc., vol. 1942, no. December, pp. 3–8, 2018.

[128] M. Rabiei et al., "X-ray diffraction analysis and williamson-hall method in usdm model for estimating more accurate values of stress-strain of unit cell and super cells (2 × 2 × 2) of hydroxyapatite, confirmed by ultrasonic pulse-echo test," Materials (Basel)., vol. 14, no. 11, 2021.

[129] L.Baghriche, « élaboration et caractérisation des couches minces d'oxyde de zinc et sulfure de zinc préparé par spray ultrasonique », thèse doctorat, université Mentouri –Constantine, 2015, page55.

[130] F. Hanini, « Etude des propriétés physiques de couches minces TiO_2 élaborées par différentes techniques », thèse doctorat, université Mentouri –Constantine, 2014, page 39.

[131] M.Hemara, « Etude structurale et optique de matériaux composites », mémoire magistère, université Mentouri –Constantine, 2015, page 49.

[132] F. Bouanaka « Spectroscopie d'émission optique (SEO) par analyseur optique multicanaux d''un plasma basse pression », mémoire magistère, université Mentouri -Constantine, 2008, page 11.

[133] H.Bensouyad, « élaboration et caractérisation des couches minces nanostructures d'oxyde de titane TiO2 dopées et non dopées avec le ZrO_2 et le ZnO obtenu par voie sol –gel », thèse doctorat, université Mentouri –Constantine, 2011, page 73,74.

[134] H.Belkacemi, «Dépôt et caractérisations des couches minces de ZnO avec différentes Sources de Zinc », mémoire magistère, université Mohamed Kheider-Biskra, 2011, page 28.

[135] S. Chelouche, « Propriétés des fenêtres optiques ZnO : Al pour cellules solaires en couches minces à base de CIGS », mémoire magistère, université Ferhat Abbas Sétif, 2012, page 43.

[136] M. O.Lakbita, « Photo catalyseurs à base de Ag_2CO_3 et TiO_2 déposés par voie humide (sol-gel, précipitation) et sèche (mécano synthèse) sur des supports argileux d'origine naturelle», thèse doctorat, université de Toulouse, 2016, page 60.

[137] L.Yang, «Caractérisation de couches minces de ZnO élaborées par la pulvérisation cathodique en continu », thèse doctorat, université de la littorale côte d'opale, 2012, page 28.

[138] I. Chadli, « Synthèse et caractérisation des sels précurseurs Par la méthode sol-gel », thèse doctorat, université Mohamed Kheider-Biskra, 2017, page 59.

[139] J.A. Resende , « Copper-based p-type semiconducting oxides: From materials to devices », doctoral thesis , Liège university,2017 page 66.

[140] Jday Rawen , « Caractérisation microstructurale du graphite sphéroïdal formé lors de la solidification et à l'état solide » ,thèse doctorat, Université de Toulouse, 2017, page31.

[141] A. Atyraou, « Elaboration de TiO2 sous forme de couche mince dopée et nano tubulaire : caractérisation électrochimique et performance photo catalytique », thèse doctorat, université Tunis el Manar, 2013, page 58.

[142] O. A. Maslova, « Spectroscopie et imagerie Raman de matériaux inhomogènes »,

Thèse doctorat, université d'Orléans, 2014, page 19,20.

[143] F. Labrèche « Elaboration et caractérisation des films minces d'oxyde de titan pur et dopés Nd et Ag »thèse doctorat, université Jijel, 2018, page 45.

[144] M. Hellal , « Elaboration et caractérisation des couches minces nanocristallines », mémoire magistère, université Mentouri -Constantine, 2014, page 24,25.

[145] S.Yahiaoui, «L'effet de la molarité des différentes sources d'étain sur les propriétés des couches minces d'oxyde d'étain SnO2 élaborées par Spray ultrasonique », mémoire magistère, université Mohamed Kheider-Biskra, 2014, page 52.

[146] K. Bouzid « Élaboration et caractérisation de couches minces ZnO d'oxyde de zinc pyrolyse-pulvérisation par ultrasonique et Application », thèse de doctorat, université Kasdi Merbah – Ouargla, 2012 page43,46.

[147] E.Benyahia, «Caractérisation structurale et optique de couches minces formées par des agrégats des nano cristaux de ZnO », », mémoire magistère, université Mentouri -Constantine, page 59 .

[148] A.Boughelout, «Elaboration et caractérisation de couches minces d'oxyde de zinc dopées aux métaux pour des applications photovoltaïques et en détection de gaz », thèse doctorat, université Houari Boumediene, 2019, page 34.

[149] S.Boulmelh, « Élaboration et caractérisation d'un dépôt de couches minces d'oxyde de zinc par spray pyrolyse », mémoire magistère, université Mentouri –Constantine, 2015, page54.

[150] F. Labrèche , « Elaboration et caractérisation des films minces d'oxyde de titan pur et dopés Nd et Ag », thèse doctorat, université de jijel,2018,page 55 .

[151] S. Abed, « Elaboration et Caractérisation de Couches minces d'Oxyde de Zinc Obtenues par Spray Pyrolyse », mémoire magistère, université Mentouri –Constantine, page58.

[152] K. Bennaceur« Elaboration and characterization of SnO2 : In thin films deposited by spray pyrolysis technique », thèse doctorat, université Mohamed Kheider-Biskra, 2020, page 38.

[153] A Camut « Mise en place du contrôle terminal des préparations d'anticancéreux injectables par spectrométrie UV-visible-IRTF, Multispec à l'Unité de Pharmacie Clinique et Cancérologique de l'Hôpital Bon Secours de Metz : Aspects analytiques et organisationnels ». thèse doctorat ,Université Henri Poincare-Nancyi,2009, page 19.

[154] S. Hamri « Etude thermophysique de la diffusion de molécules de bas poids moléculaire dans des réseaux de polymères acryliques » thèse doctorat, université Abou Bekr Belkaid –Tlemcen, 2013, page 46.

[155] Z.Manaa « Elimination des composés pharmaceutiques par photo-fention heterogene (goethite et argile synthétique) Etude cinétique et transfert des espèces organiques à l'interface minéral solution » », mémoire magistère, université Ferhat Abbas Sétif, 2015, page 68.

[156] A. James et al., « Determination of Contact Angle for Various fluids Used in Industries », vol. 6, no 2, p. 30-31, 2017.

[157] T. Huhtamäki, X. Tian, J. T. Korhonen, and R. H. A. Ras, "Surface-wetting characterization using contact-angle measurements," Nat. Protoc., vol. 13, no. 7, pp. 1521–1538, 2018.

[158] R. Djebian, B. Boudjema, A. Kabir, et C. Sedrati, « Physical characterization of CuO thin films obtained by thermal oxidation of vacuum evaporated Cu », Solid State Sci., vol. 101, no February, p. 106147, 2020.

[159] S. D. Al Ghamdi, A. O. M. Alzahrani, M. S. Aida, et M. S. Abdel-wahab, « Influence of substrate temperature and solution molarity on CuO thin films' properties prepared by spray pyrolysis », J. Mater. Sci. Mater. Electron., vol. 33, no 18, p. 14702-14710, 2022.

[160] M. Serhan et al., « Novel CuO/Chitosan nanocomposite thin film: Facile hand picking recoverable, efficient and reusable heterogeneous photocatalyst », AIChE Annu. Meet. Conf. Proc., vol. 2019-Novem, 2019.

[161] B. T. Sone, A. Diallo, X. G. Fuku, A. Gurib-Fakim, et M. Maaza, « Biosynthesized CuO nano-platelets: Physical properties & enhanced thermal conductivity nanofluidics », Arab. J. Chem., vol. 13, no 1, p. 160-170, 2020.

[162] C. Chimeno-Trinchet, A. Fernández-González, J. Á. García Calzón, M. E. Díaz-García, et R. Badía Laíño, « Alkyl-capped copper oxide nanospheres and nanoprolates for sustainability: water treatment and improved lubricating performance », Sci. Technol. Adv. Mater., vol. 20, no 1, p. 657-672, 2019.

[163] A. Boughelout, A. Bensouilah, L. Chabane, N. Zebbar, et A. H. M. Kechouane, « les propriétés optique et électriques des couches minces de ZnO déposées par pulvérisations cathodique a basse pression », vol. 9075, 2008.

[164] N. Y. Mostafa, A. Badawi, et S. I. Ahmed, « Influence of Cu and Ag doping on structure and optical properties of In2O3 thin film prepared by spray pyrolysis », Results Phys., vol. 10, no April, p. 126-131, 2018.

[165] F. Z. CHAFI, L. BAHMAD, N. HASSANAIN, B. FARES, L. LAANAB, et A. MZERD, « Characterization techniques of fe-doped cuo thin films deposited by the spray pyrolysis method », arXiv, p. 1-13, 2018.

[166] S. Kose, F. Atay, V. Bilgin, et I. Akyuz, « Some physical properties of copper oxide films : The effect of substrate temperature », vol. 111, p. 351-358, 2008.

[167] H. Hashim, S. S. Shariffudin, P. S. M. Saad, et H. A. M. Ridah, « Electrical and Optical Properties of Copper Oxide Thin Films by Sol-Gel Technique », IOP Conf. Ser. Mater. Sci. Eng., vol. 99, no 1, 2015.

[168] J. Y. Park, M. Y. Ha, H. J. Choi, S. Do Hong, et H. S. Yoon, « A study on the contact angles of a water droplet on smooth and rough solid surfaces », J. Mech. Sci. Technol., vol. 25, no 2, p. 323-332, 2011.

[169] A. James et al., « Determination of Contact Angle for Various fluids Used in Industries », vol. 6, no 2, p. 30-31, 2017.

[170] M. Arfan, D. Nawaid, T. Shahid, Z. Iqbal, and Y. Majeed, « Tailoring of Nanostructures : Al doped CuO Synthesized by Composite- Hydroxide-Mediated», Results Phys., vol. 13, no. March, p. 102187, 2019.

[171] X. Wang, Z. Li, W. Yan, P. Wang, and H. Zhang, «Electrical properties of Nb/Al-doped CuO-based ceramics for NTC thermistors », Process. Appl. Ceram., vol. 14, no. 1, pp. 47–55, 2020.

[172] R. M. Thyab, M. A. H. Al-Hilo, F. A. Yasseen, and H. Alshater, «Influence of Aluminum Doping on Structural and Optical Properties of the Nanostructured Copper Oxide Thin Films Prepared by CSP Method», NeuroQuantology, vol. 20, no. 3, pp. 99–104, 2022.

[173] A. De Chimie, « Hydrophobic Properties of CuO Thin Films Obtained by Sol-Gel Spin Coating Technique- Annealing Temperature Effect », vol. 45, no 6, p. 439-445, 2021.

[174] M. R. Islam, J. E. Obaid, M. Saiduzzaman, S. S. Nishat, T. Debnath, and A. Kabir, «Effect of Al doping on the structural and optical properties of CuO nanoparticles prepared by solution combustion method: Experiment and DFT investigation », J. Phys. Chem. Solids, vol. 147, p. 109646, 2020.

[175] Z. Khodair, A. Adwan, and N. Shallal, «Effect of Aluminum Doping on Structural Properties of CuO Thin Films Prepared by Chemical Spray Pyrolysis (CSP) Technique», Diyala J. Pure Sci., vol. 13, no. 3, pp. 198–208, 2017.

[176] A. B. Bodade, M. A. Taiwade, et G. N. Chaudhari, « Bioelectrode based chitosan-nano copper oxide for application to lipase biosensor », J. Appl. Pharm. Res. (JAPTRonline , vol. 5, no 1, p. 30-39, 2017.

[177] R. G. Sethuraman, T. Venkatachalam, et S. D. Kirupha, « Fabrication and characterization of Zn doped CuO nanofiber using newly designed nanofiber generator for the photodegradation of methylene blue from textile effluent », Mater. Sci. Pol., vol. 36, no 3, p. 520-529, 2018.

[178] L. Radev, I. Michailova, D. Zaimova, et T. Dimova, « In vitro bioactivity of Silver containing sol-gel glasses : FTIR analysis », Imp. J. Interdiscip. Res., no 4, p. 316-323, 2017.

[179] S. A. Naayi, A. I. Hassan, and E. T. Salim, «FTIR and X-ray diffraction analysis of Al2O3 nanostructured thin film prepared at low temperature using spray pyrolysis method», Int. J. Nanoelectron. Mater., vol. 11, no. Special Issue BOND21, pp. 1–6, 2018.

[180] M. Hinna et al., «Elaboration and Characterization of CuO Thin Films by Spray Pyrolysis Method for Gas Sensors Applications»,Proceedings, vol. 14, p. 55, 2019.

[181] C. P. Goyal et al., « Effect of Zn doping in CuO octahedral crystals towards structural, optical, and gas sensing properties », Crystals, vol. 10, no 3, 2020.

[182] S. Vural and Ö. Sari, «Synthesis and characterization of SDS assistant α-alumina structures and investigation of the effect of the calcination time on the morphology», Colloid Polym. Sci., vol. 297, no. 1, pp. 107–114, 2019.

[183] T. Jan et al., «Structural, Raman, optical and novel antibacterial characteristics of Al doped CuO nanostructures», Mater. Res. Express, vol. 6, no. 10, pp. 0–10, 2019.

[184] N. Mukherjee et al.,«CuO nano-whiskers: Electrodeposition, Raman analysis, photoluminescence study and photocatalytic activity », Mater. Lett., vol. 65, no 21-22, p. 3248-3250, 2011.

[185] T. Gnanasekar et al., «Enhanced opto-electronic properties of X-doped (X = Al, Ga, and In) CuO thin films for photodetector applications», J. Mater. Sci. Mater. Electron., vol. 33, no. 23, pp. 18786–18797, 2022.

[186] T. Jan, J. Iqbal, Q. Mansoor, G. Engineering, M. Ismail, and G. Engineering, «Synthesis , physical properties and antibacterial activity of Ce doped CuO : A novel nanomaterial», J. Phys. D. Appl. Phys., vol. 47, no. May 2015, 2014.

[187] Sarra Dridi , Eric Aubry , Nabila Bitri , Fatma Chaabouni and Pascal Briois «Growth and Characterization of Cu2MnSnS4 Thin Films Synthesized by Spray Pyrolysis under Air Atmosphere», Coatings,vol10: 963. 2020.

[188] R. Sharma, S. L. Patel, M. D. Kannan, et M. S. Dhaka, « Effect of different annealing conditions on CdZnTe thin films for absorber layer applications », Surfaces and Interfaces, vol. 33, no July, p. 102204, 2022.

[189] D. Bouras et al., «Photocatalytic degradation of orange II by active layers of Cu-DOPED ZnO deposited on porous ceramic substrates»,J. Ovonic Res., vol. 13, no. 5, pp. 271–281, 2017.

[190] N. Djebbari, D. Bouras, and H. Farh, «Effect of doping with manganese and zinc on the structural, morphological, optical and photocatalytic properties of NiO»,Appl. Phys. A Mater. Sci. Process., vol. 128, no. 10, pp. 1–10, 2022.

[191] M. Nesa, M. Sharmin, K. S. Hossain, et A. H. Bhuiyan, «Structural, morphological, optical and electrical properties of spray deposited zinc doped copper oxide thin films» , J. Mater. Sci. Mater. Electron. vol 28 ,2017.

[192] E. Benrezgua et al, «Synthesis and properties of copper doped zinc oxide thin films by sol-gel , spin coating and dipping : A characterization review» , J. Mol. Struct,2022.

[193] S. Das et T. Alford, « Structural and optical properties of Ag-doped copper oxide thin films on polyethylene napthalate substrate prepared by low temperature microwave annealing», 2013.

[194] N. D. Dinesh et K. Kumar, «Synthesis of CuO and Ag doped CuO nanoparticles from Muntingia calabura leaf extract and evaluation of their antimicrobial potential», 2019

[195] A. B. Bodade, M. A. Taiwade, et G. N. Chaudhari, « Bioelectrode based chitosan-nano copper oxide for application to lipase biosensor» , J. Appl. Pharm. Res.vol 5, 30-39,2017.

[196] Zi-Y. Chen et al., «Tuning the interface adhesion of Ag/ZnO composites by metallic dopants: A DFT study», Computational Materials Science. vol 224,2023.

[197] M. F. A. Aboud, S. Haider, et M. F. Warsi, «Fabrication of Binary Metal Doped CuO Nanocatalyst and Their Application for the Industrial Effluents Treatmen» , Ceram. Int,2020.

[198] L. Radev, I. Michailova, D. Zaimova, et T. Dimova, « In vitro bioactivity of Silver containing sol-gel glasses : FTIR analysis»,Imp.J.Interdiscip.Res,316-323, 2017.

[199] M. G. Méndez-Medrano et al. « Surface Modification of TiO2 with Ag Nanoparticles and CuO Nanoclusters for Application in Photocatalysis», J. Phys. Chem. Vol 120 ,2016.

[200] N. Mukherjee et al. « CuO nano-whiskers: Electrodeposition, Raman analysis, photoluminescence study and photocatalytic activity», Mater. Lett.vol 65, 2011.

[201] X. Chenet al, « Cu_2O nanoparticles and multi-branched nanowires asanodes for lithium-ion batteries », NANO vol 13, 1850103,2018.

[202] M. F. A. Aboud, S. Haider, et M. F. Warsi, «Fabrication of Binary Metal Doped CuO Nanocatalyst and Their Application for the Industrial Effluents Treatmen », Ceram. Int,2020 .

[203] R. Marnadu et al, « Significant enhancement in photosensitivity, responsivity, detectivity and quantum efficiency of Co_3O_4 nanostructured thin film-based photodetectors through Mo doping developed by spray pyrolysis method» , Surfaces and Interfaces, vol 34,102366,2022.

[204] R. Sharma, S. L. Patel, M. D. Kannan, et M. S. Dhaka, « Effect of different annealing conditions on CdZnTe thin films for absorber layer applications» , Surfaces and Interfaces, vol 33,102204, 2022.

[205] K. Sahu, S. Choudhary, S. A. Khan, et A. Pandey, «Thermal evolution of morphological , structural , optical and photocatalytic properties of CuO thin films» ,Nano-Structures & Nano-Objects. vol 17 92-102,2019

[206] S. Lacombe et al, « La photocatalyse pour l'élimination des polluants», Actual .Chim. 79-93 ,2007.

Study of the structural, optical, and electrical properties of copper oxide thin films undoped and doped

Abstract

In this study, copper oxide thin films undoped and doped were elaborated by two methods: pneumatic spray pyrolysis and sol-gel spin coating on a glass substrate, and used in two applications: self-cleaning and photocatalytic, respectively. All the samples are characterized by X-ray diffraction, FT-IR spectroscopy, scanning electron microscope, energy-dispersive X-ray, UV-visible spectrophotometry, and four-point method. Undoped CuO layers were made by spray pyrolysis for different spray times. The XRD analysis of these layers showed that the films have a monoclinic structure (tenorite) and a preferential growth in the (111) direction. According to Scherer's formula the crystallite size is nanometric between 14 – 23nm. The water contact angle values in all samples are greater than 90° and range from 96.4° to 103.2°, as we can see from these results that all the samples are hydrophobic films and excellent in a self-cleaning application. Thin films of copper oxide undoped and doped with aluminum and silver (5%, 15%, 25 %, and 50%) were deposited by the sol-gel spin coating method on a glass substrate. According to XRD diffraction and by Williamson-Hall plot method, the crystallite size varies between 21– 46 nm and 21– 33 nm and increases with the increase in Al and Ag doping, respectively. The electrical conductivity values increase with the presence of doping. Aluminum doping has good structural and electrical properties when compared to elemental silver. The Photocatalysis results showed that doping of copper oxide by (Al) improves the photocatalytic efficiency, and the best degradation of a dye (orange II) under UV irradiation after 5 hours reaches 61% for the use for thin layers of CuO doped with 50% Al.

Keywords:

Thin films, CuO, spray pyrolysis, self-cleaning, spin coating, doped, aluminum, silver, photocatalysis.

Etude structurale, optique et électrique des couches minces d'oxyde du cuivre dopées et non dopées

Résumé

Dans cette étude, des films minces d'oxyde de cuivre non dopés et dopés ont été élaborés par deux méthodes : spray pyrolyse pneumatique et sol gel spin coating sur un substrat de verre et les utilisent dans deux applications : autonettoyantes et photocatalytiques, respectivement. Tous les échantillons sont caractérisés par diffraction des rayons X, spectroscopie FT-IR, microscope électronique à balayage, rayons X à dispersion d'énergie, spectrophotométrie UV-visible et méthode de quatre points. Les couches de CuO non dopées ont été réalisées par spray pyrolyse pour différents temps de spray. L'analyse DRX de ces couches a montré que les films ont la structure monoclinique (ténorite) et une croissance préférentielle dans la direction (111). La taille des nanocristaux est comprise entre 14 et 23 nanomètres, selon la formule de Scherer. Les valeurs d'angle de contact avec l'eau dans tous les échantillons sont supérieures à 90° et vont de 96,4° à 103,2°, comme nous pouvons le voir à partir de ces résultats que tous les échantillons sont des films hydrophobes et excellents dans l'application de l'auto-nettoyage. Les films minces d'oxyde de cuivre non dopé et dopé par Aluminium et Argent (5%, 15%, 25% et 50%) ont été déposés par la méthode de sol gel spin coating sur un substrat de verre. Selon la diffraction DRX. Selon la formule de Williamson-Hall,la taille des cristallites varie entre 21–46 nm et 21–33 nm est augmentée avec l'augmentation du dopage Al et Ag, respectivement. Les valeurs de conductivité électrique augmentent avec la présence de dopage. Le dopage en aluminium a de bonnes propriétés structurelles et électriques par rapport à le dopage par l'argent. Les résultats de photocatalyse ont montré que le dopage d'oxyde de cuivre par (Al) améliore l'efficacité photocatalytique et la meilleure dégradation d'un colorant (orange II) sous irradiation UV après 5 heures atteint 61% pour l'utilisation pour des couches minces de CuO dopé à 50% Al.

Mots clés :

Couches minces, CuO, spray pyrolyse, autonettoyant, spin coating, dopé, aluminium, argent, photocatalyse.

الدراسة الهيكلية والبصرية والكهربائية للأغشية الرقيقة من أكسيد النحاس الغير مطعم والمطعم

ملخص

في هذه الدراسة، تم تصنيع أغشية رقيقة من أكسيد النحاس النقي والمطعم. بطريقتين مختلفتين: رذاذ الانحلال الحراري الهوائي والطلاء الدوراني على ركيزة زجاجية واستخدامها في تطبيقين: التنظيف الذاتي والتحفيز الضوئي، على التوالي. تميزت جميع العينات بحيود الاشعة السينية، المجهر الالكتروني الماسح، التحليل الطيفي للطاقة المتشتتة، القياس الطيفي المرئي للأشعة فوق البنفسجية، طريقة النقاط الأربعة والتحليل الطيفي للأشعة تحت الحمراء. تم صنع طبقات أكسيد النحاس النقية عن طريق الانحلال الحراري بالرش لأوقات رش مختلفة. اظهر تحليل الاشعة السينية لهذه الطبقات ان الاغشية لها بنية أحادية الميل (تينوريت) ونمو تفضيلي في الاتجاه (111). حجم البلورات نانومترية بين 14 و23 نانومتر وذلك حسب صيغة شيرير. قيم زاوية ملامسة الماء في جميع العينات أكبر من 90 درجة وتتراوح من 96.4 درجة إلى 103.2 درجة، كما يمكننا أن نرى من هذه النتائج أن جميع العينات عبارة عن أغشية كارهة للماء وممتازة في تطبيق التنظيف الذاتي. تم ترسيب الأغشية الرقيقة من أكسيد النحاس النقي والمطعم بالألومنيوم والفضة (5٪، 15٪، 25٪ و50٪) بواسطة طريقة الطلاء الدوراني على طبقة زجاجية. وفقا لتنائج الاشعة السينية و حسب صيغة ويليامسون هول فان حجم البلورات يتراوح بين 21-46 نانومتر و21-33 نانومتر فهي تزداد مع زيادة المنشطات بالألومنيوم والفضة. تزداد قيم التوصيل الكهربائي مع وجود المنشطات. منشطات الألمنيوم لها خصائص هيكلية وكهربائية جيدة مقارنة بالمنشطات بالفضة. أظهرت نتائج التحفيز الضوئي أن تعاطي أكسيد النحاس لمنشطات عنصر الالمنيوم يحسن كفاءة التحفيز الضوئي وأفضل تحلل للصبغ البرتقالي الثاني تحت الاشعة الفوق البنفسجية بعد 5 ساعات يصل الى61 ٪ باستخدام الاغشية الرقيقة من اكسيد النحاس مخدرة ب 50٪ من الالومنيوم.

الكلمات المفتاحية :

الأغشية الرقيقة، أكسيد النحاس، رذاذ الانحلال الحراري، التنظيف الذاتي، الطلاء الدوراني، مطعم، الألومنيوم، الفضة، التحفيز الضوئي.